MODIS Land-Surface Temperature Algorithm Theoretical Basis Document (LST ATBD)

Version 3.2

Contract Number: NAS5-31370

ZHENGMING WAN
WILLIAM SNYDER
Institute for Computational Earth System Science
University of California, Santa Barbara

P.I. : ZHENGMING WAN
Address: Institute for Computational Earth System Science
University of California
Santa Barbara, CA 93106-3060

Phone: (805) 893-4541
FAX: (805) 893-2578
Email: wan@icess.ucsb.edu

December 1996

TABLE OF CONTENTS

MODIS Land-Surface Temperature Algorithm Theoretical Basis Document (LST ATBD)

1. Introduction

This is version 3.1 of the ATBD for MODIS (Moderate Resolution Imaging Spectroradiometer) Land-Surface Temperature (LST), level-2 and level-3 at-launch data products that include two parameters:

MODIS Product No. 11, Land_sfc Temperature, Parameter No. 2484.
MODIS Product No. 11, Land_sfc Emissivity, Parameter No. 3323.

This is an evolutionary document of the theoretical basis of the MODIS LST algorithm. Some major changes were made in the version 2 after the first ATBD review in 1994 (see Appendix A: Comments and Corrections to the Version 1 ATBD). The following major updates have been made since the last version (v2.2, 1 November 1994) of the ATBD: 1) The solution A (multi-channel method) evolved into the generalized split-window LST algorithm [Wan and Dozier, 1996], which has been and is being validated by MAS (MODIS Airborne Simulator) data and field measurements. 2) Other LST methods evolved into a new physics-based day/night LST algorithm [Wan and Li, 1996], which is designed specifically for the MODIS instrument. The day/night LST algorithm has been validated by ground-based measurements in the sun-shadow method [Wan et al., 1996] and is being validated by MAS data. 3) LST validation plan has been completed and it is being implemented. Comments and suggestion from the peer review panel on the EOS (Earth Observing System) AM1 Land Workshop in May 1996 have been considered fully in the recent revision.

This document describes the theoretical basis for the LST algorithms, the development process, and the functional flow of the LST process. The LST product was proposed by the MODIS Science Team as a daily daytime and nighttime 1km global land product, and includes derivative products at lower temporal frequencies and spatial resolutions. This is an at-launch product of the MODIS instrument on board the EOS AM and PM platforms. The thermal infrared signature received by satellite sensors is determined by surface temperature, surface emissivity/reflectivity, and atmospheric emission, absorption and scattering actions upon thermal radiation from the surface, and the solar radiation in daytime. LST will be retrieved from MODIS thermal channel data for the entire Earth's land surface including evergreen forest and shrubs, deciduous forest and shrubs, crop and grass lands, inland water bodies, snow and ice, barren lands of exposed soil, sands and rocks, and urban areas. A database has been established for MODIS thermal band radiance values from accurate atmospheric transfer simulations for a wide range of atmospheric and surface conditions. Based on this simulated database, a look-up table and interpolation scheme has been developed for comprehensive studies of the effects of surface temperature and emissivity, atmospheric water vapor, and temperature profiles on MODIS TIR band radiance, and for the development and error analysis of LST algorithms for different land surface situations, with the goal of 1 °K LST accuracy. Existing spectral emissivity measurement data of terrestrial materials show that the band average emissivities in MODIS bands 31 and 32 are relatively stable and known within approximately 0.01 for some land cover types including dense evergreen canopies, lake surface, ice and snow, and most soils. A view-angle dependent split-window LST algorithm has been developed for correcting atmospheric and emissivity effects for these land cover types. In most cases, the accuracy of the generalized split-window LST algorithm is better than 1 °K for those surfaces with known band emissivities by optimization of its parameters for specific viewing angle and column water vapor ranges. A new physics-based day/night LST algorithm has been developed to simultaneously retrieve surface band emissivities and temperatures for cover types with emissivities that are difficult to predict.

Land-surface Temperature is one of the MODIS Land products. It will be used as an input variable for other MODIS Atmospheric and Land products such as aerosol, atmospheric profiles, land-cover, evapotranspiration, and net primary

productivity, and for a variety of EOS interdisciplinary research projects.

This document is organized into three sections. The first will discuss the rationale for the development of the LST algorithms, provide a historical context and background information, and discuss MODIS in terms of its unique ability to retrieve LST on the regional and global scales. The next section will give theoretical and practical descriptions of the LST algorithms, and discuss the calibration needs and the validation plan for these algorithms. The final section will address potential constraints and limitations.

2. Overview and Background Information

2.1. Experimental Objective

LST is a good indicator of the energy balance at the Earth's surface and the so-called greenhouse effect because it is one of the key parameters in the physics of land-surface processes on a regional as well as global scale. It combines the results of surface-atmosphere interactions and energy fluxes between the atmosphere and the ground [Mannstein, 1987; Sellers et al., 1988]. Therefore it is required for a wide variety of climate, hydrologic, ecological and biogeochemical studies [Camillo, 1991; Schmugge and Becker, 1991; Running, 1991; Zhang et al., 1995; Running et al., 1994]. For example, accurate Arctic snow and ice surface temperature is needed to improve our estimation of the heat budget in the polar region and our understanding of its link to the global climate change [Yu et al., 1995]. In the central Arctic, the climatological mean difference between air temperature and the surface temperature for all skies is within 1.5 °K, varying from -0.2 °K in September and June to 1.5 °K in February, and averages approximately 0.5 °K during winter [Maykut, 1978; Key et al., 1994]. A long-term data set of satellite-derived land-surface temperature, such as that from MODIS can be used to answer questions about the greenhouse effect and climate change in the polar region. In addition, canopy temperature may be used to estimate sensible heat flux [Vining and Blad, 1992], soil surface temperature may be used to estimate sensible and latent heat fluxes [Kimura and Shimiru, 1994], and satellite-measured surface temperature may be used to improve models and methods for evaluating land-surface energy balance [Diak and Whipple, 1993; Crag et al., 1995]. Further, atmospheric general circulation model (GCM) simulations indicate that stronger summer monsoons are associated with higher land temperatures [Meehl, 1994]. Radiative transfer simulations based on observed surface temperature data show a positive correlation between the normalized greenhouse effect and the surface temperature [Sinha, 1995]. For agriculture, the canopy temperature may be also used to evaluate water requirements of wheat [Jackson et al., 1977], to determine frosts in orange groves [Caselles and Sobrino, 1989] and the frost-damaged area [Kerdiles et al., 1996]. Finally, surface emissivity is needed in the accurate calculation of outgoing longwave radiation emitted from the Earth's surface.

The accuracy specification for LST is 1 °K at 1km resolution for flat uniform or uniformly mixed land surfaces under clear-sky conditions. The accuracy specification for land-surface emissivity retrieved from MODIS data is 0.02 for bands 29, 31 and 32, and 0.05 for bands 20, 22, and 23 [Earth Observing System Output Data Products and Input Requirements, version 2.0, Science Processing Support Office, Goddard Space Flight Center, August 1992]. After the calibration of MODIS TIR data is validated by accurate ground-based measurements, it may be possible to achieve an absolute accuracy of 0.5 °K for calm lake water and playa surfaces in dry atmospheric conditions.

2.2. Historical Perspective

During the past decade, significant progress has been made in estimation of land-surface emissivity and temperature from airborne TIR data. Kahle et al. [1980] developed a technique to estimate the surface temperature based on an assumed constant emissivity in one channel and previously determined atmospheric parameters. This temperature was then used to estimate the emissivity in other channels [Kahle, 1986]. Other techniques such as thermal log residuals and alpha residuals,

have been developed to extract emissivity from multispectral thermal infrared data [Hook et al., 1992]. Based on these techniques and an empirical relationship between the minimum emissivity and the spectral contrast in band emissivities, a temperature emissivity separation (TES) method has been recently developed for one of the ASTER (Advance Spaceborne Thermal Emission and Reflection Radiometer) products [ATBD-AST-03, 1996].

In addition, three types of methods have been developed to estimate LST from space: the single infrared channel method, the split window method which is used in various multi-channel sea-surface temperature (SST) algorithms, and a new day/night MODIS LST method which is designed to take advantage of the unique capability of the MODIS instrument.

The first method requires surface emissivity and an accurate radiative transfer model and atmospheric profiles which must be given by either satellite soundings or conventional radiosonde data [Price, 1983; Susskind et al., 1984; Chedin et al., 1985; Ottle and Vidalmadjar, 1992].

The second method makes corrections for the atmospheric and surface emissivity effects with surface emissivity as an input based on the differential absorption in a split window [Price, 1984; Becker, 1987; Wan and Dozier, 1989; Becker and Li, 1990; Sobrino et al., 1991; Vital, 1991; Kerr et al., 1992; Ottle and Stoll, 1993; Prata, 1994; Wan and Dozier, 1996].

The third method [Wan and Li, 1996] uses day/night pairs of TIR data in seven MODIS bands for simultaneously retrieving surface temperatures and band-averaged emissivities without knowing atmospheric temperature and water vapor profiles to high accuracy. This method improves upon the Li and Becker's method [1993], which estimates both land surface emissivity and LST by the use of pairs of day/night co-registered AVHRR images from the concept of the temperature independent spectral index (TISI) in thermal infrared bands and based on assumed knowledge of surface TIR BRDF (Bidirectional Reflectance Distribution Function) and atmospheric profiles.

Recent progress in SST algorithms [Barton et al., 1989; Harris and Mason, 1992; Sobrino et al., 1993] also provided useful information for the development of LST algorithms. Sobrino et al. [1993] has shown that including column water vapor in the split-window algorithm could improve the SST accuracy. The atmospheric water vapor content over ocean may be retrieved with an accuracy of 5% independent of its absolute value [Harris and Mason, 1992].

Because of the difficulties in correcting both atmospheric effects and surface emissivity effects, the development of accurate LST algorithms is not easy. The accuracy of atmospheric corrections is limited by radiative transfer methods and uncertainties in atmospheric molecular (especially, water vapor) absorption coefficients and aerosol absorption/scattering coefficients and uncertainties in atmospheric profiles as inputs to radiative transfer models. Atmospheric transmittance/radiance codes LOWTRAN6 [Kneizys et al., 1983], LOWTRAN7 [Kneizys et al., 1988], MODTRAN [Berk et al., 1989], and MOSART [Cornette et al., 1994] have been widely used in development of SST and LST algorithms. A common method used for calculation of radiative flux in these codes is the two-stream approximation. A single scattering approximation is used in LOWTRAN6, while a three-term K-distribution multiple scattering parameterization is used in LOWTRAN7, and a multiple scattering approximation without K-distribution and an option of the discrete-ordinates method [Stamnes et al., 1988] are used in MODTRAN. Other different approximations used in these codes include the Curtis-Godson approximation, and Beer's law to calculate optical depth (although atmospheric transmission does not obey Beer's law). Quantitative comparisons of the transmissions from these codes indicate that these approximations are accurate in the 0.5-2% range within the 3.4-4.1 and 8-13 μm atmospheric windows. Moreover, MODIS TIR band transmittance may differ by 6% within these windows and by more than 30% near the edges of these windows because of different molecular band absorption models used in LOWTRAN7 and MODTRAN [Wan and Dozier, 1992]. A review for measurements of water vapor absorption in the 8-13 μm atmospheric window reveals a considerable variation in its magnitude over the past

20 years [Grant, 1990]. The accuracy of water vapor continuum absorption in five of the measurements reviewed is approximately 10%; adequate experimental measurements are lacking at temperatures below 280 °K. Recent theoretical studies [Ma and Tipping, 1992; Ma and Tipping, 1994] on water vapor continuum absorption have led to significant progress in understanding the physical mechanisms and temperature dependence of the continuum absorption. But it is still premature to theoretically determine the magnitude and the temperature dependence of the water vapor continuum absorption coefficients. Barton [1991] explored the possibility to derive infrared continuum water vapor absorption coefficients from satellite TIR data in two AVHRR bands, radiosonde data, and in-situ radiometric measurements of the sea-surface temperature. Clough [1995] made a new correction to the water vapor continuum based on the measurements of the atmospheric downwelling radiance at Kavieng, New Guinea by Westwater et al. [1994] and the measurements by Revercomb and colleagues at the University of Wisconsin. This new continuum formulation has been implemented in version 3 of the MODTRAN code in 1994.

One of the major difficulties in development of LST algorithms is the considerable spectral variation in emissivities for different land-surface materials. For many of them, emissivities have been measured only for the spectrally integrated range from 8 to 14 μm [Griggs, 1968; Nerry et al., 1990; Salisbury and D'Aria, 1992; Rees, 1993]. Emissivity may also vary with the viewing angle [Dozier and Warren, 1982; Labed and Stoll, 1991; Rees and James, 1992], an effect that is more important over land than over water because the combination of surface slope and MODIS scan angle routinely results in local viewing angles greater than 60 °. In laboratory measurements of bare soils, Labed and Stoll [1991] verified the angular effect and showed that this effect is smaller at wavelengths 10.6 and 12.0 μm than at 3.7 μm. Oblique viewing results in a shift of the signature, the spectral features being essentially unchanged. At a viewing angle of 60 °, this angular effect does not exceed 1.5% for sand and silty materials but it may be up to approximately 5% for agricultural soils. Soil emissivity may vary with soil particle size [Salisbury and D'Aria, 1992]. And because of atmospheric effects, the emissivity spectra derived from field measurement and airborne sensor data may be different from the spectra derived from laboratory data [Rivard et al., 1993] if the atmospheric effect is not fully corrected. In order to accurately measure directional-hemispherical surface emissivity, information about the surface BRDF may be needed. The conventional method to measure surface emissivity with an integrating sphere assumes that the reference surface and a sample surface have a similar BRDF pattern. Otherwise, the uncertainty in measured emissivity may be up to ±5% in cases of mixed diffuse and nondiffuse samples and reference [Hanssen, 1989] and the uncertainty depends on the non-Lambertian feature of the integrating sphere [Hanssen, 1996] if an appropriate baffle is not configured in the integrating sphere. The knowledge of surface BRDF is even more important in making correction of the solar beam reflected by the surface in order to accurately determine surface emissivity from field measurement data. In vegetation, the emitted radiation varies with the viewing angle, because of the angular effect in canopy temperature in additional to the angular effects in the emissivity [Kimes, 1981; Lagouarde et al., 1995].

It is essential to measure spectral emissivities of natural cover types for the development of LST algorithms. An active method was used in emissivity and BRDF measurements of a grass field in the early 80s [Becker et al., 1981]. Rapid advances in performances of portable PC and TIR interferometers in the recent years made it possible to establish a comprehensive surface emissivity and TIR BRDF knowledge-base of land cover types through laboratory and field measurements.

The strategy for the development of MODIS LST algorithms consists of: 1) apply experiences in the development of existing SST and LST algorithms; 2) establish a land-surface emissivity and BRDF knowledge-base in a joint effort with the EOS ASTER Science Team so that the development of MODIS LST algorithms has a solid basis and so that it is possible to measure LST with an accuracy better than 1 °K for ground-based validation of the product; 3) use accurate radiative transfer models and to incorporate new theoretical and experimental advances in atmospheric absorption into radiative transfer

simulations; and 4) establish a database from accurate radiative transfer simulations and develop a look-up table and interpolation scheme so that efficient and accurate physics-based LST algorithms for retrieving surface emissivity and temperature could be used in operational production.

It should be pointed out that the MODIS LST product based on thermal infrared data will only be available in clear sky conditions. Microwave techniques have the great advantage of having an all-weather capability. McFarland et al. [1990] derived surface temperature over crop/range, moist soils, and dry soils areas in the Central Plains of the United States from the DMSP Special Sensor Microwave/Imager (SSM/I) data. A regression analysis among all of the SSM/I channels and minimum screen air temperatures (representing the surface temperatures assumed) showed correlations with root mean-square errors of approximately 3 °C. They also determined that snow-surface temperature retrieval is very difficult, if not impossible, because snow emissivity varies with depth, density, and grain size, and that land surfaces with large areas of water present, such as lakes and flooded soils, also present problems because of the integrated influence of the much lower brightness temperatures and higher polarization differences for water. Moreover, the presence of falling rain masks the radiation emitted from the surface. Microwave remote sensing has been better used to retrieve soil moisture [Schmugge et al., 1986; Jackson and Schmugge, 1986; Wigeron et al., 1993] because of the large contrast between the dielectric constant of water (≈ 80) and that of dry soil (3.5). In the microwave range, soil emissivities vary from 0.6 for the wet soil (≈ 30% volumetric soil moisture) to 0.9 for the dry soil (≈ 8%) [Jackson and O'Neill, 1987]. As indicated by Ulaby et al. [1986], although satellite-borne microwave radiometers have been providing information about atmospheric and oceanic parameters for several years, they have not provided land parameters, with the exception of snow monitoring, because 1) the spatial resolution of the satellite radiometers flown to date is more compatible with the dimensions associated with the spatial variations of most atmospheric and oceanic parameters than with those of most land parameters and 2) the mechanisms responsible for microwave emission from land surfaces and volumes are not well understood, in part because land targets generally have complicated dielectric and geometric properties. Because of much higher variations in the surface emissivities of land surfaces in the microwave range and the dependence of microwave brightness temperatures on surface roughness and structures, it is not possible to retrieve global land-surface temperature at an accuracy of 1-2 °K by the use of microwave techniques alone. In order to meet the requirement for LST in climate, hydrologic, ecological and biogeochemical studies in both clear-sky and cloudy conditions, a close synergism of MODIS LST with the National Meteorological Center's (NMC) model forecasts [White et al., 1993] may be a feasible solution. MODIS LST can be used as an input to update the NMC model over areas under clear-sky conditions and the NMC model provides forecasts of LST values for areas under cloudy atmospheric conditions. Comparisons of NCAR (National Center for Atmospheric Research) climate models with land-surface temperature data have provided valuable information for making modifications in the optical properties of clouds in the solar and longwave radiative transfer parameterization [Hahmann et al., 1995] and improvements to the model surface-layer parameterization [Betts et al., 1996]. In the EOS program, MODIS LST will be used as input to the 4-D atmosphere-ocean-land Data Assimilation Office (DAO) system and the NCAR Community Climate Model version 2 (CCM2) [Jin et al., 1996].

2.3. Instrument Characteristics

In order to understand the entire Earth system better on the global scale, the Earth Observing System will provide surface kinetic temperatures at specified accuracies of 0.3 °K for oceans and 1 °K over land, respectively. The international Tropical Ocean Global Atmosphere (TOGA) program has specified the sea surface temperature (SST) accuracy of 0.3 °K as a requirement for global numerical models of climate. Compared to the accuracy of approximately 0.7 °K achieved by the AVHRR instruments on the NOAA satellites [McClain et al., 1985; Barton et al., 1989], these accuracies specified for SST and LST in EOS represent great improvements in the sensor design and algorithm developments. MODIS is an instrument

that will serve as the keystone instrument for global studies of atmosphere, land, and ocean processes [Salomonson et al., 1989]. It scans ±55° from nadir. It has 36 bands with bands 1-19 and band 26 in the visible and near infrared range, and remainder bands in the thermal range from 3 to 15 μm. It will provide daylight reflection and day/night emission spectral imaging of any point on the Earth every 1-2 days. It uses 12 bits for quantization in all bands. The specifications of the EOS MODIS bands are shown in Table I.

The thermal infrared bands have an IFOV of approximately 1km at nadir. The MODIS instrument will view cold space and a full-aperture blackbody before and after viewing the Earth scene in order to achieve the calibration accuracy specification better than 1% absolute for thermal infrared bands (0.75% for band 20; 0.5% for bands 31 and 32). MODIS is particularly useful for the LST product because of its global coverage, radiometric resolution and dynamic ranges for a variety of land cover types, and high calibration accuracy in multiple thermal infrared bands designed for retrievals of SST, LST and atmospheric properties. Specifically, band 26 will be used for cirrus detection [Gao and Kaufman, 1995], thermal infrared bands 20, 22, 23, 29, 31-33 for correcting atmospheric effects and retrieving surface emissivity and temperature. Multiple bands in the medium wave infrared range will provide for the first time a good opportunity to make accurate corrections of the solar radiation effects so that the solar radiation can be used as a TIR source for the purpose of retrieving surface emissivity in the medium wave infrared range in the day/night MODIS LST method.

The MODIS Critical Design Review went well in January 1994. All TIR bands except band 36 are within sensitivity specifications. Its Engineering Model has been completed and tested in 1995. The spectral response functions measured from the MODIS Engineering Model have been used in the development of MODIS LST algorithms.

There are two more EOS sensors [Asrar and Greenstone, 1995], that can be used to retrieve the surface temperature. One is the ASTER on board the first EOS AM platform. It has five thermal infrared channels between 8 and 12 μm with 90-m resolution. Another is the Atmospheric Infrared Sounder (AIRS) on board the first EOS PM platform. The AIRS's high spectral resolution data will be used to retrieve atmospheric and surface parameters including surface temperature and emissivity at a horizontal spatial resolution of 13.5km at nadir [Susskind and Chahine, 1993].

3. Algorithm Description

3.1. Theoretical Description

A fundamental theoretical description for the LST algorithm development is given briefly in the following [Wan and Dozier, 1989].

Emitted spectral radiance L at wavelength λ from a surface at thermodynamic temperature T_s is given by multiplying the Planck function by spectral emissivity $\varepsilon(\lambda)$

$$L(\lambda, T) = \varepsilon(\lambda)\, B(\lambda, T_s) \ . \tag{1}$$

In general, azimuthally dependent radiance in an absorbing, emitting, and scattering layer is governed by the monochromatic radiative transfer equation

$$\mu \frac{dL(\tau, \vec{\Omega})}{d\tau} + L(\tau, \vec{\Omega}) = J(\tau, \vec{\Omega}) \ , \tag{2}$$

τ is optical depth, and $L(\tau, \vec{\Omega})$ is the radiance at level τ along direction $\vec{\Omega}$, which is composed of zenith angle $\arccos\mu$ and azimuth ϕ. The spectral designation is omitted from the equation for simplicity.

The source function J is

$$J(\tau, \vec{\Omega}) = \frac{\tilde{\omega}}{4\pi} \int_{4\pi} P(\tau, \vec{\Omega}; \vec{\Omega}') L(\tau, \vec{\Omega}) \, d\Omega' + Q(\tau, \vec{\Omega}) \ , \tag{3}$$

here $P(\tau, \vec{\Omega}; \vec{\Omega}')$ is the scattering phase function.

The Q term in (3) represents internal sources. By separating direct radiation from diffuse radiation, it is convenient to consider the radiation scattered from the direct beam or the specularly reflected direct beam as caused by some internal pseudo-source. Then the total internal source is

$$Q(\tau, \vec{\Omega}) = Q_t(\tau, \vec{\Omega}) + Q_s(\tau, \vec{\Omega}) + Q_{sp}(\tau, \vec{\Omega}) \ , \tag{4}$$

Q_t is the thermal source, and Q_s and Q_{sp} are the direct and specular pseudo-sources.

By applying the interaction principle [Grant and Hunt, 1969] and the doubling/adding method [Wiscombe 1976], a matrix form of this integro-differential radiative transfer equation can be applied to a vertically inhomogeneous, multi-layer atmosphere [Li et al., 1987]. The top and bottom boundary conditions that need to be satisfied are that $L^{\downarrow}(0)$ must be specified (usually zero) and

$$L^{\uparrow}(\tau_0) = R_g \, L^{\downarrow}(\tau_0) + \vec{\varepsilon} B(T_s) \ + \mu_0 \, E_0 \ e^{-\tau_0/\mu_0} \, f_r(\mu_0) \ . \tag{5}$$

Radiances $L^{\downarrow\uparrow}$ are vectors of $m \times n$ elements on a discrete angular space composed of m zenith and n azimuth angles. R_g is the surface diffuse reflection matrix, T_s is the temperature of the surface, $f_r(\mu_0)$ is the surface BRDF vector to the direct beam, and $\vec{\varepsilon}$ is the emissivity vector.

The directional emissivity and BRDF f_r are related by Kirchhoff's law.

$$\varepsilon(\mu) = 1 - \int_0^{2\pi} \int_0^1 \mu' \, f_r(\mu; \mu', \phi') \, d\mu' \, d\phi' \ . \tag{6}$$

Numerical results obtained by the use of the doubling/adding method have been compared with and validated by results obtained by the use of discrete-ordinate method [Stamnes and Conklin, 1984]. The doubling/adding method is used in our radiative transfer simulations because of its advantages in easy implementation of surface interfaces, such as the air-water interface and interfaces for specular reflectance or bidirectional reflectance, and in efficiently getting solutions for multiple boundary conditions.

As described thus far, the model is for the monochromatic case only. For the model to work for the atmosphere, we need to know the atmospheric optical properties. Among them the most important are optical thickness τ_0, single scattering albedo $\tilde{\omega}$, and the scattering phase function P which depend on atmospheric profiles (temperature, pressure, water vapor, ozone, and aerosol density distributions). LOWTRAN7 [Kneizys et al., 1988] and MODTRAN [Berk et al., 1989] provide absorption band absorption coefficients for calculations of atmospheric molecular transmission functions averaged within wavenumber interval $5\,\mathrm{cm}^{-1}$ and $1\,\mathrm{cm}^{-1}$, respectively. They are not monochromatic transmittance. This averaging causes violation of the Lambert-Bouguer-Beer law because of the complexity of molecular band absorption even in a narrow wavenumber interval. A solution to this problem is to expand radiative transmission functions calculated from LOWTRAN or MODTRAN by the use of exponential-sum fitting [Wiscombe and Evans, 1977]. The monochromatic radiative transfer model is applied separately to each term in the exponential-sum expansion, and the results are then summed. So described atmospheric radiative transfer model will be referred as ATRAD-LOW or ATRAD-MOD, depending on the exponential-sum

tables derived from LOWTRAN or MODTRAN transmission functions. By solving the radiative transfer equation over the whole wavelength range of a thermal band of a satellite sensor, we get the angular distribution of average spectral radiance.

$$\overline{L^{\uparrow}} = \frac{\int_{\lambda_1}^{\lambda_2} \Psi(\lambda)\, L^{\uparrow}(\lambda, 0)\, d\lambda}{\int_{\lambda_1}^{\lambda_2} \Psi(\lambda)\, d\lambda}\ , \tag{7}$$

$L^{\uparrow}(\lambda, 0)$ is the vector of upward spectral radiances at the top of the atmosphere and Ψ is the sensor response function, for the wavelength band whose lower and upper boundaries are $[\lambda_1, \lambda_2]$.

From the theoretical point of view, the success of the LST algorithm depends on 1) accurately accounting for the atmospheric effects; 2) accurately accounting for the surface emissivity effects; and 3) the quality of TIR data including the stability of the spectral response function, signal-to-noise ratio, radiometric resolution, and calibration accuracy.

3.1.1. Physics of Problem

In clear-sky conditions, the spectral infrared radiance $L(\lambda, \mu)$ at the top of the atmosphere is composed of surface thermal emittance, thermal path radiance $L_a(\lambda, \mu)$, path radiance resulting from scattering of solar radiation $L_s(\lambda, \mu, \mu_0, \phi_0)$, solar beam and solar diffuse radiation and atmospheric thermal radiation reflected by the surface,

$$\begin{aligned} L(\lambda, \mu) = {} & t_1(\lambda, \mu)\, \varepsilon(\lambda, \mu)\, B(\lambda, T_s) + L_a(\lambda, \mu) + L_s(\lambda, \mu, \mu_0, \phi_0) + t_2(\lambda, \mu, \mu_0)\, \mu_0\, E_0(\lambda)\, f_r(\mu; \mu_0, \phi_0) \\ & + \int_0^{2\pi} \int_0^{1} \mu'\, f_r(\mu; \mu', \phi')\, [t_3(\lambda, \mu)\, L_d(\lambda, -\mu', \phi') + t_4(\lambda, \mu)\, L_t(\lambda, -\mu', \phi')]\, d\mu'\, d\phi'\ , \end{aligned} \tag{8}$$

where μ is cosine of the viewing zenith angle, $\varepsilon(\lambda, \mu)$ is the surface spectral emissivity, $B(\lambda, T_s)$ is the radiance emitted by a blackbody at surface temperature T_s, $E_0(\lambda)$ is the spectral solar irradiance incident on the top of atmosphere (normal to the beam), μ_0 is cosine of the solar zenith angle, ϕ_0 is the relative azimuth between viewing direction and the solar beam direction, $f_r(\mu; \mu', \phi')$ is the BRDF function, $L_d(\lambda, -\mu', \phi')$ is downward solar diffuse radiance, $L_t(\lambda, -\mu', \phi')$ is atmospheric downward thermal radiance, their incident direction is represented by $-\mu'$ and ϕ', and $t_i(\,)$, $i = 1, \ldots, 4$ are transmission functions for the corresponding terms.

The wavelength, λ, in (8) is the wavelength center of a narrow wavelength interval because there is no way to measure the exact monochromatic signal as a continuous function of wavelength by satellite sensors. Equation (8) is the form used in the thermal infrared range 8-14 μm [Wan and Dozier, 1990] generalized into a wider wavelength range of 3-14μm. It requires complete calculations of the atmospheric radiative transfer to determine the values of all terms on the right-hand side. After the zenith and azimuth dependent radiance at any level from the Earth's surface to the top of the atmosphere (TOA) is provided by accurate atmospheric radiative transfer simulations, the TOA radiance can be represented by its components in the form of (8). Its special form has been used for a long time in many atmospheric radiation models including LOWTRAN [Kneizys et al., 1983], MODTRAN [Berk et al., 1987], and MOSART [Cornette et al., 1994] models. In the special form, $t_3(\lambda, \mu) = t_1(\lambda, \mu)$ and $t_4(\lambda, \mu) = t_1(\lambda, \mu)$ are assumed.

TABLE I. Specifications of the EOS MODIS bands.

band	bandwidth (nm)	IFOV	primary use	band	bandwidth (μm)	IFOV	$NE\Delta T$ (°K)	primary use
1	620- 670	250m	L	20	3.660-3.840	1km	0.05	O, L
2	841- 876	250m	A, L	21	3.929-3.989	1km		fire, volcano
3	459- 479	500m	L	22	3.929-3.989	1km	0.07	A, L
4	545- 565	500m	L	23	4.020-4.080	1km	0.07	A, L
5	1230-1250	500m	L	24	4.433-4.498	1km	0.25	A
6	1628-1652	500m	A, L	25	4.482-4.549	1km	0.25	A
7	2105-2155	500m	A, L	27	6.535-6.895	1km	0.25	A
8	405- 420	1km	O	28	7.175-7.475	1km	0.25	A
9	438- 448	1km	O	29	8.400-8.700	1km	0.05	L
10	483- 493	1km	O	30	9.580-9.880	1km	0.25	ozone
11	526- 536	1km	O	31	10.780-11.280	1km	0.05	A, L
12	546- 556	1km	O	32	11.770-12.270	1km	0.05	A, L
13	662- 672	1km	O	33	13.185-13.485	1km	0.25	A, L
14	673- 683	1km	O	34	13.485-13.785	1km	0.25	A
15	743- 753	1km	O	35	13.785-14.085	1km	0.25	A
16	862- 877	1km	O	36	14.085-14.385	1km	0.35	A
17	890- 920	1km	A					
18	931- 941	1km	A					
19	915- 965	1km	A					
26	1360-1390	1km	cirrus					

Note: A - atmospheric studies; L - land studies; O - ocean studies.

Ref: MODIS Level 1B Algorithm Theoretical Basis Document, 1995, NASA/GSFC, Greenbelt, MD.

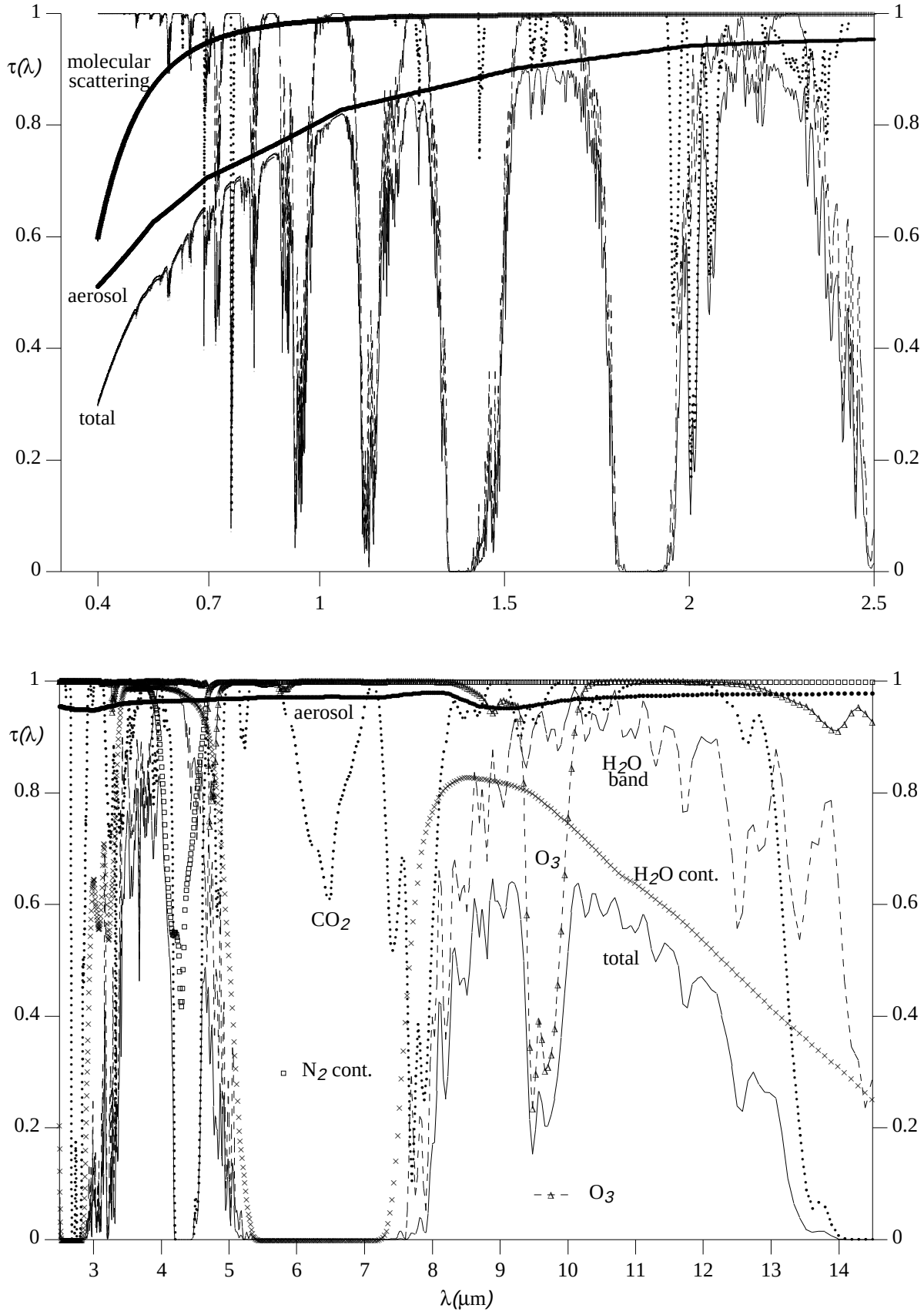

Figure 1, Atmospheric transmissions at view angle 45° in mid-latitude summer condition (cwv = 2.9cm, vis. = 23km).

In order to retrieve surface emissivity and temperature from (8), we need to use suitable TIR bands. According to the MODIS band specifications in Table I and the atmospheric transmission at viewing angle 45° from nadir in mid-latitude summer condition (column water vapor, cwv = 2.9cm; surface visibility at 0.55μm, vis = 23km) in Fig. 1, bands 20, 22, and 23 are in the transparent atmospheric window in the medium wavelength range 3.5-4.2 μm, bands 29-32 are in the atmospheric window range 8-13 μm, while band 33 is just on the edge of this atmospheric window. Band 30 is strongly affected by ozone absorption, so using this band does not help the retrieval of surface temperature. As shown in Fig. 1, major absorbers in bands 20, 22, and 23 are CO_2, N_2, and water vapor. Major absorbers in bands 29, and 31-33 are water vapor and CO_2. The transmission corresponding to aerosol scattering and absorption in these bands is approximately 0.95-0.98. So using average aerosol distribution in atmospheric radiative transfer is usually good enough unless volcano eruptions strongly change the aerosol distribution. Because CO_2 and O_2 mixing ratios are almost constant, their densities are determined by atmospheric pressure and temperature. Water vapor is the most variable absorber in the Earth's atmosphere. Therefore, if we know atmospheric water vapor and temperature profiles, we can calculate all atmospheric terms in the above equation to a quite high accuracy, which is limited mainly by the accuracy of the coefficients of the water vapor continuum and band absorptions. The MODIS sounding channels can be used to retrieve atmospheric temperature and water vapor profiles [Smith et al, 1985; Menzel and Purdom, 1994]. But retrieving atmospheric profiles needs the knowledge of surface emissivity in order to separate the surface contribution from the sounding data. Therefore, the quality of retrieved profiles might not be very good in areas for which surface emissivities are highly variable such as in semi-arid and arid areas. Although the absolute values of the retrieved profiles are not accurate, the shapes of the atmospheric temperature and water vapor profiles may be reasonably well obtained. Radiative transfer simulations show that the radiance at the top of the atmosphere, in MODIS TIR bands 20, 22, 23, 29, 31-33, is almost not affected by changing atmospheric temperature and water vapor profiles above 9km elevation. If the shapes of temperature and water vapor profiles in the lower troposphere can be accurately retrieved from the MODIS sounding data, we can use two variables to describe the atmospheric variations. One is the amount of shift in the temperature profile up to 9km elevation. Another is the scale factor for the water vapor profile so that we can determine the column water vapor with the shape and the scale factor. Then we use the atmospheric temperature at the surface level, T_a, as the representative variable of the tropospheric temperature profile. Similarly, we can use the column water vapor (cwv) as the representative for the water vapor profile. Alternatively, we can consider it as the first order of approximation to describe the atmospheric condition by the use of these two variables.

In order to make practical use of multi-temporal and multi-channel data, we need to simplify (8) by the use of some realistic assumptions about the surface optical properties. We assume: 1) The surface emissivity changes with vegetation coverage and surface moisture content, but it does not significantly change in several days unless dew, rain and/or snow occurs during the short period of time particularly for bare soils in arid and semi-arid environments, for which the surface of the ground is dry most of time [Kerr et al., 1992]. We will consider the dew effect in section 3.1.2.3 because dew may occur in clear-sky conditions. 2) There are quite strong spectral variations in surface reflectance for most terrestrial materials in the medium wavelength range 3.5-4.2μm [Salisbury and D'Aria, 1994] but their BRDF anisotropic factor in this wavelength range has very small variations (≈ 2%) [Snyder and Wan, 1996(b); Snyder et al., 1996(d)]. So it seems appropriate to assume that a single BRDF anisotropic factor can be used for the surface-reflected solar beam in MODIS bands 20, 22 and 23 located in this wavelength range. This anisotropic factor is defined by the ratio of the surface-reflected solar beam at the view direction of the MODIS sensor to the radiance that would have resulted if the surface reflected isotropically (such a surface is called a Lambertian surface),

$$\alpha_r = \frac{\pi f_r(\mu; \mu_0, \phi_0)}{r} \quad , \tag{9}$$

where r is reflectance of the assumed Lambertian surface. 3) Atmospheric radiative transfer simulations show that in clear-sky conditions the surface-reflected diffuse solar irradiance term is much smaller than the surface-reflected solar beam term in the thermal infrared range, and the surface-reflected atmospheric downward thermal irradiance term is smaller than surface thermal emission. So the Lambertian approximation of the surface reflection does not introduce a significant error in thermal infrared region 3-14 μm. Then we can replace the BRDF function $f_r(\mu, \mu', \phi')$ in (8) with r/π and link it to the surface emissivity ε by $r = 1 - \varepsilon$ according to the Kirchhoff's law.

It is important to point out that in (8) we separate the surface-reflected solar beam term from its irradiance term (the integral of the downward solar diffuse radiance) because the change of solar zenith angle has different effects on these two terms. As the solar zenith angle increases, the solar beam at the surface level decreases, but the downward solar diffuse irradiance may increase in some situations. If the solar beam is included in the total solar irradiance incident on a surface and surface reflectance (also called as hemispherical reflectance or albedo in the visible and near-infrared range) is defined as the ratio of the total solar radiance reflected from the surface to the total solar irradiance, the surface reflectance will be dominated by the BRDF of the solar beam and therefore the reflectance depends on the solar zenith angle significantly [Schaaf and Strahler, 1993]. After the solar beam is separated from the total downward solar irradiance, we can use the BRDF anisotropic factor to calculate the surface-reflected solar beam and use the surface reflectance to calculate the surface-reflected solar downward irradiance. In this way, the solar angle and viewing angle dependences in the surface reflectance will be smaller so that we can assume the surface as a Lambertian surface.

Based on above assumptions, the radiance measured in MODIS band j can be expressed as

$$L(j) = t_1(j)\,\varepsilon(j)\,\mathrm{B}_j(T_s) + L_a(j) + L_s(j) + \frac{1-\varepsilon(j)}{\pi}\left[t_2(j)\,\alpha_r\,\mu_0\,E_0(j) + t_3(j)\,E_d(j) + t_4(j)\,E_t(j)\right], \tag{10}$$

where all terms are band-averaged, $\varepsilon(j)$ is the band emissivity which will be discussed later, similarly for $\mathrm{B}_j(T_s)$, $L_a(j)$, $L_s(j)$, and $E_0(j)$. $E_d(j)$ and $E_t(j)$ are the band-averaged solar diffuse irradiance and atmospheric downward thermal irradiance at surface. And $t_i(j)$, $i = 1, .., 4$ are the band effective transmission functions weighted by the band response function and the corresponding radiance and irradiance terms. Note that we have neglected the in-band spectral variation of the surface emissivity in reducing (8) into (10), and omitted symbols of view angle and solar angle for most terms in the above equation. On the right-hand side of this equation, $\varepsilon(j)$, α_r, and $\mathrm{B}_j(T_s)$ depend on surface properties and conditions, all other terms depend on atmospheric water vapor and temperature profiles, solar angle and viewing angle. These terms can be given by numerical simulations of atmospheric radiative transfer. The spectral response functions measured from the Engineering Model of the MODIS instrument have been used as weights in calculations of band averages of these terms.

It is important to point out that in (10) t_3 and t_4 may differ from t_1 by several percent. This is also true in simulation results from the MODTRAN code, which assumes these three transmission functions to be equal at wavenumber interval 1 cm^{-1}. So errors will be introduced by replacing these three band transmission functions with a single transmission when the band emissivity is significantly less than 1. In a wide range of column water vapor in the clear-sky tropical atmosphere from very dry to very wet conditions, replacing t_3 and t_4 with t_1 in (10) causes an error of 0.7-1.9 °K in surface temperature T_s estimated from band radiance of MODIS band 29 if band emissivity ε(29) is 0.75 and T_s is close to the surface air temperature. The corresponding errors in cases of MODIS bands 31 and 32 are 0.4-0.8 °K and 0.4-1.3 °K, respectively. The physical meaning in these different transmission functions is the wavelength-dependent selective effect of the molecular band absorption. We need to consider the wavelength-dependence in radiation sources as well. It is easy to understand if

we imagine a single band as a series of conjunctive narrow intervals and use multiple terms to represent the molecular band absorption. For atmospheric radiation, the downward irradiance is strongest where molecular band absorption is large, but the band transmission for these wavelengths is lowest so radiance reflected by the surface that reaches the top of the atmosphere has a lower value. For the solar radiation, only those wavelengths where the atmospheric molecular band absorption is low will reach the surface, but the band transmission for these wavelengths is high so the radiance reflected by the surface that reaches the top of the atmosphere will be relatively large. This example clearly show the importance of an accurate radiative transfer model in the development of LST algorithms.

In emissive measurements, the band average emissivity is defined by

$$\bar{\varepsilon} = \frac{\int_{\lambda_1}^{\lambda_2} \Psi(\lambda)\,\varepsilon(\lambda)\,B(\lambda, T)\,d\lambda}{\int_{\lambda_1}^{\lambda_2} \Psi(\lambda) B(\lambda, T)\,d\lambda}, \tag{11}$$

which is a function of the surface temperature. But in the Earth surface environment, this temperature-dependence is usually very small. In an extreme example of coarse sands, the spectral emissivity increases by approximately 0.2 from the lower end to the upper end in AVHRR channel 3 at 3.75 μm, its band average emissivity changes only 0.004 as the temperature changes from 240 °K to 320 °K. But the temperature dependence in band average emissivity becomes larger for pixels mixed with two or more components that may have different emissivities and temperatures [Wan and Dozier, 1996]. If the emissive measurements are made from a far distance, the atmospheric transmission should be also included in (11) as a weight function. However, the band emissivity calculated from laboratory reflectance spectra of a pure material

$$\bar{\varepsilon} = \frac{\int_{\lambda_1}^{\lambda_2} \Psi(\lambda)\,\varepsilon(\lambda)\,d\lambda}{\int_{\lambda_1}^{\lambda_2} \Psi(\lambda)\,d\lambda}, \tag{11'}$$

is independent of the surface temperature. We used this band emissivity in our simulations.

From the point of view of satellite remote sensing, the land surface is the top layer of the interface or biosphere between the lower boundary of the atmosphere and the solid Earth. In the thermal infrared region, the thickness of this top layer is within a few millimeters. Our measurements show that the transmittance of thermal infrared radiation is smaller than 10% for a single thin leaf and is close to zero for a single thick leaf. The entire Earth's land surface consists of evergreen forest and shrubs, deciduous forest and shrubs, crop and grass lands, inland water bodies, snow/ice cover, barren lands of exposed soil, sands and rocks, and urban areas.

3.1.1.1. Generalized Split-window LST Algorithm

Despite all these variations in the surface emissivity described in section 2.2, there is evidence showing relatively stable spectral emissivity characteristics for terrestrial land cover types in the wavelength range 10.5-12.5μm, where MODIS bands 31 and 32 are located. And spectral contrast in surface emissivities usually decreases with aggregation as spatial scale increases. Salisbury and D'Aria [1992] published spectral reflectance data of 80 terrestrial material samples including igneous, metamorphic, and sedimentary fresh rocks; varnished rock surfaces, lichen-covered sandstone, soil samples, green foliage, senescent foliage, water, ice, and water surfaces with suspended quartz sediment and oil slicks, as shown in Table II.

The band average emissivities in seven MODIS bands and two MODIS bands (bands 31 and 32) calculated from these reflectance spectra are shown in Fig. 2. The solid line represents the grey body relation $\varepsilon_{31} = \varepsilon_{32}$ and the upper and lower dashed lines represent $\varepsilon_{32} - \varepsilon_{31} = 0.023$ and $\varepsilon_{32} - \varepsilon_{31} = -0.012$, respectively. We can gain the following insights into the band average emissivities of terrestrial materials: 1) all ε_{31} and ε_{32} are larger than 0.825; 2) a general relation $-0.012 \le \varepsilon_{32} - \varepsilon_{31} \le 0.023$ holds for all samples except fresh rocks, distilled water smooth ice, and senescent beech foliage; and a narrower specific relation could be developed for fresh foliage samples, senescent foliage samples, soil samples, varnished and lichen-covered rock samples, and water and ice samples; 3) all ε_{31} and ε_{32} are larger than 0.91 for fresh foliage samples, soil samples, varnished and lichen-covered rock samples, and water and ice samples. Further, Salisbury and D'Aria [1992] also indicate that multiple scattering within the canopy of radiation emitted primarily by leaves will have its spectral contrast reduced. Vertical-leaf canopies tend to have higher emissivities than horizontal-leaf canopies [Norman et al., 1990]. Because of volumetric effects, the emissivities of typical tree, bush, and grass are quite close to unity. This is supported by our recent measurements and simulations with modified BRDF kernel models [Snyder and Wan, 1996(a)]. From these measurements and simulations, a constant emissivity approximation of 0.97-0.99 in MODIS band 32 appears quite good for all natural land cover types except exposed rocks and sands. Although more field measurements are needed to confirm this approximation, it indicates that the band emissivities in MODIS bands 31 and 32 are relatively stable and known within approximately 0.01 for dense evergreen canopies, lake surface, snow and ice, and most soils. Because their band emissivities are very close to the emissivities of water, the effects of dew and rain are small.

A view-angle dependent split-window LST method has been developed [Wan and Dozier, 1996] for correcting atmospheric and emissivity effects for land cover types with known band emissivities. In the development of this generalized split-window LST algorithm, a database for MODIS atmospheric thermal radiance values in bands 31 and 32 has been established from accurate atmospheric radiative transfer simulations for 12 atmospheric temperature profiles, which cover the range of surface air temperatures, T_{air}, from 256 °K to 310 °K (it will be extended to 240-325 °K in the near future). The water vapor profile was scaled from the near saturated level down to 5% of the saturated level for each temperature profile. The land-surface temperature, T_s, ranges from $T_{air} - 16$ °K to $T_{air} + 16$ °K, and the surface emissivity ranges from 0.8 to 1.0 for each atmospheric temperature profile. Based on this simulated database, a look-up table and interpolation scheme has also been developed with an accuracy better than 0.05 °K, the specification for the MODIS noise equivalent differential temperature (NEΔT). Comprehensive error analysis has been made in wide ranges of atmospheric and surface conditions. In most cases, the accuracy of the generalized multi-channel LST algorithm is better than 1 °K for land cover types with known emissivities by optimization of its parameters for viewing angle and column water vapor ranges. MODIS products of land-cover, snow, and vegetation index will be used to infer band average emissivities of land-surface pixels. If the pixel is of dense evergreen canopy, lake surface, ice/snow cover, the corresponding values of the band average emissivities of MODIS bands 31 and 32 in the emissivity knowledge base will be used as inputs to the generalized split-window LST algorithm.

The success of the generalized split-window LST algorithm depends on our knowledge of the band emissivities ε_{31} and ε_{32} for the real land surfaces. We cannot simply apply the emissivities of single leaves measured with an integrating sphere to a scene pixel of vegetation canopy. Simulations indicate that with leaf component emissivities ranging from to 0.90 to 1.0, the canopy emissivity ranges from 0.96 to 1.0 [Olioso, 1995]. Field measurements of the true spectral emissivities of prarie grasses show an emissivity of 0.99 ± 0.01 [Palluconi et al., 1990]. We have developed modified kernel models [Snyder and Wan, 1996(a)], that calculate the BRDF, reflectance, and emissivity of a scene pixel from small-scale component measurements, land cover classification and NDVI (normalized difference vegetation index). We measured structured leaves of 13 different species, their mean emissivities in MODIS bands 31 and 32 are 0.989 and 0.988 with standard deviations of 0.005 and 0.004, as shown in Table III. We have also developed a sun-shadow method [Wan et al., 1996],

which can measure spectral emissivity of a canopy with a spot size of approximately 50cm so that the effects of surface structure and roughness may be included.

TABLE II. List of terrestrial material samples used in LST simulations.

sample no.	sample name	type of material	sample no.	sample name	type of material
1	basalt.f	fresh rough surface	41	0135	soil (Entisols)
2	basalt.v	desert vanish coated rock	42	0145	soil (Ultisols)
3	ijolite.f	fresh rough surface	43	0211	soil (Molisols)
4	ijolite.v	desert vanish coated rock	44	0219	soil (Alfisols)
5	rhyolite.f	fresh rough surface	45	0226	soil (Inceptisols)
6	rhyolite.v	desert vanish coated rock	46	0475	soil (Vertisols)
7	crustose.10	lichens coated rock	47	1530	soil (Aridisols)
8	crustose.65	lichens coated rock	48	4717	soil (Oxisols)
9	basalt.h7	igneous rock	49	foliose.1	veg., lichens
10	dunite.h1	igneous rock	50	indiangr.ass	veg., green foliage
11	granite.h1	igneous rock	51	redoak	veg., green foliage
12	syenite.h1	igneous rock	52	white.ine	veg., green foliage
13	greywack.eh1	sedimentary rock	53	senbeech	veg., senescent foliage
14	limeston.eh1	sedimentary rock	54	senpine	veg., senescent foliage
15	limeston.eh2	sedimentary rock	55	senredoa.kh1	veg., senescent foliage
16	limeston.eh3	sedimentary rock	56	senryegr.ass	veg., senescent foliage
17	sandton.eh1	sedimentary rock	57	oakbark.1	veg., tree bark
18	sandton.eh2	sedimentary rock	58	pinebark.1	veg., tree bark
19	sandton.eh4	sedimentary rock	59	ypoplarb.ark	veg., senescent foliage
20	shale.h3	sedimentary rock	60	conifer.ous	veg. decomposing litter
21	shale.h5	sedimentary rock	61	decidu.ous	veg. decomposing litter
22	shale.h6	sedimentary rock	62	wood	veg. decomposing litter
23	siltston.eh1	sedimentary rock	63	seawater	water
24	siltston.eh2	sedimentary rock	64	distwa.ter	water
25	gneiss.h1a	metamorphic rock	65	distice1.00g	ice
26	gneiss.h3a	metamorphic rock	66	distices.moo	ice
27	gneiss.h4	metamorphic rock	67	seaice.10.ogr	ice
28	marble.h2	metamorphic rock	68	seaicesm.oot	ice
29	marble.h3	metamorphic rock	69	qtzwater.23	suspended sediments
30	marble.h4	metamorphic rock	70	qtzwater.64	suspended sediments
31	quartzit.eh1	metamorphic rock	71	qtzwater.7	suspended sediments
32	quartzit.eh4	metamorphic rock	72	foam	water coatings
33	quartzit.eh6	metamorphic rock	73	oil15465	water coatings
34	schist.h3a	metamorphic rock	74	oil34792	water coatings
35	schist.h6a	metamorphic rock	75	oil39076	water coatings
36	schist.h7	metamorphic rock	76	oil42667	water coatings
37	slate.h1a	metamorphic rock	77	soilfl.oat	water coatings
38	slate.h2a	metamorphic rock	78	qtzfloat	water coatings
39	slate.h3	metamorphic rock	79	oil35473	water coatings
40	0127	soil (Spodosols)	80	qtz.hem	quartz

TABLE III. Band-averaged emissivities of 13 structured leaves in MODIS bands 31 and 32.

species	ε_{31}	ε_{32}
Algerian ivy	0.993	0.992
magnolia	0.993	0.991
coral	0.997	0.993
laurel	0.989	0.988
Indian laurel	0.984	0.984
Indian hawthorn	0.989	0.988
bird paradise	0.992	0.992
cedar	0.983	0.982
cypress	0.988	0.988
spruce	0.991	0.990
pine	0.986	0.987
fire thorn	0.980	0.979
sod grass	0.992	0.992
mean	0.989	0.988
standard deviation	0.005	0.004

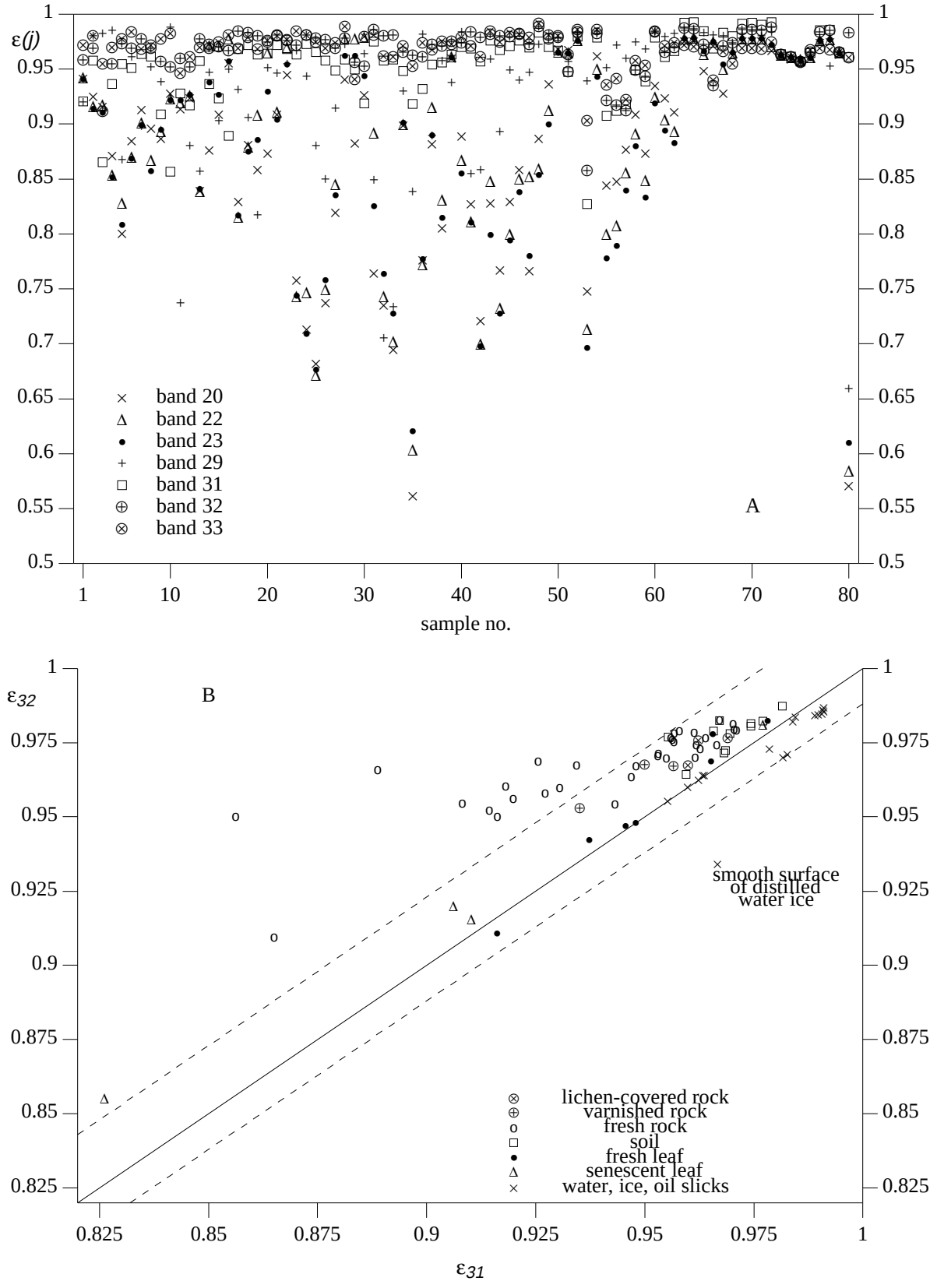

Figure 2. Averaged emissivities of terrestrial materials in seven MODIS bands (A) and in bands 31 and 32 (B).

3.1.1.2. Day/Night LST Algorithm

For land cover types with variable and unknown emissivities, obviously there is insufficient information (mathematically under-determined) to retrieve surface temperature and band-averaged emissivities from a one-time measurement of N thermal infrared channels even when atmospheric temperature and humidity profiles are known exactly, because there are N + 1 unknowns (N band emissivities plus surface temperature). Several methods have been proposed to reduce the number of unknowns, for example, emissivity-ratio method [Watson et al., 1990], two-temperature method [Watson, 1992], and the temperature-emissivity separation (TES) method used by the EOS ASTER team. In the emissivity-ratio method, the atmospheric condition is assumed temporally invariant or spatially invariant. In general, these assumptions are not valid, especially for atmospheric conditions over land. Our experience from AVHRR, HIRS/2 data, and MAS data indicates that it is difficult to verify the horizontal homogeneity of the atmosphere. Jedlovec [1990] indicated that column water vapor may vary significantly at the mesoscale (5-10km). The basic assumption in the two-temperature method and the band-differential method proposed in version 2.2 of the LST ATBD is that the differences in band radiances are caused by the surface temperature change and nothing else. This may be true for sea surface for which the vertical component of the circulation may bring colder water to the surface making the sea surface temperature different by several degrees kelvin at different locations under horizontally homogeneous atmospheric conditions. But it is not easy to explain how similar phenomena could happen to land surface in general situations. The two-temperature method is also very sensitive to the system signal-to-noise ratio and the residual uncertainty in atmospheric corrections. In the TES method, a statistical relation of the band emissivities is used as a constraint to make the retrieval problem well posed. A good statistical relation between the max-min difference and the minimum band emissivity in MODIS bands 29, 31, and 32 has been determined. We applied the TES method to simulated MODIS data in these three bands. If we know the atmospheric temperature and water vapor profiles exactly, the rms errors in retrieved daytime and nighttime LST values are smaller than 1 °K and relative band emissivities can also be well retrieved. But an error of 10% in column water vapor or an error of 3 °K in the atmospheric temperature profile would increase the rms errors in retrieved LST values by 2 °K. However, the accuracies of relative band emissivities retrieved by this method are less sensitive to the uncertainties in atmospheric temperature and water vapor profiles. We will give more details on the TES simulations in section 3.1.2.3 when we investigate the dew effect. Because the surface emission and the atmospheric effects are always mixed in the thermal infrared signal received by space-borne sensors, retrieving atmospheric temperature and water vapor profiles needs to know the surface emissivity. Without using the true surface emissivity in the profile retrieval processing, the errors in atmospheric temperature and water vapor profiles retrieved from MODIS thermal band data may be much larger over land cover types with unknown variable emissivities. Therefore, we need to use multi-temporal and multi-channel data and consider variations in the atmospheric condition if we want to retrieve surface temperature and emissivity at an acceptable accuracy.

Becker and Li [1993] used TISI values in their AVHRR day/night LST algorithm and indicated that TISI values are not very sensitive to the atmospheric conditions and the variation of surface temperature. MODIS has almost all the channels in AVHRR and HIRS/2 at the same 1km resolution. The MODIS atmospheric sounding channels can be used to estimate atmospheric temperature and water vapor profiles for making atmospheric corrections. But values of the band emissivities are also needed in calculating TISI values. Our error analysis shows that the error in $TISI_{45}$ for AVHRR channels 4 and 5 may be larger than 4% if we do not know that $\varepsilon_4 = 0.89$ and $\varepsilon_5 = 0.96$ so 0.96 is used for both ε_4 and ε_5 in calculating $TISI_{45}$ given column water vapor larger than 4cm. If we want to keep the error in $TISI_{45}$ less than 2%, we have to set 2.25cm as the upper limit for the range of column water vapor over which this method could be used to retrieve band emissivities without its *a priori* knowledge. Because of its multiple bands in the medium wave infrared range, MODIS provides an unique opportunity for the development of a physics-based MODIS day/night LST algorithm [Wan and Li, 1996]. The solar beam

in the spectral range 3.5-4.2 μm can be used as an active source for obtaining the information of surface reflectance so that the surface emissivity and temperature can be retrieved. There is no requirement for using TISIs and *a priori* knowledge of band emissivities, and no limitation to the column water vapor in the MODIS day/night LST algorithm. Based on the knowledge of solar cycle variations in the fraction of the Sun's disc covered with active regions and of their contrasts, it was estimated [Lean, 1991] that in the medium wavelength range (2-5 μm) the variation of the solar irradiance at the top of the atmosphere is well below 0.1%. Therefore, in this spectral region the solar beam at the Earth's surface can be calculated accurately based on the solar angle and the atmospheric conditions.

3.1.2. Mathematical Description of Algorithm

3.1.2.1. Unknown variables in LST problem

In the 3.5-4.2 μm and 8-13 μm atmospheric windows, the atmospheric properties of absorption/emittance and scattering depend, in an approximately decreasing priority, on atmospheric water vapor profile, temperature profile, and other molecular and aerosol profiles. So there are at least one or two unknown variables of the atmosphere in LST determination if atmospheric water vapor and temperature profiles are not available. Now the problem is how to determine the land-surface temperature if we have TIR data in N MODIS bands? In the special case for which the surface can be well approximated by a Lambertian surface and the surface emissivity can be inferred from the type of land cover, the surface temperature is the only unknown variable for the surface. So two or three bands in the 8-13 μm window can be used to correct the atmospheric effects by the use of the differential absorption in the split-window so that LST can be retrieved by the split-window method without explicitly solving the radiative transfer problem. In the general case, there are at least additional N+1 unknowns, including band emissivities and the temperature of the land surface, if it is a Lambertian surface, and even more unknowns for a non-Lambertian surface. So it is an underdetermined problem to simultaneously solve temperature and surface emissivity in N bands solely from a one-time observation of N bands even if we know the exact atmospheric condition. If we use 2 measurements (day and night) in N MODIS TIR bands, we have 2 N observations. Unknown variables include N band emissivities, daytime surface temperature T_{s-day}, nighttime surface temperature $T_{s-night}$, 4 atmospheric variables (T_a and cwv at two times), and the anisotropic factor α_r, totaling N + 7. The number of observations must be equal to or larger than the number of unknowns, $2N \geq N + 7$. So $N \geq 7$. Note that it is necessary to apply independent shapes of atmospheric temperature and water vapor profiles for daytime and nighttime so that temporal variations and temperature inversion (more often at night) could be considered in the LST retrieval. For the MODIS day/night LST algorithm, we use seven bands, i.e., MODIS bands 20, 22, 23, 29, 31-33. According to the experience from the Engineering Model of the MODIS instrument, the NEΔT in band 33 may be reduced from 0.25 °K to 0.12 °K, and it appears to be possible to achieve the goal for absolute calibration accuracy, 0.5-0.75%, for these seven TIR bands. It seems that we can get unique solutions for the above 14 unknowns by the use of 14 observations. But it is not the case because: 1) the atmospheric profile is a continuous function of height and there are only a finite number of MODIS sounding bands so that the atmospheric temperature and water vapor profiles can be retrieved only at a finite number of levels, 2) there are always uncertainties in the retrieved atmospheric profiles and even in their shapes, 3) there is always instrument noise in the measurement data, 4) there are uncertainties in the atmospheric optical properties including water vapor absorption coefficients that we used in the development of LST algorithms. Therefore all we can do is to use the best combination of available bands and use an appropriate method to obtain the best estimates of the unknown variables. We also need to use some *a priori* knowledge and constraints of the atmosphere and the surface as "virtual measurements" to make the retrieval problem well-posed [Rogers, 1976]. In the day/night LST algorithm, we use the shapes of the atmospheric temperature and water vapor profiles retrieved from MODIS sounding channels as the reasonable constraints. After comprehensive numerical simulations and analysis, we decided to implement only two LST algorithms, one is the generalized split-window

algorithm, and another is the day/night algorithm.

3.1.2.2. Generalized split-window LST algorithm

If we know the spectral emissivity of land surfaces, the multi-channel SST method can be generalized into the LST algorithm for correcting atmospheric effects of an unknown atmosphere [Wan and Dozier, 1989]. The major differences between this method and other methods are: 1) it does not require precise atmospheric profiles; 2) it does not need radiative transfer simulations pixel by pixel; 3) its accuracy depends on the knowledge of the surface emissivity. The generalized split-window LST algorithm uses a simple form so that it requires less computing time although computing time cannot be saved in radiative transfer simulations in its development stage. This method is proposed as the first method for the at-launch MODIS LST algorithm, based on the following considerations of variations in atmosphere, LST and land surface emissivity: 1) atmospheric conditions, especially the water vapor profile, are highly variable with time in both vertical and horizontal directions, and it is not easy to measure the relative humidity profile at an accuracy better than 10%; 2) LST varies with region and time, and is less coupled with surface air temperature, the difference between daytime and nighttime temperatures of land cover types may be larger than 10 °C [Betts et al., 1996]; 3) the emissivity of most land cover types in MODIS bands 31 and 32 is relatively stable and is within a certain range as shown in Figure 2B.

According to the experience in development of SST algorithms, we know that there is a relatively simple and stable relation between the atmospheric effects in NOAA AVHRR channels 4 and 5, in a wide range of atmospheric conditions from sub-arctic winter to tropical, as shown in Fig. 3. The wavelength locations for MODIS bands 31 and 32 are located in the same spectral range for AVHRR channels 4 and 5, but the bandwidth and spectral response functions are different. Data in this figure come from radiative transfer simulations with models LOWTRAN7, MODTRAN, and ATRAD-MOD. ATRAD-MOD-Q means that a quadratic regression procedure is used to produce the temperature and pressure scaling factors in the effective absorber amount that is used in the exponential-sum-fitting scheme [Dozier and Wan, 1994]. The surface emissivity is assumed to be 0.98 in both channel 4 and 5. The surface air temperature T_{air} and the Earth surface temperature $T_s = T_{air} + \Delta T_s$ are given in the figure. Four pairs of band temperature deficit $T_s - T_j$ at viewing zenith angles (θ_v) 11.4 °, 26.1 °, 40.3 ° and 53.7 ° have been used to show the viewing angle effect. Note that the relation in Fig. 3 is not very sensitive to radiative transfer models [Barton et al., 1989; Wan and Dozier, 1992]. The emissivity effect is also shown in Fig. 3. The symbol black square represents $\varepsilon_4 = \varepsilon_5 = 0.95$ to 0.99 at θ_v 11.4 ° and/or 53.7 °, the symbol plus represents $\varepsilon_4 = 0.95$ and $\varepsilon_5 = 0.99$, and the symbol star represents $\varepsilon_4 = 0.99$ and $\varepsilon_5 = 0.95$. We can gain the following insights into the emissivity effect: 1) the effect caused by a consistent emissivity change in both bands (say, from 0.99 to 0.95) is relatively small because the emissivity effect is partially compensated by the reflectance of the downward atmospheric radiation and is similar to the atmospheric effect. This is the reason that the sea-surface emissivity has not been included in various split-window SST algorithms besides the difficulty to have independent wind speed data, although the sea-surface emissivity varies with viewing angle (typical values of 0.993 and 0.967, at zenith angles 0 ° and 60 °, respectively, at wavelength 11 μm for a calm sea surface) and surface wind speed (0.957 at 60 ° as surface wind speed increases to 15 m/s at the same wavelength) [Masuda et al., 1988]; 2) the effect caused by changes in the band differential emissivity, $\varepsilon_4 - \varepsilon_5$, is much larger as shown by symbols ∗ and + in Fig. 3; 3) the emissivity effect is more significant in dry cold atmospheric conditions because the compensation by reflected downward atmospheric radiation is weaker.

If we assume that the relation in Fig. 3 is a straight line as the first order of approximation

$$T_s - T_5 = a\,(T_s - T_4) + b \quad , \tag{12}$$

we get a simple LST algorithm

$$T_s = T_4 + \frac{1}{a-1}(T_4 - T_5) - \frac{b}{a-1} \quad . \tag{13}$$

This is similar to the form of the split-window SST algorithm [McClain et al., 1985]

$$T_s = 1.0346\, T_4 + 2.5779\,(T_4 - T_5) - 10.05 \quad . \tag{14}$$

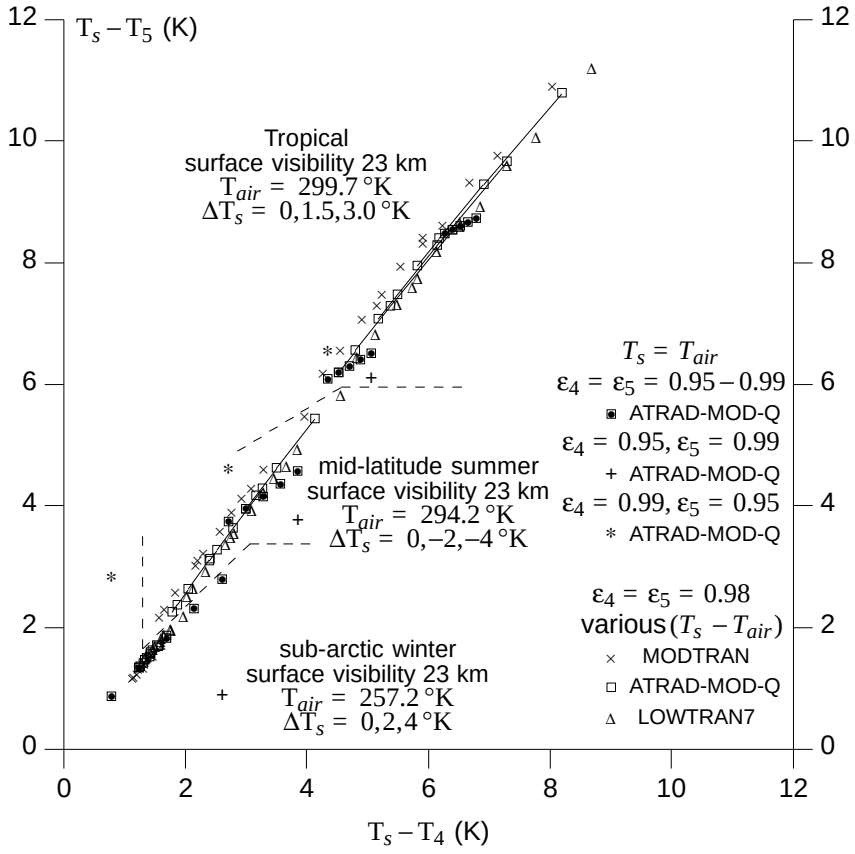

Figure 3. The atmospheric effect on NOAA-7 AVHRR band temperatures in different models.

From Fig. 3, we can see the following possible improvements: 1) the viewing angle should be included; 2) it is necessary to take regional and seasonal variations into consideration so that the regional and seasonal LST algorithm will be more accurate. It is obvious that the relation between $T_s - T_5$ and $T_s - T_4$ in sub-arctic winter is different from the relation in tropical and mid-latitude summer because the atmospheric absorption is dominated by the absorption of uniformly mixed gasses in sub-arctic winter, but it is dominated by the water vapor absorption in tropical and mid-latitude summer.

It is a common feature on the Earth's land surface that there are significant spatial variations in surface emissivity and temperature in the scale of a few kilometers, and there are several types of land cover in a single MODIS pixel. A first order of approximation method in the MODIS LST to deal with this mixed-pixel problem is to determine the average emissivity and the effective radiometric temperature of the mixed surface at the pixel level. It is expected that this approximation method works at least for certain types of mixing, uniformly distributed mixing of vegetation with soil or bare land, for example. Numerical simulations show that average band emissivities and a single effective radiometric temperature can be used to express the band radiance in MODIS bands 31 and 32 without any significant error for mixed pixels because of the small difference between wavelengths of these two bands. The difference between effective radiometric temperatures in different bands increases with the band wavelength difference.

Some LST algorithms only deal with pixels within the viewing angle range of 45 ° because the accuracy gets poor at larger viewing angles. Because the maximum MODIS viewing angle is 65 ° from nadir, pixels with viewing angle larger than 45 ° account for nearly 30% of the total pixels, or almost 50% of the total coverage area within each swath. It is better to develop LST algorithms for the whole viewing angle range in order to provide a global coverage for LST. Although a LST algorithm in a quadratic form of combinations of μ, the cosine of the viewing angle (θ_v), and TIR band brightness temperatures T_i [Wan and Dozier, 1989], gives better accuracy in cases for which surface emissivity characteristics are well known, it may be very sensitive to uncertainties in emissivity characteristics and noise in band radiance data caused by subpixel clouds. So we generalized the linear form of the Wan-Dozier LST algorithm into a view-angle dependent split-window LST algorithm for MODIS [Wan and Dozier, 1996], which is similar to Becker and Li's local split window method [1990],

$$T_s = (A_1 + A_2 \frac{1-\varepsilon}{\varepsilon} + A_3 \frac{\Delta\varepsilon}{\varepsilon^2}) \frac{T_{31}+T_{32}}{2} + (B_1 + B_2 \frac{1-\varepsilon}{\varepsilon} + B_3 \frac{\Delta\varepsilon}{\varepsilon^2})(T_{31} - T_{32}) + C \quad , \tag{15}$$

where $\varepsilon = 0.5(\varepsilon_{31} + \varepsilon_{32})$ and $\Delta\varepsilon = \varepsilon_{31} - \varepsilon_{32}$. A_1 is not fixed at 1, so there is one more variable coefficient in this form than in Becker-Li algorithm.

Our extensive error analysis shows that viewing angle and atmospheric column water vapor must be considered in the LST algorithm in order to achieve the 1 °K accuracy over the wide atmospheric and surface conditions except in very cold and dry regions. The optimal coefficients in the above algorithm are obtained in the following ways: 1) the atmospheric temperature profiles are separated into groups according to the surface air temperature, say, T_{air} <= 280 °K or >280 °K, so that winter dry atmospheres are included in the first group, summer and warm atmospheres are included in the second group; 2) the atmospheric column water vapor is separated into intervals of 0.5cm; 3) the land-surface temperature condition is separated into two groups according to $T_{air} - 16\,°K \le T_s \le T_{air} + 4\,°K$ or $T_{air} - 4\,°K \le T_s \le T_{air} + 16\,°K$ so that the first group would most likely represent the nighttime condition and the second group would most likely represent the daytime condition; 4) the band emissivities are specified by $0.89 \le \varepsilon \le 1$ in steps of 0.01 and $-0.025 \le \Delta\varepsilon \le 0.015$ in steps of 0.005; 5) 9 viewing angles are selected to cover the MODIS surface viewing angle range from nadir to 65.5 °. In short, the coefficients in the daytime and nighttime algorithms will be determined by separate regression analyses of the simulated data in each air surface temperature group, in each column water vapor interval at these 9 viewing angles. The coefficients at other viewing angles can be interpolated from the coefficients at these 9 viewing angles. The air surface temperature and column water vapor are given by the MODIS atmospheric profile product. The rms error in the resulting LST is less than 1 °K and the maximum error is less than 3 °K except at the scan edge (surface viewing angle > 55 °) when the column water vapor is larger than 4cm. These errors can be reduced by optimizing the algorithm in several overlapped narrower subranges of the air surface temperature and by the use of iterations. Details are given in Wan and Dozier's paper [1996].

A better LST algorithm must have the following two features: 1) it retrieves LST more accurately; 2) it is less sensitive to uncertainties in our knowledge of surface emissivities and atmospheric properties, and to the instrument noise. According to Equation (15), the factors on the emissivity terms $(1-\varepsilon)/\varepsilon$ and $\Delta\varepsilon/(\varepsilon^2)$ are

$$\alpha = A_2 \frac{T_4+T_5}{2} + B_2 \frac{T_4-T_5}{2} \quad , \tag{16}$$

and

$$\beta = A_3 \frac{T_4+T_5}{2} + B_3 \frac{T_4-T_5}{2} \quad . \tag{17}$$

The view-angle dependencies of the emissivity sensitivities for the θ_v-dependent and θ_v-independent LST algorithms in relatively cold, dry atmospheric conditions ($T_{air} \leq 287.2$°K and column water vapor in 0.5-1 cm) are shown in Fig. 4. There is no significant difference in maximum α values of these two LST algorithms, but the maximum β values are very different. Max (β) values in the θ_v-independent LST algorithm are close to 160, larger than twice the values in the θ_v-dependent algorithm. This means that the θ_v-independent algorithm will have a LST error up to 1.6 °K if there is an uncertainty of 0.01 in the value of $\Delta\varepsilon/(\varepsilon^2)$. We expect that this uncertainty may be around 0.005 for well known land surfaces. Then the θ_v-independent algorithm will have a 0.8 °K error in the whole range of viewing angle. The θ_v-dependent algorithm is much less sensitive to the value $\Delta\varepsilon/(\varepsilon^2)$, giving a maximum LST error around 0.37 °K at the nadir viewing angle. In warm, dry atmospheric conditions (294 °K $\leq T_{air} \leq$ 300 °K and column water vapor 0.5-1 cm), the maximum β value in the θ_v-independent algorithm is as large as 180, its corresponding value in θ_v-dependent algorithm is approximately 90 at nadir. As expected, all LST algorithms are more sensitive to uncertainty in $\Delta\varepsilon$ in dry atmospheric conditions. This sensitivity decreases as atmospheric column water vapor increases, because of the compensative effect of the reflected downward atmospheric thermal infrared radiation.

In order to investigate the sensitivity of the θ_v-dependent LST algorithm to instrument noise, we simulate the instrument noise by synthetic quantization. The radiance values of AVHRR bands 4 and 5 saturate at approximately 325 °K. The radiance values are expressed by a 10-bit integer through synthetic quantization and then converted to a double precision floating point number by multiplying by the quantization step. We compare the rms and maximum LST errors by applying the same θ_v-dependent algorithm to the original simulation data and the data after synthetic quantization. For the whole viewing angle range up to 69 °, the rms and maximum LST errors are smaller than 0.08 °K and 0.4°K. It will be more stable with 12-bit MODIS data.

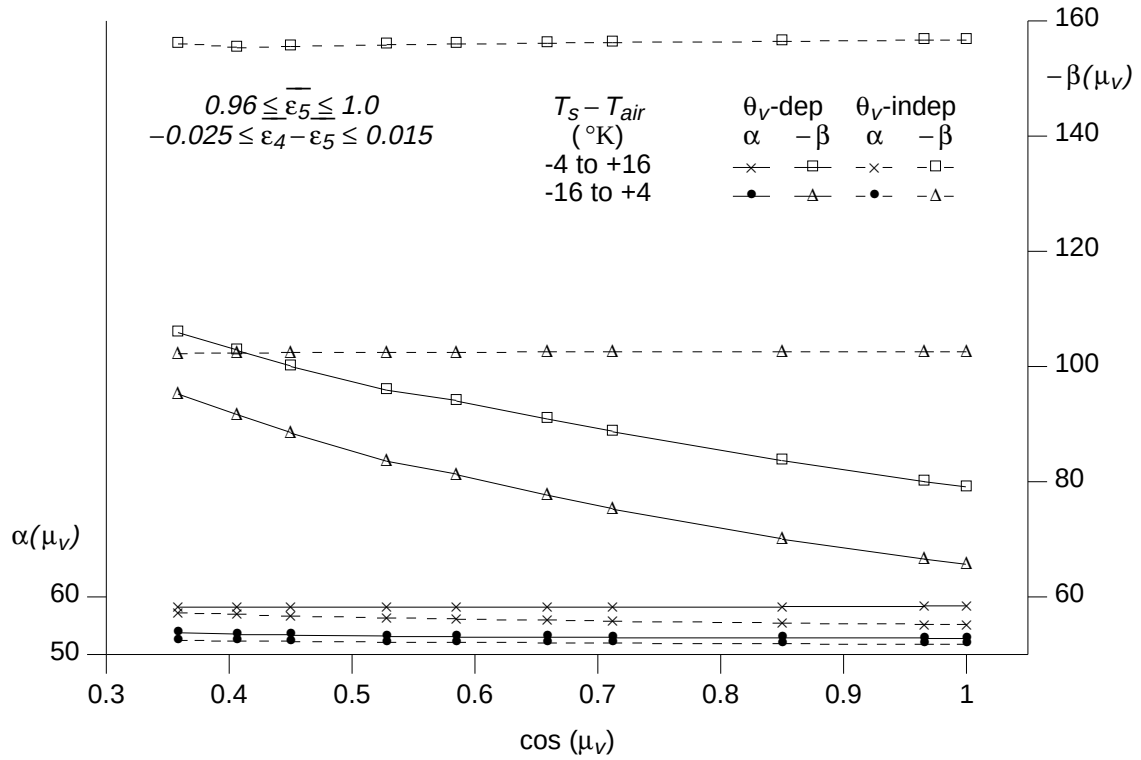

Figure 4. The maximum sensitivities of emissivity variations in the generalized LST algorithm in relatively cold atmospheric conditions ($T_{air} \leq 287$°K and column water in 0.5-1cm).

3.1.2.3. Day/night LST algorithm

In order to save computational time on numerical simulations of atmospheric radiative transfer for calculating the atmospheric and solar terms in (10), look-up tables will be used in the day/night LST algorithm. In this way, we only need to make a complete series of radiative transfer simulations once to build these look-up tables. The path radiance resulting from scattering of the solar radiation in (10), $L_s(j)$, does depend on the relative azimuth between viewing direction and the solar beam direction. This dependence is determined by the aerosol loading, its size distribution, type and scattering phase function. These aerosol information and properties are not readily available in most situations. Radiative transfer simulations indicate that the total aerosol effect on the transmission function in the thermal infrared range is small in normal clear-sky conditions. The value of L_s is only several percent of the direct solar beam value at the surface level, and the azimuth dependence in L_s is less than 10%. So it is appropriate to neglect this azimuth dependence and use the azimuth-averaged value of L_s in the day/night LST algorithm. We used version 3 of the MODTRAN3 code with the 8-stream discrete ordinate option for establishment of these look-up tables. Because multi-dimension interpolations are involved in our look-up table method, linear interpolation is most efficient. This requires smaller intervals (or steps) for these look-up tables. For example, the step for the atmospheric temperature variation is 2 °K, the step for atmospheric column water vapor is 10% of the average value, the step for solar zenith angle and viewing zenith angle is 10 ° for angles smaller than 30 ° and 5 ° for larger angles. The upper limits for solar and viewing zenith angles are 75° and 65°, respectively. Similarly, a look-up table in a step of 0.1 °K is also built for the band-averaged Planck functions in the temperature range 200-400 °K. It is required that errors caused by look-up tables and interpolation methods should be smaller than NEΔT. If this resolution scheme is used to build a look-up table for the 3 solar terms in (10) for initially 24 basic atmospheric profiles, the total size of the look-up table is approximately 60MB. If use of small look-up tables is a high priority, we can use 3-point interpolation method so that 6 steps are enough for viewing and solar angles. However, 3-point interpolation takes much more computational time than linear interpolation. The sizes of look-up tables for other 3 atmospheric terms (transmission, thermal infrared path radiance, and downward thermal infrared irradiance) are much smaller.

It is important that a practical LST algorithm should accommodate atmospheric variations in a range that is wide enough to cover all possible real situations. For LST retrieval, we only consider atmospheric variations in clear-sky conditions. In the thermal infrared range, the most important atmospheric variables are atmospheric water vapor and atmospheric temperature profiles. Atmospheric absorption and thermal emission occur mainly in the lower troposphere. Radiative transfer simulations show that the effect of changing atmospheric water vapor and temperature profiles at elevations above 9km is almost negligible. We assume that the MODIS product of the atmospheric temperature and water vapor profiles retrieved from MODIS sounding channel gives the shapes of the profiles better than their absolute values because of the difficulties in decoupling the atmosphere-land interaction. Atmospheric temperature and water vapor at any level will be interpolated from their values retrieved at fixed levels. Given the shapes of temperature and water vapor profiles, we can use only two variables to describe variations of the clear-sky atmospheric condition: a shift of the temperature profile below 9km, and a scaling factor for the water vapor profile. The column water vapor can be determined by the shape and the scaling factor. In order to build a database for the atmospheric and solar terms in (10), we will select initially 24 basic atmospheric profiles considering different shapes of temperature and water vapor profiles, and the range of air surface temperatures in different regions and seasons. Some basic atmospheric profiles include temperature inversion layers. Then we add more variations to each of these basic atmospheric profiles in the following ways. 1) A δT is added to the atmospheric temperature profile at all levels between surface and elevation 9km, δT varies from -10 °K to +20 °K in steps of 2 °K. The modified atmospheric temperature at the surface level, T_a, will be used as representative of the entire atmospheric temperature profile. 2) The atmospheric water vapor profile at all levels between the surface and 9km is scaled in steps of 10% so that the column water vapor varies from 10% to 120% of the basic value.

In the simulation study of the day/night LST algorithm, we consider LST variations in a wide range. In all the numerical examples of this LST algorithm in this ATBD, the daytime surface temperature varies from atmospheric surface temperature T_{a-day} to $T_{a-day} + 24\,°\text{K}$ in steps of $6\,°\text{K}$, the nighttime surface temperature varies from $T_{a-night} - 13.5\,°\text{K}$ to $T_{a-night} + 4.5\,°\text{K}$ in steps of $4.5\,°\text{K}$. We also considered LST variations in a wider range.

We have developed two approaches to solve the LST retrieval problem. The first one uses a statistical regression method, and the second uses other numerical methods to solve the set of nonlinear equations (10).

In a linear approximation of equation (10) around the reference values of surface temperature and band emissivities, the left-hand side reduces to the band brightness temperature and the right-hand side reduces to surface temperature and band emissivities. Combining 14 equations together, the solution for surface temperature and band emissivities should be a linear combination of the band brightness temperatures, each of which corresponds to one of the 14 observations. Its mathematical form is

$$x_i = \sum_{j=1}^{14} w_{i,j}\ y_j + w_{i,0}\ , \tag{18}$$

where x is a vector of the 14 variables including surface temperatures and band emissivities, y_j is the band brightness temperature for observation j, and $w_{i,j}$, i = 1, ..., 14 and j = 1, ..., 14 are coefficients. And $w_{i,0}$ is the coefficient for the offset term. We can determine these coefficients in two steps. In step 1, we construct a large set of simulated observation values in wide ranges of atmospheric and surface conditions. In step 2, we make a statistical regression analysis using the band brightness temperatures associated with these simulated band radiance values as independent variables and using the given surface band emissivities and temperatures, and atmospheric parameters as dependent variables. The output of this regression analysis will be the coefficients in (18). The process of statistical regression analysis takes a large amount of computational time, but it needs only to be done once. The values of x_i provided by this approach are the best estimates of these unknown variables in the statistical sense.

If we have better information on the shapes of the atmospheric temperature and water vapor profiles for the observation time which makes it possible to have a clear-sky day/night pairs of MODIS data, we can use other methods to numerically solve the set of nonlinear equations (10). We tried the Quasi-Newton method [Dennis and Schnabel, 1983] and the Least-Squares Fit (χ^2 fit) method [Bevington 1969]. As Rodgers [1976] pointed out, the retrieval problem in remote sensing is generally nonlinear. The main sources of the nonlinearity in (10) are: 1) the temperature dependence of the atmospheric transmission, 2) the dependence of transmission on absorber concentration, 3) the temperature dependence of the Planck function, 4) the wavelength dependence of the Planck function across a spectral band, 5) the wavelength dependence of the Planck function between spectral bands, and 6) nonlinear constraints.

The initial values of the 14 unknown variables are given in their constrained ranges based on reasonable guesses or statistical analysis. The Quasi-Newton method is slightly more computationally efficient. It gives similar results as the χ^2 fit method in cases not including noise. It is well known [Bevington, 1969; Dennis and Schnabel, 1983] that global convergence to the correct solution is not guaranteed for nonlinear problems, especially when noise is included. The χ^2 fit method is selected in the day/night LST algorithm because it is more stable in our simulation studies. We are only interested in real situations for which there is noise in remote measured data caused by instrument noise and turbulence in the atmosphere.

A measure of the goodness of χ^2 fit is defined by [Bevington, 1969]

$$\chi^2 = \sum_{j=1}^{14} \{ \frac{1}{\sigma_j^2} [L_j - L(j)]^2 \} \quad , \tag{19}$$

where L_j is the scaled band radiance observation value, j = 1, 7 for daytime, j = 8, 14 for nighttime. $L(j)$ is the scaled band radiance function in (10), which depends on unknowns x_i , i = 1 , 14. We use the values of band-averaged Planck functions at a reference temperature, 300 °K, to scale the band radiance in corresponding bands so that the scaled differential radiance may be comparable. The term σ_j is the uncertainty in observation value L_j. In cases without noise, σ_j is identically equal to unity. However, for cases which include noise NEΔT, σ_j will be

$$\sigma_j = L_j \frac{n_j \ \Delta T_{neq}(j)}{T_b(j)} \tag{20}$$

based on the following approximation for the band-averaged Planck function

$$L_j \simeq C_j \ T_b^{n_j}(j) \quad , \tag{21}$$

where $\Delta T_{neq}(j)$ is the NEΔT value in band j, and $T_b(j)$ is the brightness temperature corresponding to band radiance L_j. In the temperature range 240-400 °K, regression analysis gives the best fitting values for n_j, they are 12.91, 12.25, 11.98, 6.00, 4.70, 4.11, and 3.74 for MODIS bands 20, 22, 23, 29, 31-33. Note that this approximation is used only in calculation of σ_j, which determines the weight in (19). The effect of errors caused by this approximation on the solutions is negligible.

One of the difficulties in the χ^2 fit processing is that there may be more than one local minimum for χ^2 within a reasonable range of values for variable x_i, particularly in cases including noise. Therefore the final solution may depend on their initial values. We use two different ways to make the initialization. In the first way, we use 12-20 sets of initial values that are spread over preassigned ranges all from minimums to maximums to get different solutions and select the solution associated with the minimum χ^2 value. In noisy situations, this minimum χ^2 solution may not be the best one. An alternative way is to use the estimates provided by the statistical regression method as the initial values. We use the second way in our LST algorithm. Typically, the χ^2 fit method takes 3-5 iterations to reach the final solution.

We made various sensitivity and error analyses of the χ^2 fit day/night LST algorithm. In the first numerical simulation experiment, we did not include any noise in the data construction. This experiment tested the numerical method for solving the nonlinear problem and evaluated the errors caused by the use of look-up tables and interpolation methods. We used the temperature and water vapor shapes in the ‘‘averaged’’ mid-latitude summer atmospheric condition (MODTRAN model 2) and set the daytime and nighttime atmospheric surface temperatures at 298.2 °K and 290.2 °K. The column water vapor was set at 2.6cm for both daytime and nighttime for simplicity. In practice, we use independent variables for the column water vapor in daytime and nighttime. We set anisotropic factor as 1, solar zenith angle at 45 °, viewing angle at nadir for daytime and nighttime, 5 different daytime surface temperatures ranging from 298.2 °K to 322.2 °K, and 5 different nighttime surface temperatures ranging from 276.7 °K to 294.7 °K. There are 25 cases of different daytime and nighttime surface temperatures for each sample of 80 surface materials. The band emissivities of these 80 terrestrial material samples cover the range from 0.55 to almost unity. The standard deviations of errors in retrieved surface temperatures are 0.27 and 0.21 °K for daytime and nighttime, the standard deviations of errors in retrieved emissivities are in 0.005-0.008 for bands 20, 22-23, 29, 31-32, and 0.012 for the last band because of the low transmission of MODIS band 33 in the atmospheric condition. The standard deviations of errors in retrieved BRDF anisotropic factor, atmospheric temperatures, and column water vapor are 0.08, 0.10-0.15 °K, and 0.06cm, respectively. These numbers indicate that look-up tables are appropriate and the χ^2 fit method works well.

In the second simulation experiment, we set the NEΔT values for the seven bands at 0.05, 0.07, 0.07, 0.05, 0.05, 0.05, and 0.12 °K, set 0.5% as the systematic calibration error for all bands, and keep all other parameters as in the first experiment. In our simulation, NEΔT is treated as a random noise. We consider four different atmospheric conditions in mid-latitude summer, one is the ‘‘average’’ condition used in MODTRAN code (model 2), two (labeled by A109 and A117) are selected from the satellite TOVS Initial Guess Retrieval (TIGR) atmospheric profile database and the fourth (labeled by ‘‘average-4K’’) is the variant of the ‘‘average’’ one by shifting -4 °K on the temperature profile but keeping its water vapor profile unchanged. As shown in Fig. 5, three of them have almost the same air temperature at the surface level, but they have very different shapes in the temperature and water vapor profiles. The temperature discrepancy between the ‘‘average’’ profile and profile A109 may be as large as 10 °K at elevations near 2km and between 6-10km. The difference in water vapor profiles in atmospheric conditions of ‘‘average’’, A109, and A115 may be 20% to 50% or even larger. We established separate data-bases of the atmospheric terms in (10) through atmospheric radiative transfer simulations for these different atmospheric conditions. The separate data-bases will be used to calculate the daytime and nighttime band radiances in seven MODIS bands in wide ranges of surface temperature for 80 surface samples. These calculated band radiances are then used as simulated observations. The coefficients in (18) were obtained by statistical regression analysis on the observations simulated for the ‘‘average’’ atmospheric condition. In order to make this sensitivity study, we assume that there is enough information available for the ‘‘average’’ atmospheric condition, but there is no information available on the shapes of the atmospheric profile for atmospheric conditions A109 and A115. In the statistical approach, we apply the same set of regression coefficients to the 4 sets of simulated observations data for retrieving surface temperatures and emissivities. In the χ^2 fit approach, these surface temperatures and band emissivities retrieved by the regression approach are used as initial values for further iterative processing. The rms errors in surface temperatures and band emissivities retrieved by the statistical regression method are given in the first part of Table IV, and those retrieved by the use of the χ^2 fit method are given in the second part. Comparing the results from the statistical approach and the χ^2 fit approach for the ‘‘average’’ atmospheric condition indicated that the χ^2 fit method gives significant improvements on retrieved surface temperatures and band emissivities. This is because we know the shapes of the atmospheric temperature and water vapor profiles well enough so that we can select the right set of the regression coefficient and the right parts from the look-up tables for the atmospheric and solar terms in (10). But for atmospheric conditions A109 and A115, we do not have the information for making these right selections. So the results retrieved from the χ^2 fit approach may be worse than those from the statistical approach. However, for the case with the shifted ‘‘average’’ temperature profile, the rms errors in surface temperatures retrieved by the use of the χ^2 approach is reduced by a factor of 2, and the accuracies of retrieved band emissivities are improved by approximately 50% because the shapes of atmospheric temperature and water vapor profiles in this case are the same as those in the ‘‘average’’ profiles. From this experiment, we gained the following insights: the statistical method is less accurate, but it is also less sensitive to uncertainties in the atmospheric profile shapes; and the χ^2 fit method may be more accurate, but it is more sensitive to uncertainties in the profile shapes. In the following, we assume that the profile shapes are available so it is appropriate to pursue the χ^2 fit approach.

In the first test of the third simulation experiment, we set the NEΔT values for the seven bands at 0.05, 0.07, 0.07, 0.05, 0.05, 0.05, and 0.12 °K, set 0.5% as the systematic calibration error for all bands, and keep all other parameters as in the first experiment. The errors in surface temperatures retrieved by the χ^2 fit method for a total of 2,000 different cases are shown in Fig. 6A. The errors in retrieved band emissivities in MODIS bands 31 and 32 are shown in Fig. 6B. The standard deviations of errors in retrieved surface daytime and nighttime temperatures are in range of 0.4-0.5 °K, and the standard deviations of errors in band-averaged emissivities in MODIS bands 31 and 32 are 0.009 over a wide range of surface temperatures in the mid-latitude summer atmospheric condition. We can see the effect of the 0.5% systematic calibration error in Fig. 6A. This forces the retrieved temperature to shift to the positive direction by approximately 0.2 °K.

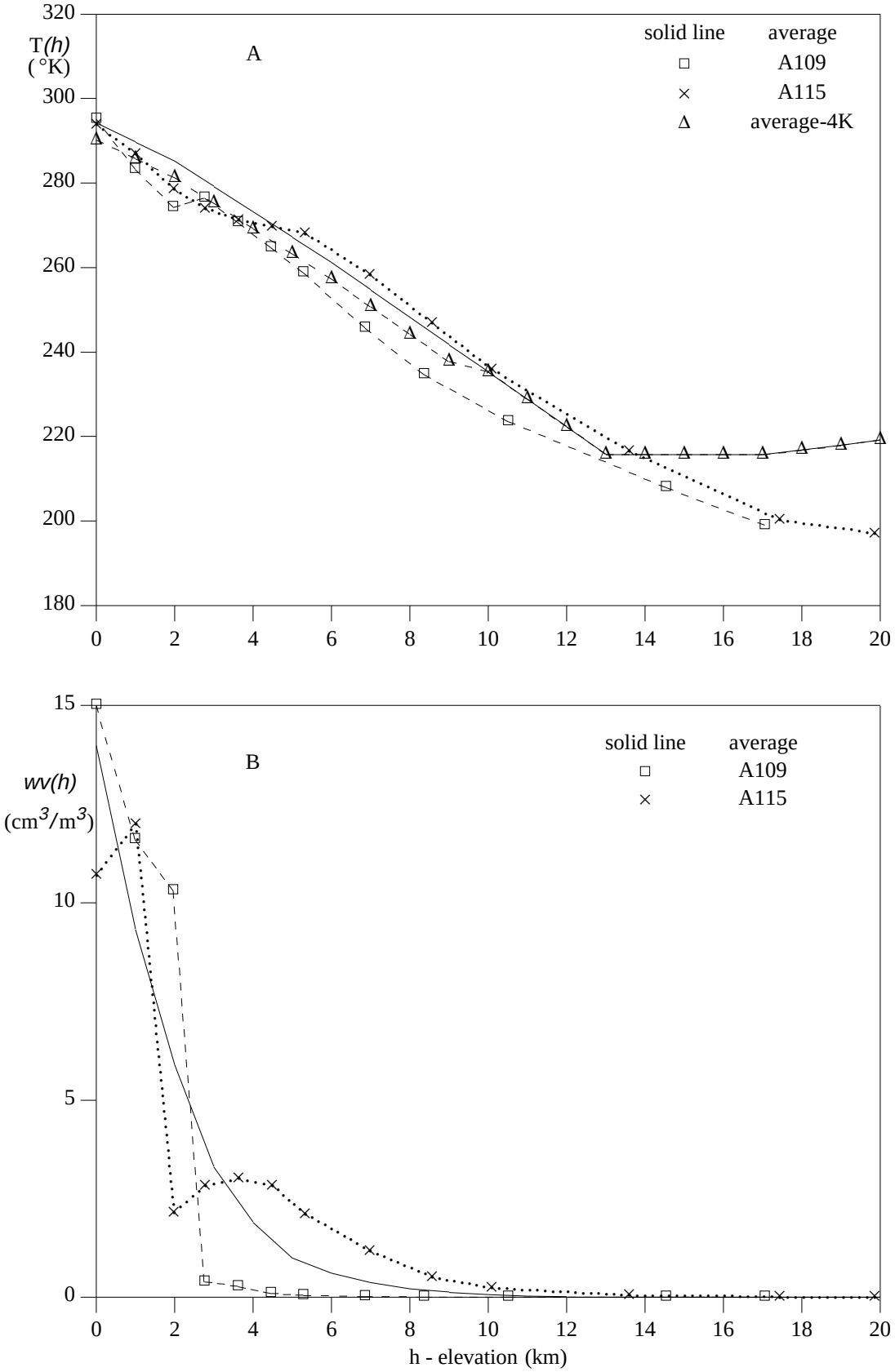

Figure 5, Atmospheric temperature profiles (A) and water vapor profiles (B) in mid-latitude summer.

TABLE IV. The standard deviations of errors in surface temperature and emissivities retrieved with two approaches of the day/night LST algorithm.

atmospheric profile	δT_{s-day} (°K)	$\delta T_{s-night}$ (°K)	$\delta\varepsilon_{20}$	$\delta\varepsilon_{22}$	$\delta\varepsilon_{23}$	$\delta\varepsilon_{29}$	$\delta\varepsilon_{31}$	$\delta\varepsilon_{32}$	$\delta\varepsilon_{33}$
with the statistical regression approach									
average	0.91	0.73	0.021	0.025	0.027	0.013	0.012	0.014	0.012
A109	0.82	0.75	0.026	0.024	0.027	0.032	0.013	0.018	0.014
A115	1.18	0.73	0.021	0.027	0.033	0.015	0.013	0.016	0.013
average-4K	0.94	0.64	0.019	0.022	0.024	0.013	0.013	0.014	0.013
with the χ^2 fit approach									
average	0.51	0.36	0.015	0.014	0.016	0.008	0.009	0.009	0.012
A109	2.13	1.91	0.057	0.068	0.076	0.030	0.036	0.043	0.014
A115	0.97	0.58	0.028	0.024	0.032	0.023	0.017	0.020	0.013
average-4K	0.45	0.32	0.014	0.013	0.015	0.008	0.009	0.009	0.013

The histograms of errors in retrieved surface temperatures and emissivities in bands 31 and 32 for a total of 2,000 cases are shown in Fig. 7A and 7B. We also applied the day/night LST method to ‘‘mixed sample’’ that contain a mixture of two samples of the 80 terrestrial materials at different surface temperatures. Similar results have been obtained as long as band emissivities of the mixed sample are calculated from the components with their proportions as weights and its effective surface temperature is calculated from the total thermal radiation in MODIS band 31. The effective surface temperature of a mixed sample does depend on band number, but this dependence is very small (at the instrument noise level) in normal surface conditions. We do not consider forest fires in the LST processing because the MODIS TIR bands may be easily saturated by subpixel fires at a small size and there is no sufficient knowledge on the optical properties of fires and smoke for making atmospheric corrections. In test 1 of this experiment, the maximum error in the retrieved LST is 3.2 °K for only one case (for the Indian grass sample at temperature 322.2 °K). Without considering this extreme case, the maximum error in retrieved LST will be 2.2 °K. Note that we simulated the surface temperature variation in a very wide range. For each sample, the surface temperature varies in a range of 24 °K in daytime, and in a range of 18 °K in nighttime. These ranges are too wide for some land cover types in real situations. For example, the temperature of snow cover and ice could not be above a few degrees C even considering possibly some small proportion of other land cover types mixed in the scene, and the temperature of water surface and green vegetation leaves is not likely to be warmer than the surface air temperature by 24 °K. In favorable conditions (for example, higher solar elevation and surface temperature being in a normal range are favorable conditions for land cover types with low reflectances), the solar beam can be effectively used as an active TIR source for remote measurements of the surface reflectance in the medium wavelength range so that the band emissivities in MODIS bands 31 and 32 can be retrieved at an accuracy better than 0.01. Then these retrieved emissivities can be used in the generalized split-window LST algorithm [Wan and Dozier, 1996] to quickly retrieve LST in the same area for a period of one or more weeks depending on season and weather conditions, if there is no appropriate day-night pair of clear-sky data during the period of time.

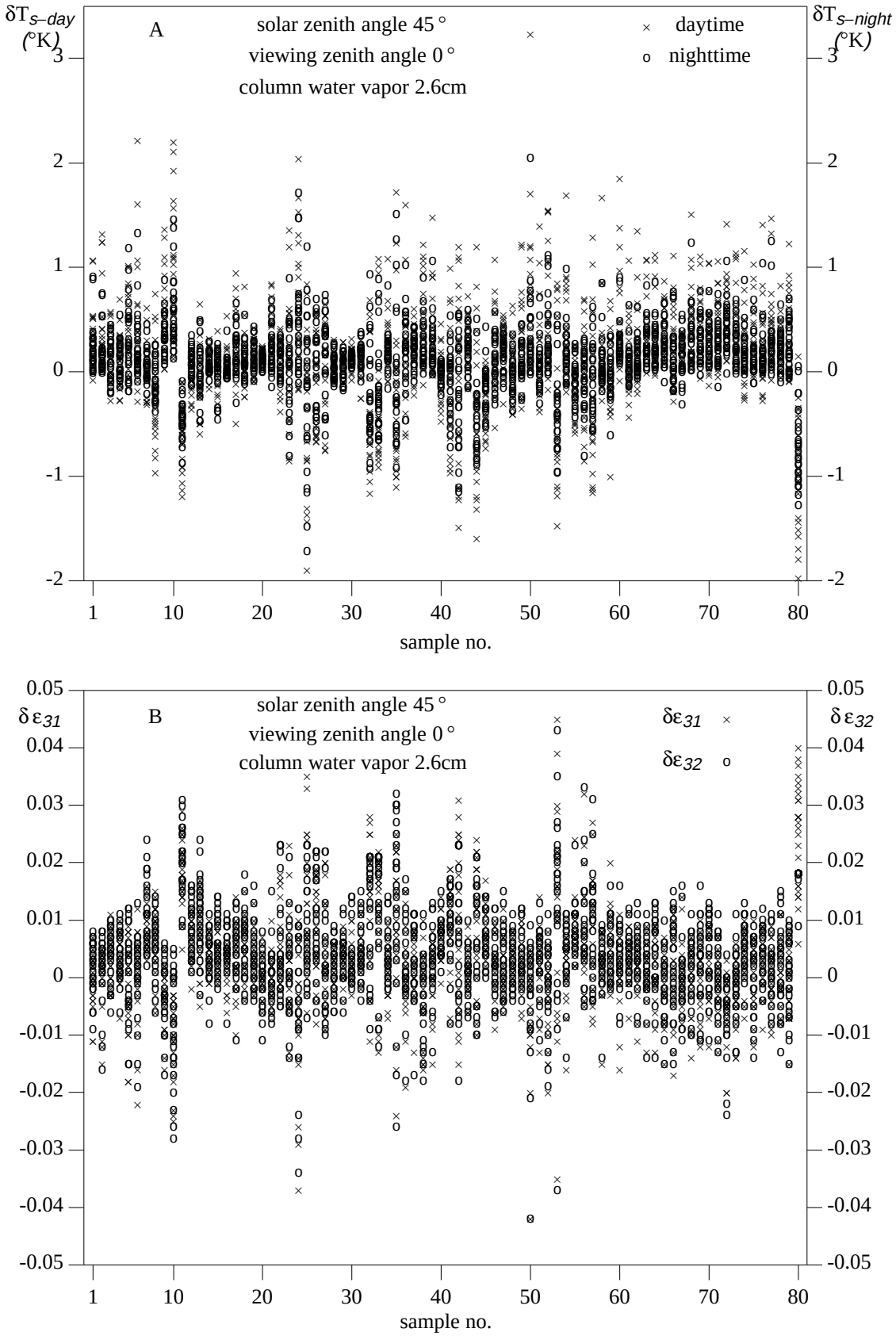

Figure 6, Errors in surface temperatures (A) and emissivities (B) retrieved by the χ^2 fitting LST method.

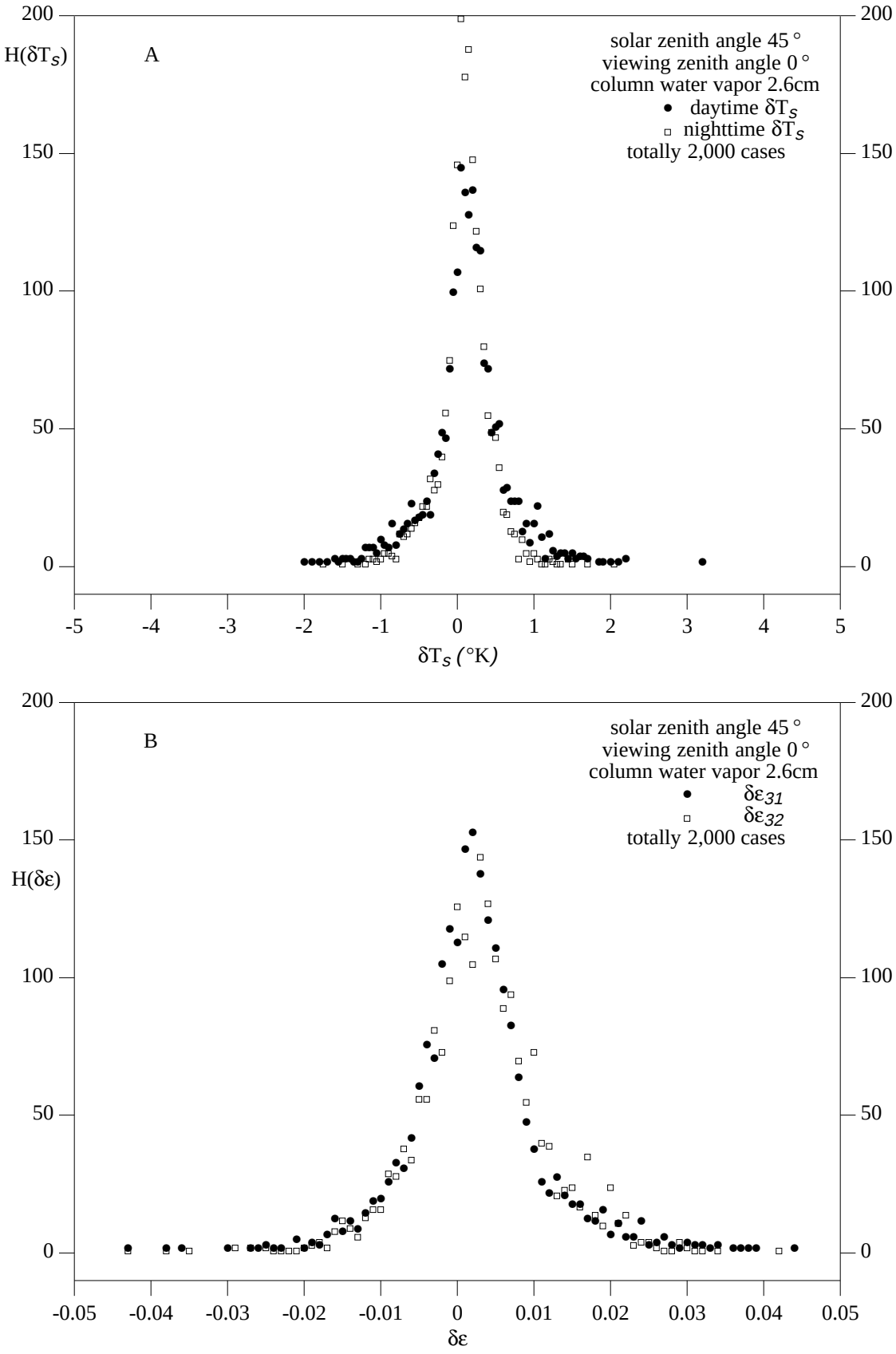

Figure 7, Histogram of errors in surface temperatures (A) and emissivities (B) retrieved by the χ^2 fit method.

Now we check whether it is possible to relax the three assumptions of surface optical properties made in section 3.1.1. The first row in Table V gives standard deviations of the surface temperature and emissivities retrieved in test 1 of this experiment. In tests 2 and 3, we introduce some variations for the nighttime surface band emissivities to simulate its possible change with surface moisture content. In test 2, the nighttime band emissivities increase by 0.01 and they are only limited by its maximum value 1. In test 3, the emissivity increment depends on its value, a lower band emissivity could increase more. This may be the case for sands, its emissivity in MODIS band 20 is approximately 0.56, it could increase to 0.604 at night. The standard deviations of errors in daytime and nighttime surface temperatures, and band emissivities retrieved by the χ^2 fit method are increased slightly. Note that the retrieved emissivities are compared to daytime emissivities only. In tests 4 and 5, we set different BRDF anisotropic factors for the three bands in the mid-infrared range by differences of 5% and 10%. There is no significant change in the retrieved surface temperature and emissivities. In tests 6 and 7, we use non-Lambertian reflectance for the surface-reflected solar diffuse irradiance and atmospheric downward irradiance terms. They differ from the reflectance of a Lambertian surface by ±20%. The effect of the non-Lambertian reflectance is also not significant. Comparing the standard deviations in tests 2 through 7 to those in test 1 shows that the maximum difference in standard deviations of errors in retrieved surface temperatures is 0.17 °K, the maximum difference in standard deviations of errors in retrieved band emissivities is 0.005, they are comparable to or smaller than the effects caused by NEΔT and calibration errors of the instrument. Therefore, we do not need to understand the three assumptions of surface optical properties described in section 3.1.1 as strict constraints to the day/night LST algorithm.

In the fourth simulation experiment, we keep the atmospheric and surface temperature parameters as in the first experiment, but change NEΔT and calibration error values in a series of tests, as shown in Table VI. The first column in the table indicates the test number. Seven NEΔT values for seven bands used in the day/night LST algorithm are listed in the second column block, and a systematic calibration error for all bands in the third column. Standard deviations (δT_s) and maximum errors (ΔT_s) of the retrieved daytime and nighttime surface temperatures are given in columns 4-7. The standard deviations of errors in retrieved emissivities for MODIS bands 31 and 32 are given in the last two columns. A comparison between test 1 and test 2 indicates that the effect caused by a systematic calibration error of 0.5% is comparable to the effect of the given NEΔT values. Test 3 indicates that doubling the NEΔ*T* values increases the standard deviation of retrieved daytime surface temperature by approximately 0.2 °K. Comparing tests 4 and 5 to test 2 indicates that errors in retrieved surface temperatures and band emissivities become larger as the calibration error increases. In order to achieve the 1 °K requirement for the LST accuracy and retrieve band emissivities in MODIS bands 31 and 32 at an accuracy of the 0.01 level, the calibration error should be smaller than 1%. The day/night LST algorithm requires small NEΔ*T* (large signal-to-noise ratio) and a high consistent calibration accuracy for the seven bands used. The split-window SST and LST algorithms also need these requirements for MODIS bands 31 and 32. However, the day/night LST algorithm needs these requirements over a much wider spectral range.

TABLE V. The rms errors in surface temperature and emissivities retrieved with the χ^2 fit approach of the day/night LST algorithm in the sensitivity study on assumptions of surface optical properties in conditions of $T_{a-day} = 298.2$ °K, $T_{a-night} = 290.2$ °K, cwv = 2.6 cm, $\alpha = 1.0$, NEΔT = 0.05–0.12 °K, and systematic calibration error = 0.5%.

test no.	test conditions	δT_{s-day} (°K)	$\delta T_{s-night}$ (°K)	$\delta\varepsilon_{31}$ (daytime)	$\delta\varepsilon_{32}$ (daytime)
1	$\varepsilon_n(j) = \varepsilon_d(j)$ $f_1 = f_2 = f_3$ Lambertian surface	0.51	0.36	0.009	0.009
2	$\varepsilon_n(j) = \varepsilon_d(j) + 0.01$	0.75	0.55	0.013	0.013
3	$\varepsilon_n(j) = \varepsilon_d(j) + 0.1\,(1 - \varepsilon_d)$	0.51	0.41	0.009	0.009
4	$f_r(22) = 0.95\,f_r(23)$, $f_r(20) = 0.90\,f_r(23)$	0.71	0.58	0.012	0.011
5	$f_r(20) = 1.10\,f_r(23)$, $f_r(22) = 1.05\,f_r(23)$	0.68	0.60	0.011	0.011
6	non-Lambertian surface (80%)	0.61	0.43	0.011	0.010
7	non-Lambertian surface (120%)	0.58	0.41	0.010	0.010

TABLE VI. The dependences of standard deviations (δT_s) and maximum errors (ΔT_s) in surface emissivities and temperatures retrieved with the χ^2 fit approach of the day/night LST algorithm on NEΔT and calibration errors.

test no.	NEΔT (°K)	calibration errors (%)	δT_{s-day} (°K)	$\delta T_{s-night}$ (°K)	ΔT_{s-day} (°K)	$\Delta T_{s-night}$ (°K)	$\delta\varepsilon_{31}$	$\delta\varepsilon_{32}$
1	0.05,0.07,0.07,0.05,0.05,0.05,0.12	0.00	0.41	0.31	3.3	2.6	0.007	0.007
2	0.05,0.07,0.07,0.05,0.05,0.05,0.12	0.50	0.51	0.36	3.2	2.1	0.009	0.009
3	0.10,0.14,0.14,0.10,0.10,0.10,0.25	0.50	0.69	0.49	3.7	2.2	0.011	0.012
4	0.05,0.07,0.07,0.05,0.05,0.05,0.12	0.75	0.58	0.40	3.3	2.1	0.010	0.011
5	0.05,0.07,0.07,0.05,0.05,0.05,0.12	1.00	0.66	0.45	4.4	2.5	0.012	0.012

Now we consider the dew problem. Dew is a common global phenomenon. By model calculations and measurements of dew occurrence, Janssen and Römer [1991] showed that there were 220 dewy nights and 1600 dewy hours in the Netherlands in 1987. Six years of dew observations in the Negev Desert, Israel [Zangvil, 1996] show that the total monthly dew hours is 145 h per month from August to January, and 80 h per month from February to June and that the average duration of dew per dew night appears to follow closely the length of the night. Scherm and Bruggen [1993] used a previously verified and validated model to calculate the frequency and duration of dew occurrence with hourly weather data over a growing season (April-October) in different climate regions of California. Simulation results indicated that high dew occurrence (78-93% of the days) and long mean dew duration (8.7-9.3 per day) at coastal stations, and low occurrence (23% of the days) and short duration (0.9 h per day or 3.7 h per dew event) at the interior valley site. The dew duration is sensitive to changes in humidity and cloud cover at the coastal sites and to humidity and wind speed at the interior valley site. An empirical model to estimate the duration of dew periods by the use of dew point depression, wind speed, and relative humidity (RH) as inputs [Gleason et al., 1994], has an accuracy better by only 5-10% than a simple RH > 90% model [Sutton et al., 1984]. This indicates that the near-surface relative humidity is the primary factor in dew occurrence. Because the weather data are usually not available in remote areas, it is not easy to calculate dew occurrence with the dew models. The near-surface humidity in the MODIS atmospheric profile product may be used to reject the dew occurrence. Considering potential large errors in the temperature and water vapor in the surface boundary layer in the MODIS atmospheric profiles product, RH < 50% may be used as a conservative condition for nondew hours. Then we only need to detect night dew in our LST algorithm in relatively wet conditions (RH > 50%). When dew occurs at night the surface emissivity may be changed significantly if a land cover has a low emissivity in dry conditions, for example, in the desert environment. This significant change in surface emissivity should be shown in TIR data. If surface emissivity at night differs significantly from the value in daytime, the major link between day and night observations used in the day/night LST method will be lost. So we need to find some additional information to help the LST retrieval with only the multiband night-only observation. The empirical relationship between the minimum emissivity (ε_{min}) and the spectral contrast which is described by the maximum-minimum difference (MMD) is such an information. This relationship is used in the ASTER TES algorithm [ATBD-AST-03, 1996]. Based on 80 laboratory reflectance spectra of rocks, soils, vegetation leaves, snow, ice and water [Salisbury and D'Aria, 1992] and their mixed values with three different portions of vegetation (totally 320 samples), two empirical relationships between minimum emissivity (ε_{min}) and the spectral contrast described by MMD (maximum and minimum difference) have been calculated. One is for five MODIS bands (bands 20, 22, 23, 29 and 31), and another for the seven MODIS bands used in the day/night LST algorithm, as shown in Fig. 8. These two relationships have been added to our day/night algorithm as an option. We also made a series of numerical simulations with the enhanced day/night LST algorithm (called MMD-MIN χ^2 fitting LST method hereafter) in cases with and without night dew. Seven tests have been made to show the performance of three options of this enhanced LST algorithm: night-only, day-only, and day/night combination. In the current simulations we assume that the emissivity of a dew film has the same value of water surface emissivity. We will measure its spectral emissivity during the course of dew occurrence.

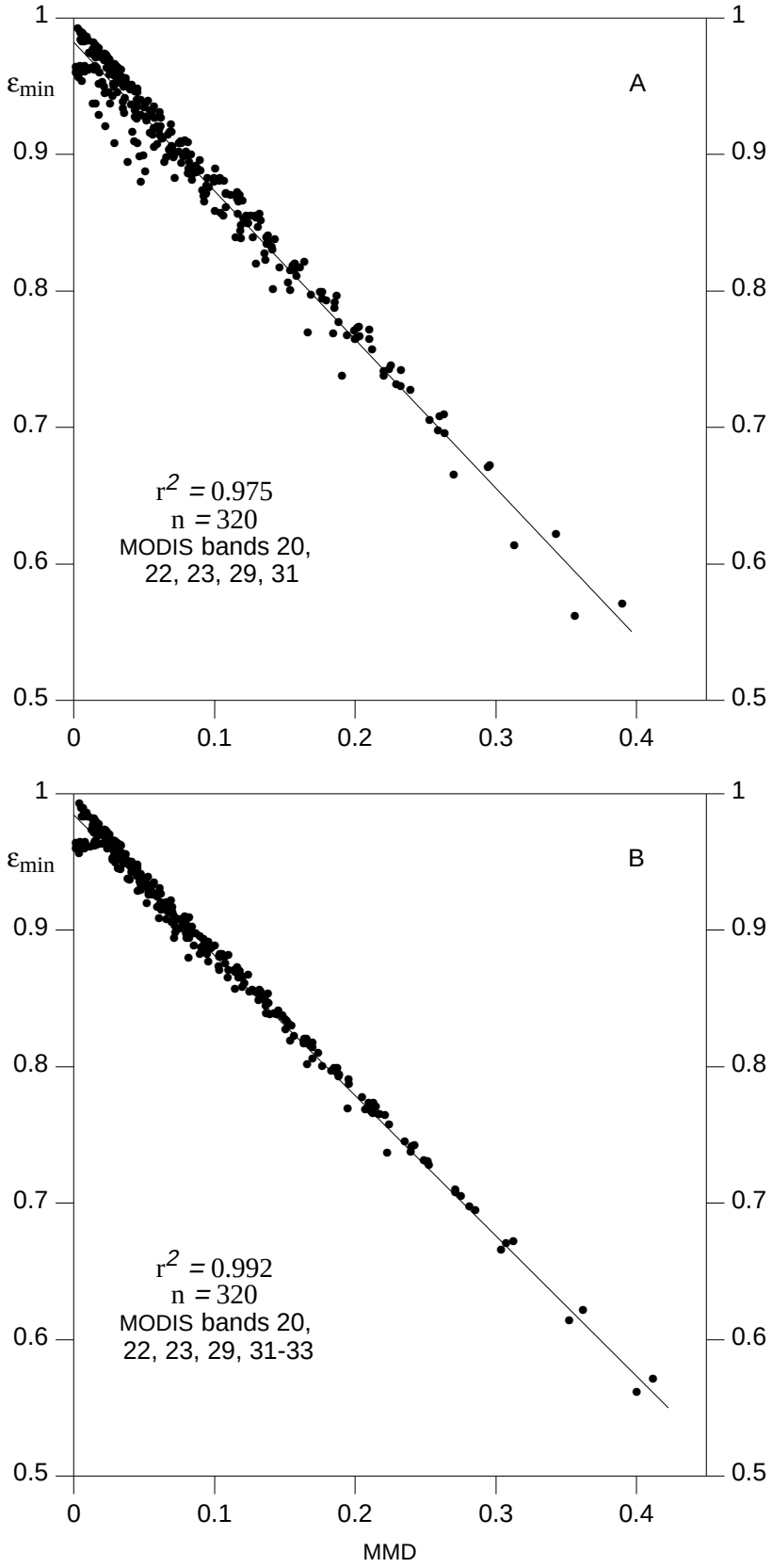

Figure 8. The empirical ε_{min} vs MMD relationships in five MODIS bands (A) and seven MODIS bands (B).

Simulation results with the statistical day/night LST algorithm and the MMD-MIN χ^2 fitting LST algorithm are shown in Fig. 9 and Table VII. We used the similar parameters as used in the third numerical experiment and assume that each of 80 samples mixed with the vegetation sample (no. 51 in Table II) in a proportion of 25 percent. Note that the spectral reflectance data of vegetation samples (no. 50 to 62) were obtained by measurements of single leaves. According to our recent measurements and simulations with modified BRDF kernel models [Snyder et al., 1996(a)], the spectral reflectance of a canopy is approximately one third of the spectral reflectance of a single leaf because of volumetric effects. We have made this adjustment for the vegetation samples in this numerical experiment in order to get a better understanding of the dew effect. After this adjustment, the emissivity of all vegetation samples is close to 0.99 so that the emissivity difference between water and vegetation is negligible. Figure 9 show the error in surface temperature and the emissivity in MODIS band 20 retrieved by the night-only method. For sample 50 to sample 79, the errors in nighttime surface temperature retrieved by both the statistical and χ^2 fitting methods are within the range of $\pm 1.5\,°K$ because dew does not change the surface emissivities of vegetation, water, and ice. But dew has a significant effect on the emissivities of most rock and soil samples as shown in Fig. 2A. As indicated in Table VII, test A is for the surface temperature and emissivities retrieved by the day/night statistical method. Because the dew effect has not been included in the statistical regression analysis, the rms and maximum errors in nighttime surface temperatures are $1.7\,°K$ and $6.6\,°K$, respectively. In test B, only the night observation in seven MODIS bands was used to retrieve the surface temperature and emissivities by the χ^2 fit method. The maximum error in the retrieved nighttime surface temperature reduces to $5.4\,°K$ if no MMD-MIN relationship is used, and it reduces to $3.4\,°K$ and $3.1\,°K$ if one or two MMD-MIN relationships are used. The rms error in retrieved band emissivities is reduced by a factor of 2-3. Figure 9A shows the error in surface temperatures retrieved by the statistical method in test A and by the χ^2 fitting method in test B. Figure 9B shows the error in surface emissivities in band 20, ε_{20}, retrieved by the the χ^2 fitting method in test B. Although errors in the retrieved ε_{20} are still large for some rock and soil samples, these errors are smaller than the emissivity difference between dew and these samples, which is shown by open circles in Fig. 9B. This means that ε_{20} retrieved by the night-only method can be used to detect dew for those land types which have low ε_{20} values in dry conditions. Then we can use this information in the following processing. Test C shows the simulations results retrieved by the night-only χ^2 fitting LST method for cases without night dew, the accuracies are much better than those in Test B for cases with night dew. Tests D and E show the results retrieved by the day-only χ^2 fitting method for cases with and without dew. The MMD-MIN relationships improve the retrieval accuracies slightly. The accuracies of retrieved emissivities in bands 20, 22, and 23 are poor because the solar effects cannot be corrected well by the use of only the daytime observation data. In Test F for cases with night dew, use of both daytime and nighttime data does not improve the accuracies, even with the dew emissivity for nighttime. This is because the surface emissivity may be changed significantly between daytime and nighttime. Test G is the results retrieved by the day/night χ^2 fitting method with and without the MMD-MIN relationships in cases without night dew. Use of the MMD-MIN relationships in Tests F and G improves the accuracies by only a small amount. From the simulation results for Tests A through G, we can gain the following insights into the capability of the day/night LST algorithm to deal with the dew effects: 1) dew does not affect the LST and emissivity retrieval for most of the Earth surface which is covered by water and vegetation. 2) dew do affect the retrieval for land surfaces with low emissivities in dry conditions, mainly in semi-arid and arid areas. In these areas, dew reduces the accuracies in retrieved LST and emissivities in bands 20, 22, and 23 roughly by a factor of 2, and reduces the emissivity accuracies in other bands slightly. Considering the low frequency of dew occurrence in semi-arid and arid regions, dew is not a serious problem for LST and emissivity retrieval but it makes the processing complicated slightly. We assume that the dew effect is needed to considered for one third of the global land (determined by the MODIS land-cover and NDVI products) at a frequency less than 50%. Because the dew detection process with the night-only LST mode takes less than half the computing time for the day/night LST mode, the total computing time will be increased by less than 10 percent. 3)

the MMD-MIN χ^2 fitting day/night LST algorithm can be used to deal with night-only and day-only observations at lower accuracies. Surface emissivities in MODIS bands 20, 22, and 23 cannot be retrieved accurately by the day-only option in all situations (with and without dew). It is also worth noting the differences between the ASTER TES algorithm and the MODIS day/night LST algorithm: 1) the ASTER algorithm uses five bands in the spectral region 8-12 μm, the MODIS algorithm uses four bands in the spectral range 8-13.5 μm and three bands in the spectral region 3.5-4.2 μm. Two of the seven MODIS bands, bands 23 and 33, are on the edges of the atmospheric windows. They are used to adjust the boundary atmospheric temperature and the column water vapor but not for retrieval of surface temperature and emissivities per se. 2) If the atmospheric temperature and water vapor profiles recovered from the MODIS sounding channels are accurate enough ($\delta T \leq 1\,°K$, the accuracy of cwv $\leq 10\%$), the ASTER algorithm can retrieve surface temperature and emissivity quite accurately. But this algorithm does not have the capability to reduce the uncertainties in the ASTER atmospheric correction product (including transmission, path radiance, and downwelling irradiance) which uses the MODIS atmospheric profiles product as input. The MODIS day/night LST algorithm uses the MODIS atmospheric profiles product only as initial conditions and has some capability to reduce the uncertainties in the atmospheric profiles by the use of self consistency in the seven MODIS bands. For water surfaces and evergreen canopies with stable and known emissivities, the LST and surface emissivity retrieved by this MODIS day/night algorithm will be compared with the values retrieved by the MODIS generalized split-window LST algorithm for additional evaluation of the self consistency. 3) The ASTER algorithm can retrieve daytime and nighttime surface temperatures and emissivities independently so that its performance will not be affected by the dew occurrence in principle. The dew occurrence will affect the MODIS day/night LST algorithm for some land-cover surfaces. Therefore, its night-only option will be used first for dew detection, and then compare the retrieved ε_{20} to its daytime value retrieved previously. If there is a significant difference, this nighttime observation data should be avoided in the day/night algorithm. If this is the only nighttime observation available in one or two weeks, it can be used for day/night retrieval at a lower accuracy and it will be flagged in the QA bits. 4) These two algorithm will produce LST and surface emissivities at different spatial resolutions. Comparison between the products by these two independent algorithms can provide useful information for validation.

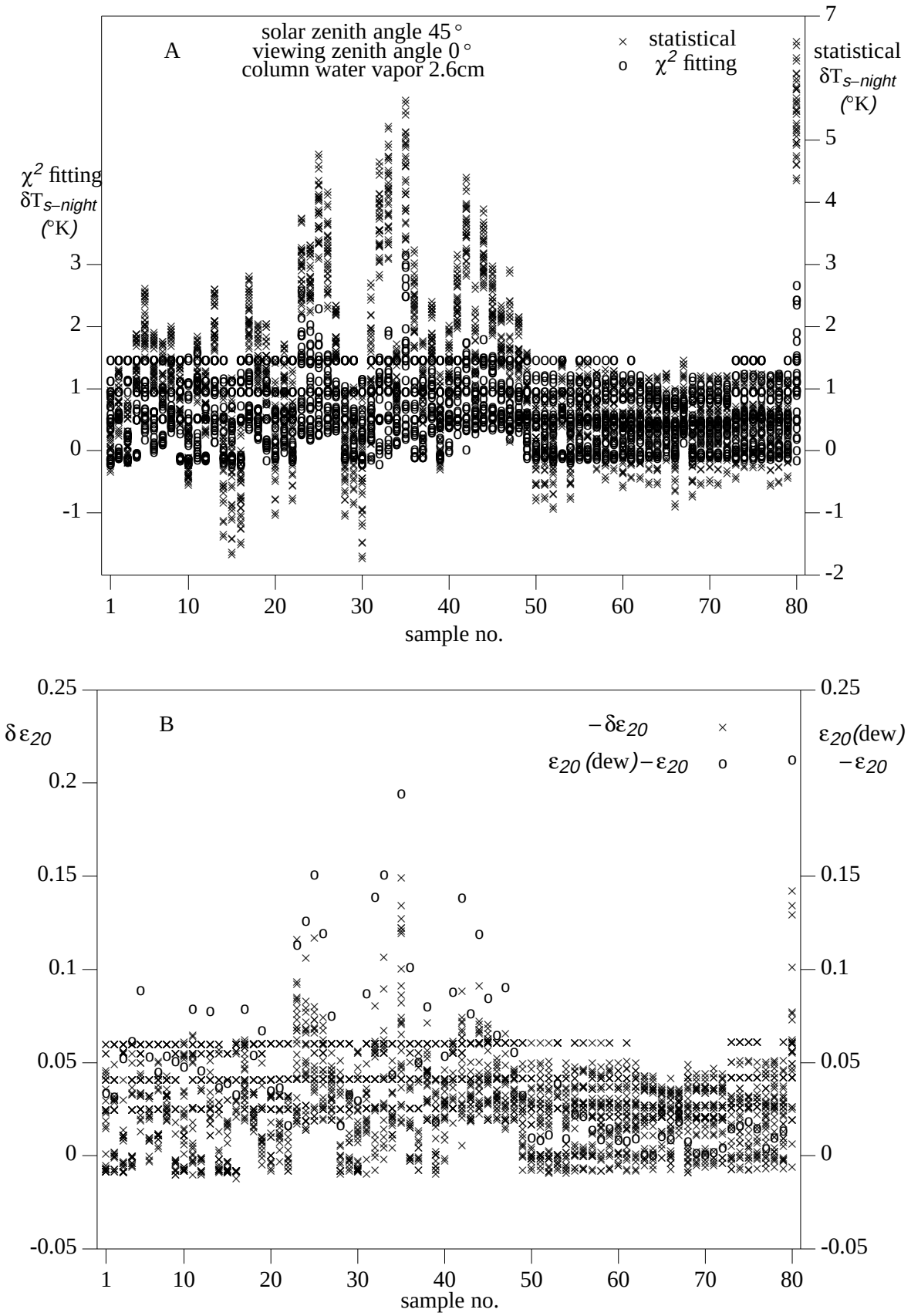

Figure 9, Errors in surface temperatures (A) and ε_{20} (B) retrieved in case of night dew.

TABLE VII. The standard deviation (δ) and maximum (Δ) errors in surface temperature and emissivities retrieved with the statistical and the MMD-MIN χ^2-fitting LST algorithms in cases with and without night dew.

test	number of MMD-MIN relations used	δT_{s-day} (ΔT_{s-day} (°K)	$\delta T_{s-night}$ $\Delta T_{s-night}$	$\delta\varepsilon_{20}$ $\Delta\varepsilon_{20}$	$\delta\varepsilon_{22}$ $\Delta\varepsilon_{22}$	$\delta\varepsilon_{23}$ $\Delta\varepsilon_{23}$	$\delta\varepsilon_{29}$ $\Delta\varepsilon_{29}$	$\delta\varepsilon_{31}$ $\Delta\varepsilon_{31}$	$\delta\varepsilon_{32}$ $\Delta\varepsilon_{32}$	$\delta\varepsilon_{33}$ $\Delta\varepsilon_{33}$)
A		day/night statistical LST method for cases with night dew (including daytime ε's only)								
	0	0.87	1.71	0.026	0.029	0.026	0.023	0.012	0.013	0.014
		(3.63	6.56	0.140	0.132	0.097	0.113	0.045	0.052	0.040)
B		night-only χ^2-fitting LST method for cases with unknown night dew (retrieving dew ε's)								
	0		1.49	0.070	0.066	0.071	0.037	0.033	0.033	0.007
			(5.37	0.221	0.204	0.214	0.123	0.109	0.116	0.037)
	1		0.84	0.039	0.038	0.042	0.019	0.015	0.014	0.007
			(3.36	0.161	0.147	0.149	0.094	0.062	0.087	0.037)
	2		0.81	0.037	0.037	0.043	0.017	0.013	0.011	0.007
			(3.14	0.149	0.137	0.146	0.094	0.068	0.071	0.037)
C		night-only χ^2-fitting LST method for cases without night dew (retrieving nighttime ε's)								
	0		0.46	0.020	0.019	0.021	0.011	0.009	0.009	0.012
			(1.75	0.063	0.058	0.064	0.057	0.037	0.034	0.031)
	1		0.44	0.020	0.019	0.021	0.012	0.010	0.011	0.012
			(1.77	0.058	0.059	0.063	0.084	0.039	0.035	0.031)
	2		0.42	0.020	0.019	0.021	0.011	0.009	0.008	0.012
			(1.81	0.068	0.075	0.080	0.092	0.035	0.037	0.031)
D		day-only χ^2-fitting LST method for cases with unknown night dew (retrieving daytime ε's)								
	0	0.74		0.021	0.055	0.059	0.014	0.012	0.013	0.014
		(2.74		0.110	0.304	0.306	0.055	0.047	0.045	0.040)
	1	0.63		0.021	0.028	0.048	0.011	0.009	0.010	0.014
		(3.19		0.111	0.215	0.296	0.046	0.041	0.053	0.040)
	2	0.64		0.021	0.028	0.047	0.011	0.009	0.009	0.014
		(2.69		0.117	0.210	0.277	0.041	0.040	0.043	0.040)
E		day-only χ^2-fitting LST method for cases without night dew (retrieving daytime ε's)								
	0	0.74		0.015	0.066	0.057	0.014	0.012	0.012	0.012
		(2.42		0.059	0.314	0.191	0.074	0.067	0.063	0.031)
	1	0.57		0.017	0.035	0.039	0.009	0.007	0.008	0.012
		(2.42		0.291	0.300	0.265	0.032	0.037	0.064	0.031)
	2	0.56		0.016	0.029	0.040	0.009	0.007	0.007	0.012
		(2.42		0.148	0.287	0.295	0.044	0.032	0.052	0.031)
F		day/night χ^2-fitting LST method for cases with known night dew (retrieving daytime ε's)								
	0	0.74	0.21	0.021	0.055	0.059	0.014	0.012	0.013	0.014
		(2.74	2.09	0.110	0.304	0.306	0.055	0.047	0.045	0.040)
	1	0.63	0.20	0.021	0.028	0.049	0.011	0.009	0.010	0.014
		(3.19	2.09	0.111	0.146	0.296	0.046	0.041	0.053	0.040)
	2	0.63	0.20	0.021	0.030	0.049	0.011	0.009	0.009	0.014
		(2.69	2.09	0.117	0.255	0.277	0.041	0.040	0.043	0.040)
G		day/night χ^2-fitting LST method for cases without night dew (retrieving averaged ε's)								
	0	0.40	0.30	0.014	0.013	0.014	0.008	0.007	0.007	0.012
		(2.02	1.49	0.073	0.065	0.072	0.110	0.033	0.034	0.031)
	1	0.37	0.28	0.013	0.012	0.013	0.007	0.006	0.007	0.012
		(1.75	1.44	0.054	0.051	0.057	0.075	0.029	0.033	0.031)
	2	0.33	0.26	0.011	0.011	0.012	0.006	0.005	0.006	0.012
		(1.77	1.20	0.051	0.055	0.060	0.053	0.027	0.031	0.031)

It is natural to link the MODIS day/night LST algorithm to the apparent thermal inertia (ATI) algorithm of the Heat Capacity Mapping Mission (HCMM) sensor [NASA, 1980; Short and Stuart, 1982; Price, 1985; Vukovich, 1984; Majumdar and Bhattacharya, 1990]. The HCMM program was the first NASA research effort directed mainly toward observations on the thermal state of Earth's land surface from an unmanned satellite. The HCMM spacecraft operated between April 1978 and September 1980. MODIS is a much more advanced instrument than HCMM in terms of the thermal remote sensing capability except for the spatial resolution, as shown in Table VIII. The nature of the analog telemetry system onboard the satellite results in some variability in the quality of the HCMM data and the data quality was also influenced by the quality of the receiving station recording [NASA, 1980]. Because there was only one TIR channel on HCMM, it was not possible to make atmospheric and emissivity corrections unless in-situ measurements of atmospheric profiles and surface emissivity were available. The ATI algorithm requires data in the 12-hour day and night coverage for estimate the day/night temperature difference. So cloud cover was a hindrance to the accomplishment of objectives [Short and Stuart, 1982]. The MODIS day/night LST algorithm does not require the 12-hour day and night coverage, it can use daytime and nighttime data collected in several days as long as the surface emissivity does not change significantly. Therefore, the chance to have a pair of daytime and nighttime data both in clear-sky conditions will be much large. It does not assume the same atmospheric conditions for daytime and nighttime because separate atmospheric variables are used for day and night.

Cloud cover is a common problem for visible and infrared remote sensing. Although the day/night LST algorithm can be used for all land surfaces, the main purpose of this algorithm is to retrieve the surface temperature and emissivity in semi-arid and arid regions where the surface emissivity varies in a wide range. The International Satellite Cloud Climatology Project (ISCCP) C2 data from 1984 to 1987 show that the world's desert regions, which result from the sub-tropical anticyclones, are areas of total cloud amount minima, less than 30% or 50% depending on the season [Drake, 1993]. From analysis of weather satellite observations, Chahine shows that the decreases in moisture and cloudiness are coupled with the increase in surface temperature over 304 °K, suggesting a positive feedback from the atmosphere perpetuating the existing desert conditions over dry and hot deserts [Chahine, 1995]. With EOS AM and PM platforms, the chance to have pairs of clear-sky day/night data will be increased significantly, especially in the dry areas.

TABLE VIII. Comparison between HCMM and MODIS TIR channels.

specification	HCMM	MODIS
orbital altitude	620km	705km
resolution	0.6km at nadir	1km at nadir
swath width	716km	2330km
spectral range	10.5-12.5 μm	3.5-14.5 μm
number of TIR channels	1	16
NEΔT	0.4 °K	0.05 °K for surface channels 0.25 °K for sounding channels
quantization	8 bits from analog data	12 bits
positioning error	≈ 3km	< 200m
spatial coverage	direct broadcast to ground stations	gloabl
launch date	April 1978	June 1998
life time	17 months	5 years

3.1.3. Prelaunch Algorithm Development and Validation

Prelaunch versions of the LST algorithms described in this document have been developed for AVHRR and MAS (MODIS Airborne Simulator) data so that the MODIS LST algorithms could be validated in the prelaunch phase.

The validation is a comparison between temperatures retrieved from in-situ measurements and those retrieved from airborne and satellite thermal infrared data. Test sites such as silt playas and inland lakes have been chosen because their in-situ surface temperatures can be measured more accurately. These areas validate primarily the atmospheric correction and emissivity-extraction portions of the MODIS LST algorithms. We also plan to make in-situ measurements of surface temperature for validation over a wider variety of land cover types. After MODIS's launch, these same techniques will be applied to validate the MODIS LST product.

The validation has spectral, spatial, temporal, and angular requirements. For the spectral requirements, spectral emissivities of various cover types need to be measured in order to validate the recovered band-averaged surface emissivities. For spatial requirements, product validation needs to be carried out for different land cover types and different latitudes. This sampling should include a range of surface temperatures and atmospheric conditions. The land cover types will include prototypes of the main groups such as desert, bare soil, crop-land, grassland, forests, water, snow and ice. For unstructured surfaces, the in-situ measurements can be made with transects large enough to represent the aerial pixel average. For structured surfaces, tower or aerial measurements will be required. Ideal test sites are flat areas with size larger than 3km by 3km with uniform or uniformly mixed surfaces so that the uncertainty in spatial sampling is significantly reduced. For in-situ measurements, the short-term changes in temperature are difficult to quantify, so weather conditions for such measurements must be stable (constant wind speed). We have analyzed validation requirements versus spatial and temporal variations of surface temperature for a silt playa [Snyder, et al., 1996(c)]. The requirements for long-term temporal sampling depend on latitude, and can be combined with the requirements for spatial sampling. In other words, we need a seasonal and global range of surface temperatures and atmospheric conditions. Finally, the surface temperature algorithm should be validated over the range of MODIS look angles. Because there is more than one look per day at high latitudes, and because MAS (MODIS Airborne Simulator) views the Earth surface at different look angles, in-situ measurements should be made at multiple view angles at ground validation sites. For daytime measurements, a range of sun angles also must be incorporated for validation of the mid-infrared band processing and for validation of the mixed-temperature model with structured surfaces.

The metric for measures of success for validation will be the difference between the surface temperature estimated from in-situ measurement data and that retrieved from airborne or satellite data. Because there are errors in both the ground measurements and the satellite measurements, the success criterion will depend on the ground measurement accuracy as well as the accuracy of airborne and satellite data. The success criterion will also depend on atmospheric and surface conditions. It is critical to have high quality ground measurements with small temporal and spatial variations in order to reduce the uncertainties in temporal interpolation, spatial sampling, and geometric co-registration. In-situ measurements should include records of the atmospheric and surface weather conditions. After collection, an error analysis of in-situ measurements and the aerial and satellite measurements is required to determine the potential validation accuracy. The LST product will be considered valid when the measurements and error analysis indicate an absolute accuracy of the aerial or satellite measurements of better than 1 °K standard deviation.

Surface temperature measurements can be made with contact sensors, hand-held infrared thermometers as wideband radiometers, and infrared spectrometers. Transects will be made with infrared thermometers. The contact sensors are for surface temperature measurements of water body and flat land surfaces such as playa. The spectrometers do not translate

easily, but they can scan a range of angles to provide temporal and angular spectral surface radiance and atmospheric downwelling radiance (from a diffuse reflector). Temperature is recovered directly from the contact sensors. The downwelling radiance, instrument calibration, and surface emissivity must be applied to compute the temperature from the non-contact sensors. Spectral directional-hemispherical emissivity can be measured with an integrating sphere system which includes a Fourier transform infrared (FTIR) spectrometer and a 5-inch infragold integrating sphere. The spectrometer has sensitivity both in the mid and thermal infrared, covering all MODIS bands of interest for LST. This instrument is primarily used for emissivity measurements of flat samples such as ice, water, silt, sand, soil, leaf surface, etc. The surface roughness of these samples is limited to a few millimeters. Field measurements of BRDF and emissivity are made with the SIBRE (Spectral Infrared Bidirectional Reflectance and Emissivity) instrument, which includes a hemispherical pointing system, FTIR spectrometer, a TIR source, and reference plates. The effect of surface temperature change caused by the thermal source heating is corrected in the processing of data from this instrument [Snyder and Wan, 1996(b)]. Samples are measured with 187 source-sensor geometries. An abbreviated measurement set of 45 geometries is an alternative for materials whose BRDF shapes are reasonably well known. For each geometry, there are 1232 spectral samples from 3.3 to 14.5 microns. These can be integrated to provide band-averaged values for MODIS or MAS. The spot size viewed by the InSb/MCT sandwich detector is approximately 3cm diameter so materials with some small-scale surface structure can be examined. We also have a beam expander that gives a 10cm spot for more structured surfaces. In addition, we can recover angular spectral emissivity (but not BRDF) from absolute radiance measurements by the use of a sun-shadow technique. Our goal for the sun-shadow method [Wan et al., 1996] is to increase the spot size to an half meter so that band-averaged emissivities and radiometric temperature of structured surfaces, such as vegetation canopy, can be measured.

We validated the sun-shadow method with measuring samples of soil, sands, grass and a black aluminum plate on the roof platform of our building at UCSB on January 19th and 26th, 1996. The solar beam is blocked for half of the samples. The TIR spectrometer views the portions in sunshine and in shadow for two separate measurements and also views a diffuse reflecting gold plate in the same spots for providing information of the solar and atmospheric downwelling radiation. After calibrating the spectrometer with blackbody at three different temperatures, another two separate measurements are made. For each sample, we obtained two pairs of data for the sunshine and shadow portions, and the diffuse reflecting gold plate. A band average procedure with the spectral response functions in seven MODIS TIR bands (i.e., 20, 22, 23, 29, 31-33) is used to achieve a high signal-to-noise ratio. Radiometric calibration is made with three blackbody temperatures, spectral emissivity of the blackbody surface and the front mirror, and the temperature of the front mirror. Then we use two methods to recover the surface temperature. In the conventional method, we use the spectral emissivity curves of samples measured with the integrating sphere system. In the sun-shadow method, we make non-linear χ^2 fit of the sun-shadow data set for recovering surface temperatures in sunshine and in shadow, and the band-averaged emissivities. The LST values of samples of sand, soil, grass and black plate in sunshine and in shadow recovered by these two methods are shown in Fig. 10. Note that the mark squares represent the first method. The standard deviations are 0.4 °K and 0.1 °K, the maximum LST differences are 0.7 °K and 0.2 °K, for the LST difference in sunshine and in shadow, respectively.

We conducted a field campaign jointly with the JPL (Jet Propulsion Laboratory) ASTER team at a large flat silt playa in Railroad Valley, Nevada, on August 3rd, 1995. MAS and TIMS (Thermal Imaging Multispectral Spectrometer) data, and field measurement data of surface spectral emissivity and temperature with TIR spectrometer and broadband radiometer were collected. Temporal and spatial analysis has been made. As shown in Table IX, LST retrieved from MAS data with the generalized split-window LST algorithm at view angle (θ_v) 18.75 ° agrees with field measurement LST values within 1 °K. In this case, the LST accuracy is mainly limited by the uncertainty in its spatial variation. The MAS was calibrated with the

new method [King et al., 1996]. Three field campaigns have been conducted in 1996. The first one was conducted over a snow field at the test site in Mammoth Lakes, California, on April 2nd, 1996. The second one was conducted jointly with other EOS teams at the same silt playa site in Railroad Valley, Nevada, on June 4th, 1996. The third one was conducted in the southern BOREAS test site on 14 August, 1996. MAS data and field measurement data were collected in early afternoon and evening during the first two field campaigns. In the field campaign at the playa site on 4 June 1996, surface temperatures were measured by three different methods: a TIR spectrometer, an infrared thermometer, and a thermistor 1mm beneath the surface. The surface temperature is also recovered from MAS data by the use of the generalized split-window and day/night LST algorithms. These results are shown in Fig. 11. Except the daytime temperature measured by the thermistor beneath the surface (it may differ from the surface temperature because of the variation in surface energy balance caused by the changing wind speed), the surface temperature values given by five methods are all within 1 °C. The band emissivities retrieved by the day/night LST method are lower than the values measured from playa samples, which were collected at the test sites, by 0.02 in bands 31-33, and 0.09 in bands 20, 22, and 23. Note the significant fluctuations in the daytime surface temperature caused by the change in wind speed.

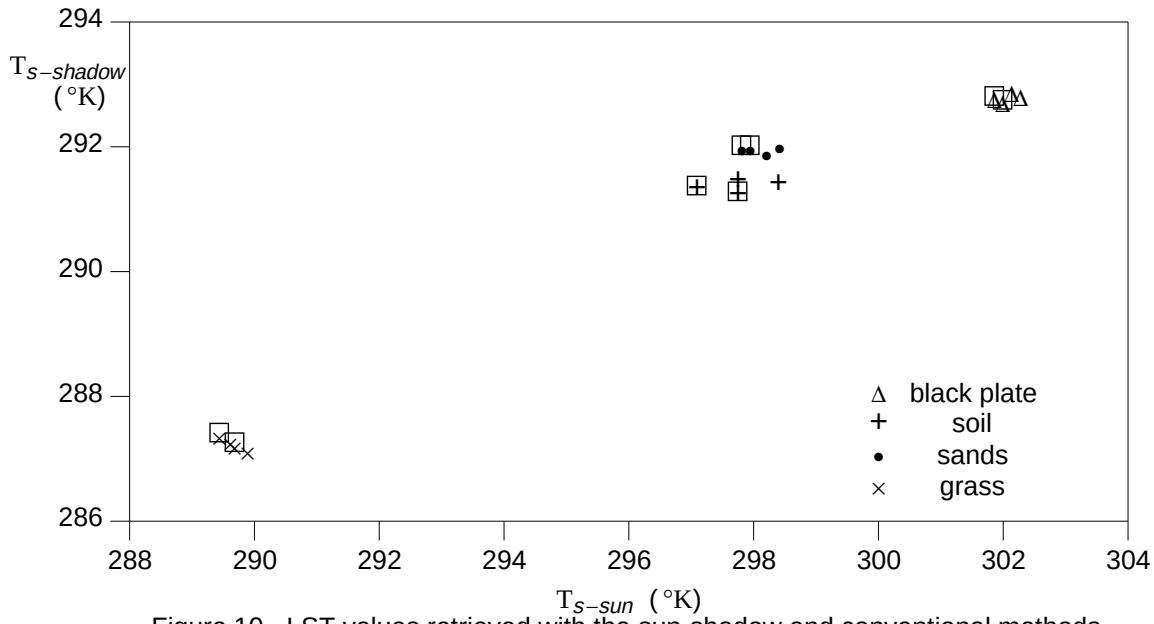

Figure 10, LST values retrieved with the sun-shadow and conventional methods.

TABLE IX. Summary of LST values over the test site (38' 31.46'N, 115' 42.74'W) in Railroad Valley, Nevada, during 1:22 and 1:30 PDT on 8/3/95. The size of one MAS pixel is approximately 50m by 50m.

size of area	mean (°C)	stdv (°C)	remarks
12 cm diameter	58.5		by radiometer
5 cm diameter	59.2		by spectrometer at θ_v 20°
1 MAS pixel	59.1		at θ_v 18.75°
3 by 3 MAS pixels	58.9	0.48	
5 by 5 MAS pixels	58.8	0.67	
7 by 7 MAS pixels	58.9	0.76	
9 by 9 MAS pixels	59.0	0.81	
11 by 11 MAS pixels	58.9	0.82	
21 by 21 MAS pixels	58.9	1.21	

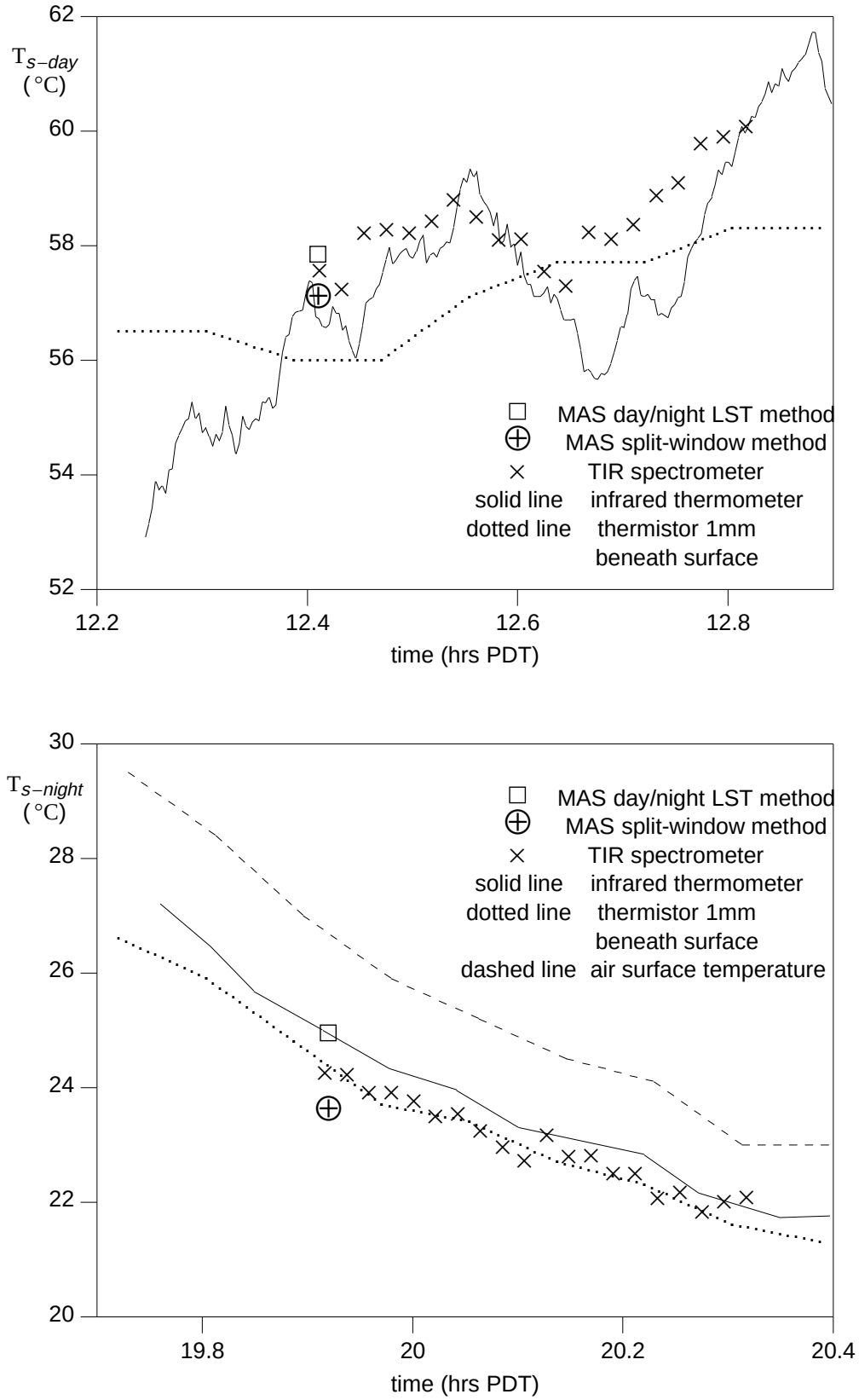

Figure 11, LST measured at a playa site in Railroad Valley, ND, on 4 June, 1996.

3.1.4. Variance and Uncertainty Estimates

For variance and uncertainty estimates, we use the multi-channel SST algorithm in (14) as an approximation of the generalized split-window LST algorithm for lake surfaces and dense vegetation canopies. We express the band brightness temperature T_i as a sum of the accurate value $\hat{T}_i$, a systematic error ΔT_i, and a random error δT_i. Similarly for the surface temperature T_s. And assume that $\Delta T_5 \approx \Delta T_4$ and $|\delta T_5| \approx |\delta T_4|$. Substituting them into (14), we get

$$\Delta T_s = 3.6125\Delta T_4 - 2.5779\,\Delta T_5 \approx \Delta T_i \tag{22-1}$$

and

$$\delta T_s = 3.6125\delta T_4 + 2.5779\,\delta T_5 \approx 6.19\,\delta T_i \tag{22-2}$$

Actually, the numerical factor on the right side of (22-2) increases with the viewing angle and the amount of the column water vapor according to our analysis of the generalized split-window LST algorithm.

3.1.4.1. Error estimates relevant to the MODIS instrument

Absolute and relative calibration accuracies. According to the accuracy budget for the MODIS internal blackbody in Hughes SBRC document 93-0204-00 (March 24, 1993), the accuracy of transfer to NIST is 0.4% for bands 31 and 32, and 0.5% for other emissive bands. An accuracy of 0.4% corresponds to a ΔT_s of approximately 0.3 °K at the typical temperature 300 °K. In order to achieve the LST absolute accuracy of 1 °K, δT_s should be less than 0.7 °K. According to (22-2), this requires δT_i to be less than 0.1 °K. The SST accuracy 0.3 °K requires δT_i to be less than 0.05 °K. This means that SST and LST require a relative calibration accuracy at the level of noise equivalent differential temperature NEΔT (Section 3.4.5.3.1 in the MODIS specifications, on Relative Radiometric Accuracy over the full range of spectral radiance) and the sensitivity of the split-window LST algorithm to the random error in band radiances (related to its relative calibration accuracy) is five times stronger than the sensitivity to its systematic error. It may be possible to reduce the absolute radiometric uncertainty of the MODIS emissive bands designed for surface temperature measurements to 0.5% through accurate ground-based calibrations by the use of high altitude lakes if MODIS performs according to or better than its specifications. This gives an uncertainty of 0.35 °K in band brightness temperatures.

Spectral response function. The spectral response function (SRF) of each emissive band should be measured over the entire wavelength range from visible to LWIR for the MODIS engineering and in-flight models. The accuracy of relative SRF should be better than 0.01% so that measured thermal infrared radiance could be accurately converted to band brightness temperature and it is possible to measure instrument characteristics including SNR, linearity, wavelength shift, and stray light effect [Hughes SBRC document 93-0204-00, March 24, 1993]. It has been noted [Khattak et al., 1991; Brush, 1993] that AVHRR channel 4 on the NOAA-12 satellite is subject to errors when sunglint occurs, but channel 5 looks unaffected. Compared with thermal infrared radiation emitted from the sea surface, the reflected solar beam radiation in the 8-13 μm range is almost negligible. It seems that this channel is not completely insensitive to the reflected solar radiation in the visible and near infrared range. Solar radiation in the visible range is two orders of magnitude larger than the thermal radiation at 300 °K in the MODIS bands 31 and 32, and at least one more order of magnitude larger in MODIS band 20. So the total out-of-band (OOB) response of MODIS emissive bands 29, 31 and 32 over the entire visible / near infrared range should be at the 10^{-4} level in order to meet the radiometric accuracy of 1%. A more strict OOB, at the 10^{-6} level, is required for bands 20, 22 and 23. If these OOB requirements cannot be achieved, it is impossible to simply use these MODIS emissive bands to accurately estimate the surface temperature in sunglint areas and for land cover types that are highly reflective in the visible / near infrared range, such as snow cover. MODIS bands in the visible and near infrared

range, and surface albedo values in these bands would be used to convert radiance values in the MODIS emissive bands into band brightness temperature. This means that the LST algorithm will be too complicated to achieve a good accuracy.

Optical system noise equivalent differential temperature (NEΔT). The NEΔT requirement of 0.05 °K is critical to SST and LST products. NEΔT, or equivalently signal-to-noise ratio, shall be determined for all bands at a minimum of three equally spaced spectral radiance levels between 0.3 $L_{typical}$ and 0.9 L_{max} to characterize the signal dependence of the system noise (Section 3.4.5.5 in the MODIS specifications).

Quantization noise equivalent differential temperature (NEΔT'). In order to characterize system noise equivalent differential temperature (NEΔT) and radiance (NEΔL) pre-launch, NEΔT' must be much less than NEΔT. Otherwise, quantization will limit MODIS emissive bands and it will be impossible to measure system noise characteristics for potential improvement of data quality in the long run. Radiative transfer simulations show that in the clear-sky ''average'' tropical atmospheric condition, the brightness temperature of AVHRR band 5 at a zenith angle of 54 ° changes only 0.035 °K as water surface temperature changes by 0.20 °K. Note that the maximum viewing angle of MODIS at the Earth surface could be up to 65 ° from nadir. Nonlinear quantization was required for MODIS bands 31 and 32 in the original specifications. In light of descope, it has been changed to linear quantization and the T_{max} was increased from 324 °K to 400 °K for both bands 31 and 32 in order to see small-size fires without saturation. The major effect of increasing T_{max} to 400 °K is that the radiometric dynamic range of bands 31 and 32 would be increased by 120% so that NEΔT' is larger. At a low temperature, 233 °K, NEΔT' will be 0.11 °K so that the quantization alone would contribute an error of approximately 0.7 °K into the surface temperature estimated with the split-window method. Therefore, the LST accuracy will be affected in the cold range.

Pointing knowledge and accuracy. The specification for MODIS pointing knowledge and accuracy is 90 arc seconds, which corresponds to approximately 200m on the ground. It is expected that the initial post-launch knowledge of pointing accuracy may be larger than 1km so that post-launch ground-based vicarious calibration activities and processing will be required to validate the geometric accuracy and to reach the specification of pointing knowledge and accuracy. This process may take several months. Therefore, it is proposed to apply the day/night LST method to pairs of daytime and nighttime data at a resolution of 5km in the first half year after launch.

3.1.4.2. Uncertainties within the LST algorithms

For uniform land surfaces with known spectral emissivity characteristics, the uncertainty in LST retrieved by the generalized split-window LST algorithm could be equal to or smaller than 0.5 °K [Wan and Dozier, 1989; Li and Becker, 1993]. The most difficult part is for pixels at the maximum scanning angle ±55 °, for which local viewing zenith angle is approximately 65 °. This difficulty has been overcome through the following improvements: 1) viewing angle considered in the algorithm; 2) the LST algorithm optimized over column water vapor and temperature ranges.

The uncertainty in day/night registration of MODIS data may be a major error source for the day/night LST algorithm. Numerical simulations have been made to evaluate the sensitivity of the day/night LST algorithm to the uncertainty in day/night registration. We assume that a vegetation component is mixed with another terrestrial material in the 80-sample database. It is assumed that the daytime proportion of the vegetation component in a mixed pixel is 0.5 and the nighttime proportion varies from 0.5 to 0.2 for simulating the mis-registration effect. The daytime canopy temperature of the vegetation component is given three values: the same surface temperature as for the another component, 4 °K warmer or cooler than the surface temperature of the another component. Its nighttime temperature is assumed to be equal to the surface temperature of the another component. The mid-latitude summer atmosphere is used in this simulation study. Note

that the same NEΔT values and the systematic calibration error 0.5% used in typical numerical experiments for the day/night LST algorithm are also used in this sensitivity study. The rms and maximum errors in surface temperatures and band emissivities retrieved by the χ^2 fitting day/night LST algorithm are shown in Table X. The band emissivities of the mixed pixel are calculated from the band emissivities in the database and the proportions. The average values of calculated daytime and nighttime band emissivities are used as the target values for retrieval. Results in Table X indicate that the day/night LST algorithm still works well as long as the nighttime proportion of the vegetation component is not smaller than 0.35, differing from the daytime proportion by less than 30%. This corresponds to a mis-registration 15% or 30%, depending on how the vegetation component distributed in the mixed pixel.

TABLE X. The sensitivity of surface emissivities and temperature retrieved by the χ^2 fit day/night LST algorithm to uncertainties in day/night registration. The proportion of vegetation within a mixed pixel in daytime differs from that in nighttime because of mis-registration.

P (veg)		rms errors					maximum errors				
day	night	δT_{s-d} (°K)	δT_{s-n} (°K)	$\delta\varepsilon_{20}$	$\delta\varepsilon_{31}$	$\delta\varepsilon_{32}$	ΔT_{s-d} (°K)	ΔT_{s-n} (°K)	$\Delta\varepsilon_{20}$	$\Delta\varepsilon_{31}$	$\Delta\varepsilon_{32}$
		$T_{s-d}(veg) - T_{s-d}(\text{background}) = -4$ °K									
0.5	0.5	0.35	0.24	0.011	0.007	0.008	3.1	1.5	0.090	0.041	0.040
0.5	0.45	0.35	0.25	0.012	0.008	0.009	1.8	1.2	0.059	0.029	0.035
0.5	0.4	0.37	0.29	0.014	0.008	0.010	1.8	2.2	0.092	0.035	0.041
0.5	0.35	0.44	0.36	0.016	0.010	0.012	2.6	3.4	0.130	0.060	0.060
0.5	0.3	0.46	0.41	0.018	0.011	0.014	2.9	3.5	0.145	0.074	0.078
0.5	0.25	0.56	0.51	0.022	0.013	0.017	4.2	4.5	0.182	0.086	0.081
0.5	0.2	0.61	0.57	0.023	0.015	0.018	4.1	3.4	0.185	0.144	0.101
		$T_{s-d}(veg) - T_{s-d}(\text{background}) = 0$ °K									
0.5	0.5	0.36	0.26	0.012	0.007	0.009	2.3	1.5	0.068	0.031	0.037
0.5	0.45	0.38	0.27	0.013	0.008	0.010	2.1	1.5	0.068	0.037	0.037
0.5	0.4	0.38	0.30	0.014	0.009	0.011	1.8	1.9	0.082	0.036	0.038
0.5	0.35	0.43	0.36	0.016	0.010	0.013	2.6	2.8	0.109	0.047	0.048
0.5	0.3	0.46	0.44	0.019	0.012	0.015	2.9	4.7	0.183	0.083	0.074
0.5	0.25	0.52	0.51	0.021	0.013	0.017	3.7	3.6	0.171	0.068	0.077
0.5	0.2	0.58	0.59	0.023	0.015	0.019	4.4	4.3	0.150	0.185	0.091
		$T_{s-d}(veg) - T_{s-d}(\text{background}) = 4$ °K									
0.5	0.5	0.39	0.25	0.011	0.007	0.009	3.2	1.5	0.088	0.037	0.037
0.5	0.45	0.40	0.26	0.012	0.008	0.010	2.4	1.4	0.069	0.033	0.037
0.5	0.4	0.45	0.32	0.014	0.009	0.012	2.6	2.3	0.096	0.039	0.046
0.5	0.35	0.50	0.38	0.016	0.011	0.014	2.9	3.3	0.128	0.059	0.059
0.5	0.3	0.57	0.45	0.019	0.012	0.016	4.0	4.5	0.178	0.083	0.068
0.5	0.25	0.65	0.54	0.021	0.014	0.018	4.7	4.3	0.163	0.072	0.062
0.5	0.2	0.73	0.62	0.024	0.015	0.020	5.3	3.9	0.182	0.063	0.068

3.1.4.3. Uncertainties in the emissivity knowledge base

It is expected that the uncertainty in the emissivity knowledge base of most land cover types is approximately ±0.005.

3.1.4.4. Root Sum Square (RSS) of uncertainties

The individual uncertainties above are combined by the use of the RSS technique [Asrar et al., 1988; Cooper and Asrar, 1989]. The RSS of uncertainties in LST retrieved by the generalized split-window LST algorithm in the T_{air} range 280-310°K is shown in Table XI. It is obvious that the RSS error depends on viewing angle and atmospheric column water vapor. Note that the range of $T_s - T_{air}$ is assumed to be from -16 °K to +16 °K in this error analysis.

TABLE XI. Error estimate by RSS of the generalized multichannel MODIS LST algorithm (the instrument calibration error 0.35 °*K* included).

uncertainties	viewing angle					
	14.9°	38.6°	51.2°	58.0°	61.6°	65.5°
	column water vapor 2-2.5cm					
error in algorithm	0.26	0.29	0.33	0.38	0.42	0.46
0.005 in mean ε	0.33	0.33	0.33	0.33	0.33	0.33
0.005 in Δε	0.62	0.64	0.66	0.67	0.68	0.68
error due to NEΔT (0.05 °K)	0.3	0.3	0.3	0.3	0.3	0.3
calibration error (°K)	0.35	0.35	0.35	0.35	0.35	0.35
RSS (°K)	0.88	0.90	0.93	0.96	0.98	1.0
	column water vapor 3-3.5cm					
error in algorithm	0.37	0.42	0.50	0.58	0.64	0.80
0.005 in mean ε	0.31	0.31	0.31	0.31	0.30	0.30
0.005 in Δε	0.57	0.60	0.63	0.65	0.65	0.64
error due to NEΔT (0.05 °K)	0.3	0.3	0.3	0.3	0.3	0.3
calibration error (°K)	0.35	0.35	0.35	0.35	0.35	0.35
RSS (°K)	0.88	0.92	0.98	1.03	1.07	1.16
	column water vapor 4-4.5cm					
error in algorithm	0.42	0.52	0.71	0.97	1.18	1.47
0.005 in mean ε	0.29	0.28	0.27	0.26	0.26	0.26
0.005 in Δε	0.55	0.58	0.61	0.58	0.54	0.47
error due to NEΔT (0.05 °K)	0.3	0.3	0.3	0.3	0.3	0.3
calibration error (°K)	0.35	0.35	0.35	0.35	0.35	0.35
RSS (°K)	0.88	0.95	1.08	1.25	1.40	1.63

We have included the effects of NEΔT and calibration error in the error analysis of the day/night LST algorithm for 80 surface samples and their mixtures in mid-latitude summer and ‘‘US standard’’ atmospheric conditions. We will extend the analysis to other atmospheric conditions in wide ranges of viewing and solar angles.

3.2. Practical Considerations

3.2.1. Numerical Computation Considerations

As discussed in Section 3.1, a practical solution for the LST problem consists of two major parts. Main tasks in the first part are to establish a generalized split-window LST algorithm to retrieve LST for pixels with known band emissivities. The

band emissivities are inferred from the land-cover type based on the previous month's MODIS land-cover product. The IGBP-type 1-km global vegetation database will be used at-launch as an alternative to the MODIS land-cover data. The numerical form of the generalized split-window LST algorithm is a linear equation of the band brightness temperatures of MODIS bands 31 and 32. A built-in look-up table in steps of 0.1 °K will be used to convert the band radiance into band brightness temperature. This LST algorithm will be very efficient in the processing. Main tasks in the second part are to establish a database of atmospheric look-up tables for MODIS bands 20, 22, 23, 29, 31-33, and to develop the day/night LST algorithm for retrieving surface band emissivities and temperature for pixels with highly variable emissivities through the statistical regression approach and χ^2 fit approach. The data-base obtained from accurate atmospheric radiative transfer simulations and look-up tables and interpolation methods will be used in these algorithms for numerical efficiency. The bubble chart for the LST generation process is shown in Fig. 12. Input data will be described in the section of Data Dependencies (3.2.6). The LST process is working on the granule basis. Each granule covers four or more tiles. The global sinusoidal grids system is divided into a large number of tiles, each with a nominal size of 1100 km by 1100 km (10 ° by 10 ° on the equator). An internal file of intermediate data, named MOD.AM1.V1.lst_update.TILE, will be used in the process MOD_PR11 for each tile. This file stores the most updated clear-sky data for brightness temperatures in MODIS bands 20, 22, 23, 29, 31-33, atmospheric temperature and water vapor profiles at lower levels, date and observation time, view angle, and related QA flags for both daytime and nighttime, and solar zenith angle, NDVI, condensed information of land-cover for daytime. The at-launch IGBP-type global vegetation database and NDVI will be used to distinguish pixels (class A) covered by dense vegetation, water, snow and ice from others (class B) in barren lands, including bare soils, semi-arid and arid regions. The generalized split-window LST algorithm will be applied to class A pixels for generating the level-2 LST product at 1km resolution. As doing an experiment, we used the global land-cover classification database (named VEG_CLSS) in the Global Data Sets for Land-Atmosphere Models, ISLSCP Initiative 1: 1987-1988, Volumes 1-5, which is available in CD-ROM from NASA Goddard DAAC Science Data Center. The spatial resolution of this database is 1 by 1 degree latitude/longitude. We can delineate semi-arid and arid regions which generally agree well with the dry regions defined by climatology [Trewartha and Horn, 1980].

The major steps in the LST process for each granule of 100 MODIS scan cube (1000 scan lines with 1354 1km-resolution samples each line) are described in the following.

1) input one tile of the previous quarter's land cover product and the intermediate file MOD.AM1.lst_update.TILE.

2) input N scan-lines of MODIS geolocation 1A and 1B data and level-2 MODIS products (cloud mask, atmospheric profiles, snow, NDVI) used as input to the LST process.

3) search for clear-sky pixels by the use of the MODIS cloud mask product, skip cloudy pixels.

4) find the grids covered with each clear-sky pixel, and calculate their coverages.

5) determine pixels with known band emissivities by the use of the previous quarter's land-cover product, MODIS snow cover, and NDVI products. These products can be used to identify dense vegetation (evergreen needleleaf forest, evergreen broadleaf forest, deciduous needleleaf forest, deciduous broadleaf forest, grasslands, croplands, if NDVI > 0.8), water, snow, ice. Their emissivities in bands 31 and 32 can be calculated from the coverages of these land cover types and the emissivity knowledge base. Then LST can be retrieved with the generalized split-window LST algorithm.

5') for other pixels, retrieve LST with the generalized split-window algorithm by the use of the emissivity values in bands 31 and 32 that were retrieved by the day/night algorithm in previous days. This retrieved LST needs to be compared with and may be refined by the values retrieved by the day/night algorithm later.

6) calculate and accumulate the values at each grid that will be used in the day/night LST algorithm.

7) back to (2) if the granule is not completed.

8) find new pairs of daytime and nighttime co-registered pixels

9) proceed the statistical regression approach for the day/night LST method to retrieve surface temperatures and emissivities.

10) proceed the χ^2 fit approach of the day/night LST method for pixels in which the MODIS atmospheric temperature and water vapor profiles product has high quality.

11) L3 LST quality assessment. The LST retrieved by the day/night algorithm will be compared with and may be refined or replaced by the values retrieved by the generalized split-window algorithm, especially for land cover types with high and stable emissivities in bands 31 and 32.

12) output L3 LST for the tile.

13) update and output the intermediate tile file.

14) L2 LST quality assessment.

15) output N scan-lines of L2 LST.

16) go to 1) if there is more tiles.

The value of N in 2) is determined by the memory requirement and the size of the main memory on the CPU. We use 50 as its initial value. If N equals to the total number of scan lines in the granule, step 7) will be skipped. If the computer system has enough main memory, all tiles can be processed with only one-time input of the granule files. But most likely it is not the case in the beginning of the at-launch processing.

The development of the LST algorithms depends on measured data of spectral response functions of MODIS bands 20, 22, 23, 29, 31-33. A prototype AVHRR-type LST code was developed and submitted to SDST in early 1994. Beta versions of MODIS LST codes were developed and submitted to SDST in 1994 and 1995. Version 1 of the LST code will be delivered in 1996. It will be updated on basis of the data of the Protoflight Model and be delivered as version 2 in 1997. The final launch version of the LST code will be delivered in January of 1998.

As ground-based calibration and validation data become available after launch, the LST algorithm may need some minor adjustments and refinements. A version number should be attached to each LST data product. It is expected that the LST product will be reprocessed only if the temperature difference is larger than 0.5 °K for one or more major land cover types.

It is expected that a major change may occur after the first EOS AM platform operates for one or one and a half years. At that time, MODIS atmospheric products [King et al., 1992] and land products (land-cover, snow, NDVI, and BRDF) will be also validated. These products can be better used in the LST production for quantitative analysis of the viewing angle effect in retrieved LST values, especially in the level 3 LST product. The major change also involves refinements of the land-surface emissivity knowledge base according to results from validating the MODIS LST product (including land-surface emissivity and temperature parameters) with field measurements and MAS data. After one-year operation of the first EOS AM platform, the chance to get a complete global coverage of land-surface emissivities will be much better, so it may be worth reprocessing the LST product.

The MODIS day/night LST algorithm at launch of the first EOS PM platform will work much better because the probability of having pairs of daytime and nighttime MODIS data in clear-sky conditions would increase by a factor of 4 over the AM data only. With MODIS data from both EOS AM and PM platforms, LST can be retrieved four times each day for most of the Earth's land surface, so the diurnal features in retrieved LST can be better used for various applications.

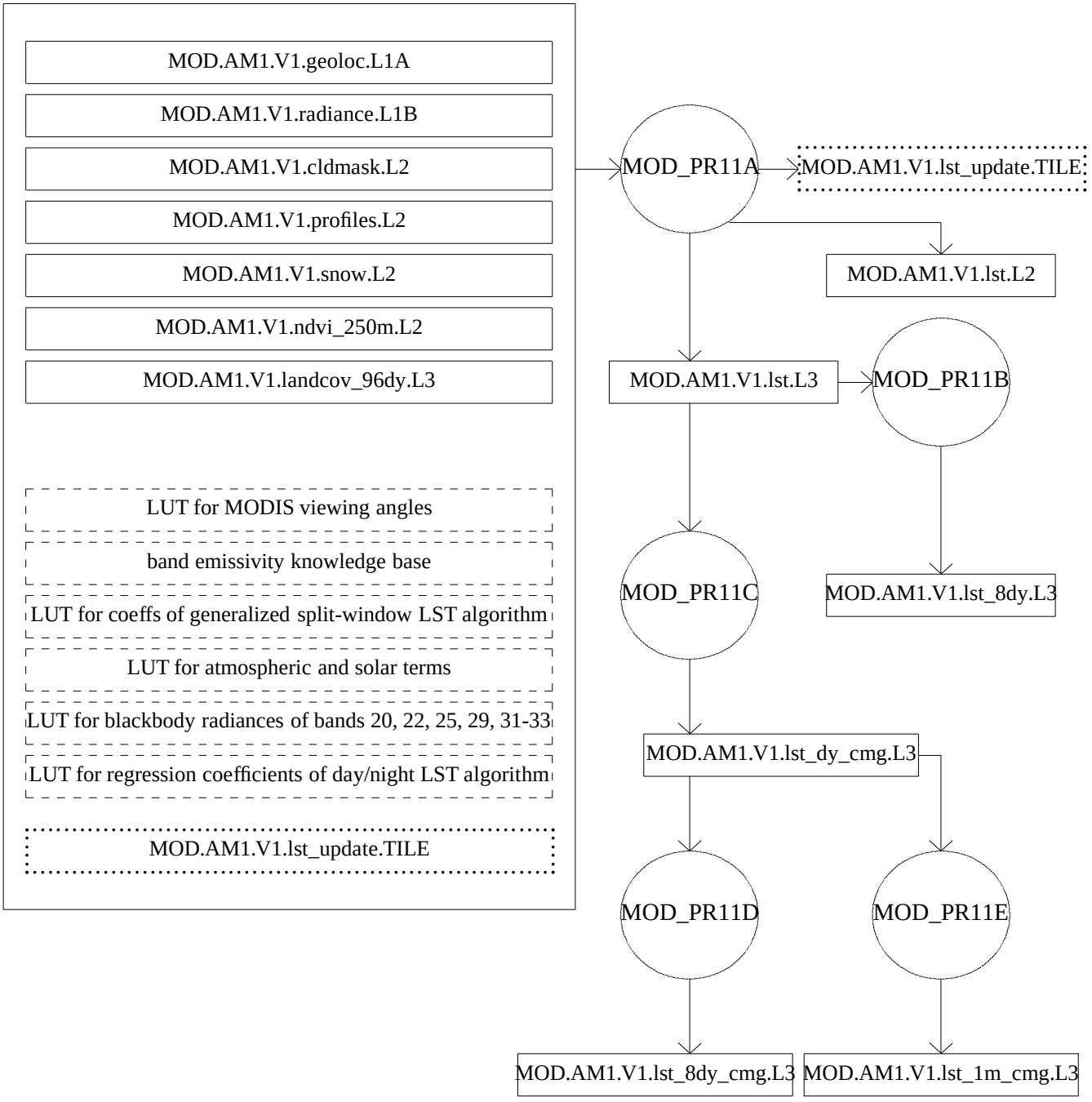

designed by Z. Wan 10/19/96

Figure 12. Bubble chart for MOD_PR11

3.2.2. Programming/Procedural Considerations

3.2.2.1. Programming Considerations

Look-up tables will be used to increase the computational efficiency as long as the LST accuracy requirement is secure. Possible look-up tables include one for conversion of scan number to cosine of the viewing angle at the Earth's surface, one for conversion of band radiance to band brightness temperature, one for atmospheric and solar radiation terms in (10).

3.2.2.2. Procedural Considerations

All procedures will be automatic.

3.2.2.3. Registration

Registration and resampling into spatial resolution 1 km will be made after the level-2 LST processing when possible in order to avoid degradation in radiometric accuracy caused by resampling. But co-registration is required in the day/night method to retrieve surface band emissivities for some land cover types with highly variable surface emissivities. Thus the day/night processing must be done after the registration and resampling.

3.2.2.4. Processing Estimate

The land surface of the Earth is approximately 1.5×10^8 sq. km. Considering some overlap of MODIS data in the high latitude region, the daily total number of pixels of land surface is approximately 2×10^8. Assuming 30% cloud-free, approximately 6×10^7 pixels are needed for LST processing. On the average, half of these pixels (3×10^7) are in the day mode. The generalized split-window LST algorithm needs 1000 flops per pixel, giving 6×10^{10} flops. Geolocation processing needs approximately 9×10^{10} flops. Adding together, it results in a need for approximately 1.5×10^{11} flops to process the LST product each day, processing rate being roughly 17 MFLOPS. Plus 15-20% overhead for I/O operations results in 20 MFLOPS. It is estimated that additional 20 MFLOPS be required for simultaneous estimation of surface emissivity and temperature in some areas under favorable conditions.

In order to reduce the overhead for I/O operations, it is desirable to input all data into core memory in a granule of 100 MODIS scan cube (1354 samples per scan line by 10 scan lines per scan cube by 100 scan cubes equals to 1354000 samples). There are 585.5 granules each day, the corresponding flops per granule is 310 MFLOPs per granule. Parallel processing is allowed for the LST process on different tiles.

3.2.3. Postlaunch Validation

The MODIS Land group will select approximately 60 sites globally to validate MODIS land products, and LTER sites will be considered as potential candidate sites. In addition to these sites, several lakes including Mono Lake and Lake Tahoe will also be used as validation sites for the LST algorithm. It is critical to select validation sites in relatively uniform and flat areas so that high quality field measurement data can be obtained for validation. Portable radiometers and a TIR spectrometer will be calibrated with the same blackbody radiation source. The former will be used to measure the surface temperature in a transect and the latter will be used at a few points to make temporal and angular measurements so that spatial and temporal variations of the surface temperature within a MODIS pixel can be analyzed. MAS flight data will be used for regional validation of LST. Information on atmospheric conditions is desirable in radiative transfer simulations for atmospheric corrections in retrieving land surface emissivity and temperature from field measurement data. According to our experience in field measurements for validation of the LST algorithms in the last two years, the temporal and spatial

variations in LST are the primary problems. In order to solve these problems, we need more thermistors with light and inexpensive automatic data recording systems and distribute them in test site of 2km by 2km. The total number of thermistors depends on the surface conditions and accuracy requirements [Snyder et al., 1996].

The EOS AM-1 land surface temperature product from ASTER data will be used for comparison with and spatial variation analysis of the MODIS LST product over test sites. The EOS PM-1 land surface temperature and emissivity product from AIRS data will be used for comparison with the MODIS LST product at coarse resolutions.

It is very important to find some good ground sites for validating the absolute calibration of the MODIS thermal bands. Radiative transfer simulations show that the atmospheric transmission function for mid-latitude summer atmosphere over a lake surface at elevation 4 km above sea level in a dry region is larger than 0.95 for most of the $10-13\,\mu m$ atmospheric window, and that the difference between the radiance at the top of the atmosphere and the upwelling radiance at the lake surface is less than 1% for the wavelength range from 10.4 to 12 μm. If a fair knowledge of atmospheric temperature and water vapor profiles is available, it seems not difficult to make an atmospheric correction to achieve an accuracy better than 0.5% for ground-based calibrations. The major uncertainty will be in measurements of the lake surface temperature. We need to make very accurate radiometric measurements. Or if we can find some partially frozen alpine lakes, then the temperature of the free water surface area is believed to be very close to $0\,°C$ without measurements. Several such lakes exist in the Tibet region. Nam Co (Tengri Nor) is located at 30.40N, 90.30E with average length 80km and width 50km at elevation of 4718m above sea level, and a frozen period of November - May. It is located approximately 100km north-west of Lhasa. It will be an ideal TIR calibration site for meteorological satellites and EOS sensors if an international joint project can be organized with funding from participating countries so that a permanent station could be established. Even without a permanent station, it can still be used as a validation site occasionally, once a year or every two years. More Tibet lakes will increase the chance for suitable validations without much ground support. An alternative high-altitude lake is Lake Titicaca which lies across the border between Peru and Bolivia. It is a large (8,100 km^2), high-altitude (3,808 m), tropical ($16\,°$ S) lake. There are four major components in the postlaunch LST validation plan as shown in Table XII: 1) participating in the MODLAND tiers 1-4 validation activities; 2) participating in the MODATM validation activities when the measurement of the clear-sky atmospheric conditions over lands is one of the primary purposes; 3) LST-specific validation activities in California and Western US states in different seasons labeled by S in Table x; 4) limited activities for validation/calibration of the MODIS TIR bands. A close collaboration with the ASTER Science Team and some LST groups in other countries have been established. It will be continued and enhanced. Two small groups (2-3 persons each group) will be formed in the MODIS LST team to conduct the validation activities of the LST product. Each group will be equipped one TIR spectrometer, several infrared thermometers and 8-16 simple thermistor systems. One group will mainly conduct validation activities in California and Western US states at variable sampling frequencies to capture the seasonal or interannual variabilities. A grassland in approximately 100 miles north of Santa Barbara will be visited each quarter or every six months. Another group will join the first group to make field measurements at another site or participate in the MODLAND and MODATM validation activities whenever the test site and schedule are appropriate. Aircraft MAS flight hours will be requested for some of the planned field campaigns.

All vicarious calibration/validation field measurement data will be archived at the designated DAAC for field data and related aircraft data. The field measurement data and related aircraft data will be also archived on CD-ROMs at the team member science computing facility. EOS investigators are encouraged to use these archived data.

3.2.4. Quality Control and Diagnostics

TABLE XII. Major postlaunch validation activities for MODIS LST products.

field campaigns (type)	1998 Q1	1998 Q2	1998 Q3	1998 Q4	1999 Q1	1999 Q2	1999 Q3	1999 Q4	2000 Q1	2000 Q2	2000 Q3	2000 Q4
MODLAND (tiers 1-4 val)							Africa				TBD	
MODATM (joint val)			ARM-1				Mid-Atlantic					
MOD-LST (tier 4, val in CA & W. US)			S	S	S	S	S	S	S	S	S	S
MOD-LST (tier 5, TIR cal)				Tibet or Bolivia								Tibet or Bolivia

There are two types of quality controls. The first one is automatic quality control on a routine basis to be performed at DAAC. For simplicity, quality flags will be provided for each LST pixel so that a quality image corresponds to a LST image. The quality flag indicates the confidence in LST processing. It will be determined by comparing LST values retrieved from the generalized split-window algorithm to those retrieved from the day/night LST algorithm and by considering the following factors: 1) radiometric calibration accuracy and geometric pointing knowledge of MODIS data; 2) spatial variations in band brightness temperatures and NDVI values; 3) confidence in land-cover classification; 4) emissivity uncertainty; 5) land-cover mixture and regional topographic effects; 6) cirrus effect; 7) others to be determined.

Van De Griend and Owe [1993] show that the thermal emissivity ε in spectral range 8-14 μm is highly correlated with NDVI for different surface types

$$\varepsilon = a + b \ln(\mathrm{NDVI}) \quad . \tag{23}$$

The MODIS Vegetation Indices will be useful to estimate green cover percentage [Jasinski, 1990; Carlson, 1991; Kerr et al., 1992; Running et al., 1994] for estimation of emissivities in mixed pixels. In arid and semi-arid regions, surface emissivity varies strongly with vegetation coverage because of the distinct difference in emissivities of vegetation and rock/sands. This correlation and the seasonal change in band emissivities retrieved by the day/night LST algorithm can also be used in quality assessment of the LST product.

Comprehensive quality diagnostics and assessment will be made at P.I.'s SCF by the use of validation data at test sites. Validation data include ground spectrometric measurement data, MAS flight data, and radiosonde data if available. ASTER data will be used for analysis of land cover mixture and sub-pixel spatial variation in MODIS LST pixels.

3.2.5. Exception Handling

Cloud pixels identified by the cloud mask will be skipped. Pixels with bad data will also be skipped and flagged.

3.2.6. Data Dependencies

Input data for the LST process are given in Table XIII. For the at-launch LST product, input data include MODIS level-1A geolocation data, level-1B TIR band radiance data (Parameter No. 2338), classification masks (Parameter No. 3660), atmospheric temperature profile (Parameter No. 3726), column water vapor profile (Parameter No. 3727), MODIS snow

TABLE XIII. Input data for the at-launch MODIS LST algorithms.

prod #	product name	parameter name	parm #	input parameter #	comments for input parameter
MOD11	Land_sfc Temperature	Land_sfc Temperature		2338	TIR bands bands level-1B radiance
				3660	cloud mask
		Emissivity	3323	3726	temperature profile
				3727	water vapor profile
				3020	1km snow cover
				2669	1km land cover
				2749	250m NDVI
				(3323)	knowledge base from measurements and retrieved band emissivities

cover, land-cover, and NDVI products, and surface emissivity knowledge base from laboratory and field measurements.

There are strong relations among the MODIS land products. The LST will be used as an input variable for other MODIS Land products such as land-cover, evapotranspiration, and net primary productivity [Running et al., 1994]. The MODIS land-cover, snow, and NDVI products will provide useful information to infer the surface band emissivity.

DEM is an important input to make pixel-specific topographic correction for localized radiometric effects (slope/aspect related illumination differences, shadowing, and reflection of radiation from adjacent pixels). Because of the limitations in platform and MODIS pointing accuracy and knowledge, it is not easy to co-register MODIS pixels with DEM. The surface elevation provided in MOD02 will be used in LST algorithms.

3.2.7. Output Product

The level-2 output of the LST product is land-surface temperature and its quality flag both in image format at a spatial resolution 1km, with 2 bytes for LST, 1 byte for associated error, and additional 2 byte for quality flag for each pixel. For the land-surface emissivity parameter, 1 byte each for band emissivity in MODIS bands 31 and 32 in binary fraction format in the range from 0.488 to 1. And 1 byte is used for MODIS viewing angle, 1 byte for observation time of MODIS viewing at the pixel.

At-launch level-3 product will be daily 1-km and 5-km equal area daytime and nighttime LST and band emissivities. Band emissivities in MODIS bands 20, 22, 23, 29, 31-33 are included in the 5-km product. Its derivative products are 0.5 or 1 degree (latitude and longitude) equal angle daily, 8-day, and monthly products. We will deal with the LST angular-dependence problem in the advanced post-launch LST level-3 product. MODIS BRDF product, and the temporal and spatial information in the level-2 MODIS LST product and LST estimated from GOES data will be used in surface modeling to provide LST normalized at nadir or some simple angular distribution of LST.

4. Constraints, Limitations, Assumptions

A major constraint for the MODIS LST as well as other MODIS land products is that they will only be available in clear sky conditions. Clouds will prevent the Earth surface from satellite observing in the visible and thermal infrared spectral ranges. The MODIS LST algorithm as well as most existing LST algorithms is based on the basic assumption that a land surface pixel could be described by different spectral emissivities and a single effective radiometric temperature in all TIR bands. But this may be not true for pixels containing sub-pixel fires. When linking pixel values to fixed grids on the Earth surface coordinates, the MODIS LST as well as all other land products will have troubles with complicated mixed pixels along land

cover boundaries in terms of their quantitative definitions, quality assessments, and applications.

4.1. Mixed-pixel Problem

It is possible to use atmospheric-corrected multichannel TIR data for estimation of subpixel temperatures and proportions of pixels mixed with two components under the assumption that emissivities of target and background were known [Dozier, 1981; Matson and Dozier, 1981]. This method works if the target temperature differs from the background temperature significantly.

Gillespie [1992] developed a linear isothermal mixing method for spectral mixture analysis of multichannel TIR data under assumptions: 1) mixing is additive, and 2) scene components in each pixel are isothermal.

No method exists to solve the difficulties in general nonisothermal and rough-surface mixing under influence of atmospheric effects unless more detail independent information is available for specific applications at a local scale. Sobrino and Caselles [1991] developed a methodology for obtaining the crop temperature from NOAA-9 AVHRR data based on additional independent information of 1) the temperature difference between crop and ground, 2) the ground and vegetation emissivities in each bands, 3) the proportion of ground in each pixel, and 4) shape factors of the vegetation. No attempt will be made to deal with such mixed-pixel problems in the global at-launch MODIS LST product. Alternatively, only effective averaged temperatures will be given for mixed pixels. The sub-pixel problem will be a post-launch research activity.

4.2. Complicated Surface Structures

It is difficult to make ground measurements with complicated surface structures. For some pixels, it may be difficult to define a pixel surface temperature without consideration of the surface structure within the pixel if there are large contrasts in its band emissivities and there are significant viewing shadows with a temperature significantly different from the temperature in other part of the pixel. For example, there are fires in shadows and band 1 has a very low emissivity while band 2 has an emissivity close to 1. The fires have no effect in band 2 because they are in viewing shadows and the band reflectivity is close to zero. But the fires have a significant effect in band 1 caused by within-pixel reflected TIR radiation emitted from the fires. This makes effective temperatures different in these two bands.

4.3. Topographic Effects in Complicated Terrains

Only the first order of topographic information, i.e., the elevation of the surface, is considered in radiative transfer simulations in the development of MODIS LST algorithms. In rugged areas for which high resolution DEM is not available, it is difficult to accurately estimate land surface temperature in one pixel without correcting the reflected thermal infrared radiation from its adjacent pixels.

ACKNOWLEDGEMENTS

The authors would like to thank the reviewers and the participants to the International Land-Surface Temperature Workshop on September 17-19, 1996 at University of California at Santa Barbara, CA, for their comments and suggestions, which helped to improve this ATBD.

REFERENCES

Note: five unpublished papers included here can be obtained by anonymous ftp to crseo.ucsb.edu in the directory pub/modis_lst.

Asrar, G., D. I. Cooper, and T. R. Harris, ‘‘Surface radiative temperatures of the burned and unburned areas in a tallgrass prairie,’’ *Remote Sens. Environ.*, vol. 24, pp. 447-457, 1988.

Asrar, G. and R. Greenstone, *MTPE EOS Reference Handbook*, Greenbelt, MD: NASA Goddard Space Flight Ctr., 1995.

Barton, I. J., ‘‘Infrared continuum water vapor absorption coefficients derived from satellite data,’’ *Appl. Optics*, vol. 30, no. 21, pp. 2929-2934, 1991.

Barton, I. J., A. M. Zavody, D. M. O’Brien, D. R. Cutten, R. W. Saunders, and D. T. Llewellyn-Jones, ‘‘Theoretical algorithms for satellite-derived sea surface temperatures,’’ *J. Geophys. Res.*, vol. 94, no. D3, pp. 3365-3375, 1989.

Becker, F., ‘‘The impact of spectral emissivity on the measurement of land surface temperature from a satellite,’’ *Int. J. Remote Sens.*, vol. 8, no. 10, pp. 1509-1522, 1987.

Becker, F. and Z.-L. Li, ‘‘Toward a local split window method over land surface,’’ *Int. J. Remote Sens.*, vol. 11, no. 3, pp. 369-393, 1990.

Becker, F., W. Ngai, and M. P. Stoll, ‘‘An active method for measuring thermal infrared effective emissivities: implications and perspectives for remote sensing,’’ *Adv. Space Res.*, vol. 1, pp. 193-210, 1981.

Berk, A., L. S. Bemstein, and D. C. Robertson, ‘‘MODTRAN: A moderate resolution model for LOWTRAN 7,’’ Rep. GL-TR-89-0122, Burlington, MA: Spectral Sciences, Inc., 1989.

Berk, A., L. S. Bemstein, and D. C. Robertson, ‘‘MODTRAN: A moderate resolution model for LOWTRAN,’’ Rep. AFGL-TR-87-0220, Burlington, MA: Spectral Sciences, Inc., 1987.

Betts, A. K., S.-Y. Hong, and H.-L. Pan, ‘‘Comparison of NCEP-NCAR reanalysis with 1987 FIFE data,’’ *Monthly Weather Review*, vol. 124, pp. 1480-1498, 1996.

Bevington, P. R., *Data Reduction and Error Analysis for the Physical Sciences*, New York: McGraw-Hill Book Company, 1969.

Brush, R. J. H., ‘‘Anomalous effects of sunglint on the AVHRR in the NOAA-12,’’ *Int. J. Remote Sens.*, vol. 14, pp. 629-634, 1993.

Camillo, P. J., ‘‘Using one- or two-layer models for evaporation estimation with remotely sensed data,’’ in *Land Surface Evaporation: Measurements and Parameterization*, ed. T. J. Schmugge and J. C. André, New York: Springer-Verlag, 1991.

Carlson, T. N., ‘‘Recent advances in modeling the infrared temperature of vegetation canopies,’’ in *Land Surface Evaporation: Measurements and Parameterization*, ed. T. J. Schmugge and J. C. André, New York: Springer-Verlag, 1991.

Caselles, V. and J. A. Sobrino, ‘‘Determination of frosts in orange groves from NOAA-9 AVHRR data,’’ *Remote Sens. Environ.*, vol. 29, no. 2, pp. 135-146, 1989.

Chahine, M. T., ‘‘Observation of local cloud and moisture feedbacks over high ocean and desert surface temperature,’’ *J. Geophys. Res.*, vol. 100, no. D5, pp. 8919-8927, 1995.

Chedin, A., M. A. Scott, C. Wahiche, and P. Moulinier, ‘‘The improved initialization inversion method: a high resolution physical method for temperature retrievals from the Trios-N series,’’ *J. Clim. Appl. Meteorol.*, vol. 24, pp. 124-143, 1985.

Clough, S. A., ‘‘The water vapor continuum and its role in remote sensing,’’ in *Proc. of Conference on Optical Remote Sensing of the Atmosphere, Salt Lake City, Utah*, pp. 76-78, 1995.

Cooper, D. I. and G. Asrar, ‘‘Evaluating atmospheric correction models for retrieving surface temperatures from the AVHRR over a tallgrass prairie,’’ *Remote Sens. Environ.*, vol. 27, pp. 93-102, 1989.

Cornette, W. M., P. K. Acharya, D. C. Robertson, and G. P. Anderson, ‘‘Moderate spectral atmospheric radiance and transmittance code (MOSART),’’ Rep. R-057-94(11-30), La Jolla, CA: Photon Research Associates, Inc., 1994.

Crag, R., M. Sugita, and W. Brutsaert, ‘‘Satellite-derived surface temperatures with boundary layer temperatures and geostrophic winds to estimate surface energy fluxes,’’ *J. Geophys. Rev.*, vol. 100, no. D12, pp. 25447-25451, 1995.

Dennis, J.E. JR. and R. B. Schnabel, *Numerical Methods for Unconstrained Optimization and Nonlinear Equations*, New Jersey: Prentice-Hall, Inc., 1983.

Diak, G. R. and M. S. Whipple, ‘‘Improvements to models and methods for evaluating the land-surface energy balance and effective roughness using radiosonde reports and satellite-measured skin temperature data,’’ *Agricul. and Forest Meteorol.*, vol. 63, no. 3-4, pp. 189-218, 1993.

Dozier, J., ‘‘A method for satellite identification of surface temperature fields of subpixel resolution,’’ *Remote Sens. Environ.*, vol. 11, pp. 221-229, 1981.

Dozier, J. and Z. Wan, ‘‘Development of practical multiband algorithms for estimating land-surface temperature from EOS/MODIS data,’’ *Adv. Space Res.*, vol. 13, no. 3, pp. 81-90, 1994.

Dozier, J. and S. G. Warren, ‘‘Effect of viewing angle on the infrared brightness temperature of snow,’’ *Water Resour. Res.*, vol. 18, no. 5, pp. 1424-1434, 1982.

Drake, F., ‘‘Global cloud cover and cloud water path from ISCCP C2 data,’’ *Int. J. Climatology*, vol. 13, pp. 581-605, 1993.

Gao, B. C. and Y. J. Kaufman, ‘‘Selection of the 1.375μm MODIS channel for remote sensing of cirrus cloud and stratospheric aerosols from space,’’ *J. Atmos. Sci.*, vol. 52, no. 23, pp. 4231-4237, 1995.

Gillespie, A. R., ‘‘Spectral mixture analysis of multispectral thermal infrared images,’’ *Remote Sens. Environ.*, vol. 42, pp. 137-145, 1992.

Gleason, M. L., S. E. Taylor, T. M. Loughin, and K. J. Koehler, ‘‘Development and validation of an empirical model to estimate the duration of dew periods,’’ *Plant Diseases*, vol. 78, no. 10, pp. 1011-1016, 1994.

Grant, I. P. and G. E. Hunt, ‘‘Discrete space theory of radiative transfer, I, Fundamentals,’’ *Proc. Royal Soc. London*, vol. A313, pp. 183-197, 1969.

Grant, W. B., ‘‘Water vapor absorption coefficients in the 8-13-μm spectral region: a critical review,’’ *Appl. Optics*, vol. 29, no. 4, pp. 451-462, 1990.

Griggs, M., ‘‘Emissivities of natural surfaces in the 8- to 14-micron spectral region,’’ *J. Geophys. Res.*, vol. 73, pp. 7545-7551, 1968.

Hahmann, A. N., D. M. Ward, and R. E. Dickinson, ‘‘Land surface temperature and radiative fluxes response of the NCAR CCM2/Biosphere-Atmosphere Transfer Scheme to modifications in the optical properties of clouds,’’ *J. Geophys. Res.*, vol. 100, no. D11, pp. 23239-23252, 1995.

Hanssen, L. M., ‘‘Effects of non-Lambertian surfaces on integrating sphere measurements,’’ *Appl. Optics*, vol. 35, no. 19, pp. 3597-3606, 1996.

Hanssen, L. M., ‘‘Effects of restricting the detector field of view when using integrating spheres,’’ *Appl. Optics*, vol. 28, no. 11, pp. 2097-2103, 1989.

Harris, A. R. and I. M. Mason, ‘‘An extension to the split-window technique giving improved atmospheric correction and total water vapor,’’ *Int. J. Remote Sens.*, vol. 13, no. 5, pp. 881-892, 1992.

Hook, S. J., A. R. Gabell, A. A. Green, and P. S. Kealy, ‘‘A comparison of techniques for extracting emissivity information from thermal infrared data for geological studies,’’ *Remote Sens. Environ.*, vol. 42, pp. 123-135, 1992.

Jackson, R. D., R. J. Reginato, and S. B. Idso, ‘‘Wheat canopy temperature: a practical tool for evaluating water requirements,’’ *Water Resour. Res.*, vol. 13, pp. 651-656, 1977.

Jackson, T. J. and P. E. O’Neill, ‘‘Salinity effects on the microwave emission of soil,’’ *IEEE Trans. Geosci. Remote Sens.*, vol. 25, pp. 214-220, 1987.

Jackson, T. J. and T. J. Schmugge, ‘‘Passive microwave remote sensing of soil moisture,’’ *Adv. Hydrosci.*, vol. 14, pp. 123-159, 1986.

Janssen, L. H. J. M. and F. G. Römer, ‘‘The frequency and duration of dew occurrence over a year: model results compared with measurements,’’ *Tellus*, vol. 43B, no. 5, pp. 408-419, 1991.

Jasinski, M. F., ‘‘Sensitivity of the normalized difference vegetation index to subpixel canopy cover, soil albedo, and pixel scale,’’ *Remote Sens. Environ*, vol. 32, pp. 169-187, 1990.

Jedlovec, G. J., ‘‘Preciptable water estimation from high-resolution split window radiance measurements,’’ *J. Appl. Meteorol.*, vol. 29, pp. 863-877, 1990.

Jin, M., R. E. Dickinson, and A. M. Vogelmann, ‘‘A comparison of CCM2/BATS skin temperature and surface-air temperature with satellite and surface observations,’’ *J. Climate*, accepted 1996.

Kahle, A. B., D. P. Madura, and J. M. Soha, ‘‘Middle infrared multispectral aircraft scanner data: analysis for geological applications,,’’ *Appl. Optics*, vol. 19, pp. 2279-2290, 1980.

Kahle, A. B., ‘‘Surface emittance, temperature, and thermal inertia derived from Thermal Infrared Multispectral Scanner (TIMS) data for Death Valley, California,’’ *Geophysics*, vol. 52, no. 7, pp. 858-874, 1986.

Kerdiles, H., M. Grondana, R. Rodriguez, and B. Seguin, ‘‘Frost mapping using NOAA AVHRR data in the Pampean region, Argentina,’’ *Agricul. and Forest Meteorol.*, vol. 79, pp. 157-182, 1996.

Kerr, Y. H., J. P. Lagouarde, and J. Imbernon, ‘‘Accurate land surface temperature retrieval from AVHRR data with use of an improved split window algorithm,’’ *Remote Sens. Environ.*, vol. 41, no. 2-3, pp. 197-209, 1992.

Key, J., J. A. Maslanik, T. Papakyriakou, M. C. Serreze, and A. J. Schweiger, ‘‘On the validation of satellite-derived sea ice temperature,’’ *Arctic*, vol. 47, pp. 280-287, 1994.

Khattak, S., R. A. Vaughan, and A. P. Cracknell, ‘‘Sunglint and its observation in AVHRR data,’’ *Remote Sens. of Environ*, vol. 37, pp. 101-116, 1991.

Kimes, D. S., ‘‘Azimuthal radiometric temperature measurements of wheat canopies,’’ *Appl. Optics*, vol. 20, no. 7, pp. 1119-1121, 1981.

Kimura, F. and A. P. Shimiru, ‘‘Estimation of sensible and latent heat fluxes from soil surface temperature using a linear air land heat transfer model,’’ *J. Appl. Meteorol.*, vol. 33, no. 4, pp. 477-489, 1994.

King, M. D., Y. J. Kaufman, W. P. Menzel, and D. Tanré, ‘‘Remote sensing of cloud, aerosol, and water vapor properties from the Moderate Resolution Imaging Spectrometer (MODIS),’’ *IEEE Trans. Geosci. Remote Sens.*, vol. 30, no. 1, pp. 2-27, 1992.

King, M. D., W. P. Menzel, P. S. Grant, J. S. Myers, G. T. Arnold, S. E. Platnick, L. E. Gumley, S. C. Tsay, C. C. Moeller, M. Fitzgerald, K. S. Brown, and F. G. Osterwisch, ‘‘Airborne scanning spectrometer for remote sensing of cloud, aerosol, water vapor and surface properties ,’’ *J. Atmos. Ocean. Technol.*, vol. 13, pp. 777-794, 1996.

Kneizys, F. X., E. P. Shettle, L. W. Abreu, J. H. Chetwynd, G. P. Anderson, W. O. Gallery, J. E. A. Selby, and S. A. Clough, ‘‘Users Guide to LOWTRAN 7,’’ Rep. AFGL-TR-88-0177, Bedford, MA: Air Force Geophys. Lab., 1988.

Kneizys, F. X., E. P. Shettle, W. O. Gallery, J. H. Chetwynd, L. W. Abreu, J. E. A. Selby, S. A. Clough, and R. W. Fenn, ‘‘Atmospheric Transmittance/Radiance: Computer Code LOWTRAN 6,’’ Rep. AFGL-TR-83-0187 (NTIS AD A137796), Bedford, MA: Air Force Geophys. Lab., 1983.

Labed, J. and M. P. Stoll, ‘‘Angular variation of land surface spectral emissivity in the thermal infrared: laboratory investigations on bare soils,’’ *Int. J. Remote Sens.*, vol. 12, no. 11, pp. 2299-2310, 1991.

Lagouarde, J. P., Y. H. Kerr, and Y. Brunet, ‘‘An experimental study of angular effects on surface temperature for various plant canopies and bare soils,’’ *Agri. and Forest Meteorol.*, vol. 77, pp. 167-190, 1995.

Lean, J., ‘‘Variations in the Sun’s radiative output,’’ *Res. Geophys.*, vol. 29, no. 4, pp. 505-535, 1991.

Li, S., Z. Wan, and J. Dozier, ‘‘A component decomposition model for evaluating atmospheric effects in remote sensing,’’ *J. Electromag. Waves Applic.*, vol. 1, no. 4, pp. 323-347, 1987.

Li, Z.-L. and F. Becker, ‘‘Feasibility of land surface temperature and emissivity determination from AVHRR data,’’ *Remote Sens. Environ.*, vol. 43, pp. 67-85, 1993.

Ma, Q. and R. Tipping, ‘‘The detailed balance requirement and general empirical formalisms for continuum absorption,’’ *J. Quant. Spectrosc. Radiat. Transfer*, vol. 51, pp. 751-757, 1994.

Ma, Q. and R. Tipping, ‘‘A far wing line shape theory and its application to the foreign-broadened water vapor continuum absorption .3,’’ *J. Chem. Phys.*, vol. 97, pp. 818-828, 1992.

Majumdar, T. J. and B. B. Bhattacharya, ‘‘Simulation of thermal inertia imagery with daytime HCMM data,’’ *Int. J. Remote Sens.*, vol. 11, no. 1, pp. 139-147, 1990.

Mannstein, H., ‘‘Surface energy budget, surface temperature and thermal inertia,’’ in *Remote Sensing Applications in Meteorology and Climatology*, ed. R. A. Vaughan and D. Reidel, NATO ASI Ser. C: Math. Phys. Sci. Vol. 201, pp. 391-410, Dordrecht, Netherlands: A Reidel Publishing Co., 1987.

Masuda, K., T. Takashima, and Y. Yakayma, ‘‘Emissivity of pure and sea waters for the model sea surface in the infrared window regions,’’ *Remote Sens. Environ.*, vol. 24, pp. 313-329, 1988.

Matson, M. and J. Dozier, ‘‘Identification of subresolution high temperature sources using a thermal IR sensor,’’ *Photogram. Engrg. Remote Sens.*, vol. 47, pp. 1311-1318, 1981.

Maykut, G., ‘‘Energy exchange over young sea ice in the central Arctic,’’ *J. Geophys. Res.*, vol. 83, pp. 3646-3658, 1978.

McClain, E. P., W. G. Pichel, and C. C. Walton, ‘‘Comparative performance of AVHRR-based multichannel sea surface temperatures,’’ *J. Geophys. Res.*, vol. 90, no. C6, pp. 11587-11601, 1985.

McFarland, M. J., R. L. Miller, and C. M. U. Neale, ‘‘Land surface temperature derived from the SSM/I passive microwave brightness temperatures,’’ *IEEE Trans. Geosci. Remote Sens.*, vol. 28, no. 5, pp. 839-845, 1990.

Meehl, G. A., ‘‘Influence of the land surface in the Asian summer monsoon: external conditions versus internal feedbacks,’’ *J. Climate*, vol. 7, pp. 1033-1049, 1994.

Menzel, W. P. and J. F. W. Purdom, ‘‘Introducing GOES-I - the 1st of a new generation of geostationary operational environmental satellites,’’ *Bull. Amer. Meteor. Soc.*, vol. 75, no. 5, pp. 757-781, 1994.

Moine, P., A. Chedin, and N. A. Scott, ‘‘Automatic classification of air mass type from satellite vertical sounding data. Application to NOAA-7 observations,’’ *Ocean-Air Interactions*, vol. 1, pp. 95-108, 1987.

NASA,, *Heat Capacity Mapping Mission User’s Guide*, 119 pp., Greenbelt, MD: NASA Goddard Space Flight Ctr., 1980.

Nerry, F., J. Labed, and M. P. Stoll, ‘‘Spectral properties of land surfaces in the thermal infrared, 1, Laboratory measurements of absolute spectral emissivity signatures,’’ *J. Geophys. Res.*, vol. 95, no. B5, pp. 7027-7044, 1990.

Norman, J. M., J. Chen, and N. Goel, ‘‘Thermal emissivity and infrared temperature dependency of plant canopy architecture and view angle,’’ *Proc. IGARSS ’90*, pp. 1747-1750, 1990.

Olioso, A., ‘‘Simulating the relationship between thermal emissivity and the normalized difference vegetation index,’’ *Int. J. Remote Sens.*, vol. 10, no. 16, pp. 3211-3216, 1995.

Ottlé, C. and M. Stoll, ‘‘Effect of atmospheric absorption and surface emissivity on the determination of land temperature from infrared satellite data,’’ *Int. J. Remote Sens.*, vol. 14, no. 10, pp. 2025-2037, 1993.

Ottlé, C. and D. Vidal-Madjar, ‘‘Estimation of land surface temperature with NOAA9 data,’’ *Remote Sens. Environ.*, vol. 40, no. 1, pp. 27-41, 1992.

Palluconi, F., A. B. Kahle, G. Hoover, and J. E. Conel, ‘‘The spectral emissivity of prairie and pasture grasses at Konza Prairie, Kansas,’’ in *Symposium on FIFE*, pp. 77-78, Boston, MA: American Meteorological Society, 1990.

Prata, A. J., ‘‘Land surface temperatures derived from the advanced very high resolution radiometer and the along-track scanning radiometer 2. experimental results and validation of AVHRR algorithms,’’ *J. Geophys. Res.*, vol. 99, no. D6, pp. 13025-13058, 1994.

Price, J. C., ‘‘Estimating surface temperature from satellite thermal infrared data - a simple formulation for the atmospheric effect,’’ *Remote Sens. Environ.*, vol. 13, pp. 353-361, 1983.

Price, J. C., ‘‘Land surface temperature measurements from the split window channels of the NOAA-7 AVHRR,’’ *J. Geophys. Res.*, vol. 79, pp. 5039-5044, 1984.

Price, J. C., ‘‘On the analysis of thermal infrared imagery: the limited utility of apparent thermal inertia,’’ *Remote Sens. Environ.*, vol. 18, pp. 59-73, 1985.

Rees, W. G., ‘‘Infrared emissivities of Arctic land cover types,’’ *Int. J. Remote Sens.*, vol. 14, pp. 1013-1017, 1993.

Rees, W. G. and S. P. James, ‘‘Angular variation of the infrared emissivity of ice and water surfaces,’’ *Int. J. Remote Sens.*, vol. 13, pp. 2873-2886, 1992.

Rivard, B., S. B. Petroy, and J. R. Miller, ‘‘Measured effects of desert varnish on mid-infrared spectra of weathered rocks as an aid to TIMS imagery interpretation,’’ *IEEE Trans. Geosci. Remote Sens.*, vol. 31, no. 1, pp. 284-291, 1993.

Rodgers, C. D., ‘‘Retrieval of atmospheric temperature and composition from remote measurements of thermal radiation,’’ *Rev. Geophys. and Space Phys.*, vol. 14, no. 4, pp. 609-624, 1976.

Running, S. W., ‘‘Computer simulation of regional evapotranspiration by integrating landscape biophysical attributes with satellite data,’’ in *Land Surface Evaporation: Measurements and Parameterization*, ed. T. J. Schmugge and J. C. André, New York: Springer-Verlag, 1991.

Running, S. W., C. Justice, V. Salomonson, D. Hall, J. Barker, Y. Kaufman, A. Strahler, A. Huete, J.-P. Muller, V. Vanderbilt, Z. Wan, and P. Teillet, ‘‘Terrestrial remote sensing science and algorithms planned for EOS/MODIS,,’’ *Int. J. Remote Sens.*, vol. 15, no. 17, pp. 3587-3620, 1994.

Salisbury, J. W. and D. M. D’Aria, ‘‘Emissivity of terrestrial materials in the 8-14 μm atmospheric window,’’ *Remote Sens. Environ.*, vol. 42, pp. 83-106, 1992.

Salisbury, J. W. and D. M. D’Aria, ‘‘Emissivity of terrestrial materials in the 3-5 μm atmospheric window,’’ *Remote Sens. Environ.*, vol. 47, pp. 345-361, 1994.

Salisbury, J. W. and D. M. D’Aria, ‘‘Infrared (8-14 μm) remote sensing of soil particle size,’’ *Remote Sens. Environ.*, vol. 42, pp. 157-165, 1992.

Salomonson, V., W. Barnes, P. Maymon, H. Montgomery, and H. Ostrow, ‘‘MODIS: advanced facility instrument for studies of the Earth as a system,’’ *IEEE Trans. Geosci. Remote Sens.*, vol. 27, no. 2, pp. 145-153, 1989.

Schaaf, C. B. and A. H. Strahler, ‘‘Solar zenith angle effects on forest canopy hemispherical reflectances calculated with a geometric-optical bidirectional reflectance model,’’ *IEEE Trans. Geosci. Remote Sens.*, vol. 31, no. 4, pp. 921-927, 1993.

Scherm, H. and A. H. C. van Bruggen, ‘‘Sensitivity of simulated dew duration to meteorological variations in different climate regions of California,’’ *Agricul. and Forest Meteorol.*, vol. 66, pp. 229-245, 1993.

Schmugge, T. J. and F. Becker, ‘‘Remote sensing observations for the monitoring of land-surface fluxes and water budgets,’’ in *Land Surface Evaporation: Measurements and Parameterization*, ed. T. J. Schmugge and J. C. André, New York: Springer-Verlag, 1991.

Schmugge, T. J., P. E. O’Neill, and P. E. Wang, ‘‘Passive microwave soil moisture research,’’ *IEEE Trans. Geosci. Remote Sens.*, vol. 24, pp. 12-22, 1986.

Sellers, P. J., F. G. Hall, G. Asrar, D. E. Strebel, and R. E. Murphy, ‘‘The first ISLSCP Field Experiment (FIFE),’’ *Bull. Amer. Meteorol. Soc.*, vol. 69, no. 1, pp. 22-27, 1988.

Short, N. M. and L. M. Stuart, Jr., *The Heat Capacity Mapping Mission (HCMM) Anthology*, Washington, DC: NASA, 1982.

Sinha, A., ‘‘Relative influence of lapse rate and water vapor on the greenhouse effect,’’ *J. Geophys. Res.*, vol. 100, no. D3, pp. 5095-5103, 1995.

Smith, W. L., H. M. Woolf, and A. J. Schriener, ‘‘Simultaneous retrieval of surface and atmospheric parameters: a physical and analytically direct approach,’’ in *Advances in Remote Sensing Retrieval Methods*, ed. A. Deepak, H. E. Fleming, and M. T. Chahine, pp. 221-232, Hampton, Va., USA: A. Deepak Publishing, 1985.

Snyder, W. and Z. Wan, ‘‘Adaptation of kernel BRDF models to predict spectral reflectance and emissivity in the thermal infrared,’’ *IEEE Trans. Geosci. Remote Sens.*, revised 1996(a).

Snyder, W. and Z. Wan, ‘‘Surface temperature correction for active infrared reflectance measurements of natural materials,’’ *Appl. Optics*, vol. 35, no. 13, pp. 2216-2220, 1996(b).

Snyder, W., Z. Wan, Y. Zhang, and Y.-Z. Feng, ‘‘Requirements for satellite land surface temperature validation using a silt playa,’’ *Remote Sens. Environ.*, submitted 1996(c).

Snyder, W., Z. Wan, Y. Zhang, and Y.-Z. Feng, ‘‘Thermal infrared (3-14 μm) bidirectional reflectance measurements of sands and soils,’’ *Remote Sens. Environ.*, in press 1996(d).

Sobrino, J. A. and V. Caselles, ‘‘A methodology for obtaining the crop temperature from NOAA-9 AVHRR data,’’ *Int. J. Remote Sens.*, vol. 38, pp. 19-34, 1991.

Sobrino, J. A., C. Coll, and V. Caselles, ‘‘Atmospheric corrections for land surface temperature using AVHRR channel 4 and 5,’’ *Remote Sens. Environ.*, vol. 38, no. 1, pp. 19-34, 1991.

Sobrino, J. A., Z.-L. Li, and M. P. Stoll, ‘‘Impact of the atmospheric transmittance and total water vapor content in the algorithms for estimating satellite sea surface temperature,’’ *IEEE Trans. Geosci. Remote Sens.*, vol. 31, no. 5, pp. 946-952, 1993.

Stamnes, K. and P. Conklin, ‘‘A new multi-layer discrete ordinate approach to radiative transfer in vertically inhomogeneous atmospheres,’’ *J. Quant. Spectrosc. Radiat. Transfer*, vol. 31, pp. 273-282, 1984.

Stamnes, K., S.-C. Tsay, W. Wiscombe, and K. Jayaweera, ‘‘Numerically stable algorithm for discrete-ordinate-method radiative transfer in multiple scattering and emitting layered media,’’ *Appl. Optics*, vol. 27, no. 12, pp. 2502-2509, 1988.

Susskind, J. and M. T. Chahine, ‘‘Determination of temperature and moisture profiles in a cloudy atmosphere using AIRS/AMSU,’’ in *High Spectral Resolution Infrared Remote Sensing for Earth’s Weather and Climate Studies*, ed. A. Chedin, M. T. Chahine, and N. A. Scott, pp. 149-161, Berlin, Germany: Springer-Verlog, 1993.

Susskind, J., J. Rosenfield, D. Reuter, and M. T. Chahine, ‘‘Remote Sensing of weather and climate parameters from HIRS2/MSU on TIROS-N,’’ *J. Geophys. Res.*, vol. 89, no. D3, pp. 4677-4697, 1984.

Sutton, J. C., T. J. Gillespie, and P. D. Hilebrand, ‘‘Monitoring weather factors in relation to plant disease of dew periods,’’ *Plant Disease*, vol. 68, no. 1, pp. 78-84, 1984.

Trewartha, G. T. and L. H. Horn, in *An Introduction To Climate*, New York: McGraw-Hill Book Company, 1980.

Ulaby, F. T., R. K. Moore, and A. K. Fung, *Microwave Remote Sensing: Active and Passive, Volume III, from Theory to Applications,* North Bergen, NJ: Book-Mart Press, Inc., 1986.

Van-De-Griend, A. A. and M. Owe, ‘‘On the relationship between thermal emissivity and the normalized difference vegetation index for natural surface,’’ *Int. J. Remote Sens.*, vol. 14, no. 6, pp. 1119-1131, 1993.

Vidal, A., ‘‘Atmospheric and emissivity correction of land surface temperature measured from satellite using ground measurements or satellite data,’’ *Int. J. Remote Sens.*, vol. 12, no. 12, pp. 2449-2460, 1991.

Vining, R. C. and B. L. Blad, ‘‘Estimation of sensible heat flux from remotely sensed canopy temperatures,’’ *J. Geophys. Res.*, vol. 97, no. D17, pp. 18951-18954, 1992.

Vukovich, F. M., ‘‘A comparison of surface temperature derived from HCMM infrared measurements with field data,’’ *Remote Sens. Environ.*, vol. 15, pp. 63-76, 1984.

Wan, Z. and J. Dozier, ‘‘Effects of temperature-dependent molecular absorption coefficients on the thermal infrared remote sensing of the Earth surface,’’ *Proc. IGARSS ’92*, pp. 1242-1245, 1992.

Wan, Z. and J. Dozier, ‘‘Effects of the atmosphere and surface emissivity on the thermal infrared spectral signature measured from MODIS-N,’’ *Proc. IGARSS ’90*, pp. 189-192, 1990.

Wan, Z. and J. Dozier, ‘‘A generalized split-window algorithm for retrieving land-surface temperature from space,’’ *IEEE Trans. Geosci. Remote Sens.*, vol. 34, no. 4, pp. 892-905, 1996.

Wan, Z. and J. Dozier, ‘‘Land-surface temperature measurement from space: physical principles and inverse modeling,’’ *IEEE Trans. Geosci. Remote Sens.*, vol. 27, no. 3, pp. 268-278, 1989.

Wan, Z. and Z.-L. Li, ‘‘A physics-based algorithm for retrieving land-surface emissivity and temperature from EOS/MODIS data,’’ *IEEE Trans. Geosci. Remote Sens.*, accepted 1996.

Wan, Z., W. Snyder, Z.-L. Li, Y. Zhang, and Y.-Z. Feng, ‘‘A sun-shadow method for in-situ measurements of land-surface temperature and emissivity,’’ *IEEE Trans. Geosci. Remote Sens.*, submitted 1996.

Watson, K., F. Kruse, and S. Hummer-Miller, ‘‘Thermal infrared exploration in the Carlin Trend,’’ *Geophysics*, vol. 55, no. 1, pp. 70-79, 1990.

Watson, K., ‘‘Two-temperature method for measuring emissivity,’’ *Remote Sens. Environ.*, vol. 42, pp. 117-121, 1992.

Westwater, E. R., J. B. Snider, J. H. Churnside, and J. A. Shaw, ‘‘Ground based microwave and infrared radiance observations during Probe,’’ in *Proc. of the Eighth Conference on Atmospheric Radiation, AMS, Nashville, TN*, pp. 272-275, 1994.

White, G. H., E. Kalnay, R. Gardner, and M. Kanamitsu, ‘‘The skill of precipitation and surface temperature forecasts by the NMC global model during DERF II,’’ *Monthly Weather Review*, vol. 121, pp. 805-814, 1993.

Wigneron, J. P., Y. Kerr, A. Chanzy, and Y. Q. Jin, ‘‘Inversion of surface parameters from passive microwave measurements over a soybean field,’’ *Remote Sens. Environ.*, vol. 46, pp. 61-72, 1993.

Wiscombe, W. J. and J. W. Evans, ‘‘Exponential-sum fitting of radiative transmission functions,’’ *J. Comput. Phys.*, vol. 24, no. 4, pp. 416-444, 1977.

Wiscombe, W. J., ‘‘Extension of the doubling method to inhomogeneous sources,’’ *J. Quant. Spectros. Radiat. Transfer*, vol. 16, no. 6, pp. 477-486, 1976.

Yu, Y., D. A. Rothrock, and R. W. Lindsay, ‘‘Accuracy of sea ice temperature derived from the advanced very high resolution radiometer,’’ *J. Geophys. Res.*, vol. 100, no. C3, pp. 4525-4532, 1995.

Zangvil, A., ‘‘Six years of dew observations in the Negev Desert, Israel,’’ *Journal of Arid Environ.*, vol. 32, pp. 361-371, 1996.

Zhang, L., R. Lemeur, and J. P. Goutorbe, ‘‘A one-layer resistance model for estimating regional evepotranspiration using remote sensing data,’’ in *Agricul. and Forest Meteorol.*, vol. 77, pp. 241-261, 1995.

ACRONYMS

AIRS	Atmospheric Infrared Sounder
ASTER	Advance Spaceborne Thermal Emission and Reflection Radiometer
ATBD	Algorithm Theoretical Basis Document
ATI	Apparent Thermal Inertia
ATSR	Along-Track Scanning Radiometer
AVHRR	Advanced Very High-Resolution Radiometer
BRDF	Bidirectional Reflectance Distribution Function
CCM2	NCAR Community Climate Model version 2
DAAC	Distributed Active Archive Center
DAO	Data Assimilation Office
DEM	Digital Elevation Model
DMSP	Defense Meteorological Satellite Program
EOS	Earth Observing System
EOS AM1	The first EOS AM platform
FOV	Field-of-View
FTIR	Fourier Transform Infrared
GCM	Global Circulation Model
GSFC	Goddard Space Flight Center
HCMM	Heat Capacity Mapping Mission
HIRS	High-Resolution Imaging Spectrometer
IFOV	Instantaneous Field-of-View
IGARSS	International Geoscience and Remote Sensing Symposium
IGBP	International Geosphere-Biosphere Program
ISCCP	International Satellite Cloud Climatology Project
ISLSCP	International Satellite Land Surface Climatology Project
JPL	Jet Propulsion Laboratory
LOWTRAN	Low Spectral Transmittance/Radiance Code
LST	Land-Surface Temperature
LTER	Long-Term Ecological Research
LUT	Look-up Table

LWIR	Long Wave Infrared
MMD	Maximum Minimum Difference
MODIS	Moderate Resolution Imaging Spectroradiometer
MODATM	MODIS Atmosphere
MODLAND	MODIS Land
MODTRAN	Moderate Spectral Transmittance/Radiance Code
MOSART	Moderate Spectral Atmospheric Radiance and Transmittance Code
NDVI	Normalized Differential Vegetation Index
NEΔT	Noise-Equivalent Temperature Difference
NIST	National Institute of Standard and Technology
NMC	National Meteorological Center
NOAA	National Oceanic and Atmospheric Administration
OOB	Out-of-Band
PDT	Pacific Daylight Time
QA	Quality Assessment
RH	Relative Humidity
RSS	Root Sum Square
SBRC	Santa Barbara Research Center (currently as Santa Barbara Remote Sensing)
SCF	Science Computing Facility
SDST	Science Data Supporting Team
SIBRE	Spectral Infrared Bidirectional Reflectance and Emissivity
SNR	Signal-to-Noise Ratio
SRF	Spectral Response Function
SSM/I	Special Sensor Microwave/Imager
SST	Sea Surface Temperature
TBD	To Be Determined
TES	Temperature Emissivity Separation
TIGR	TOVS Initial Guess Retrieval
TIR	Thermal Infrared
TISI	Temperature Independent Spectral Index
TOA	Top of the Atmosphere
TOGA	Tropical Ocean Global Atmosphere
TOVS	TIROS Operational Vertical Sounder

Appendix A: Response to the review comments to the version 1 ATBD

Summary of the ATBD review for MOD-12 in June 1994.

degree to which product meets EOS priorities	soundness (feasibility / practical) of approach	appropriateness of algorithm input	completeness sensitivity and error budget	soundness of validation strategy	results of products at launch
9	5	5	1-5	5	5
	Many assumptions are included. The theoretical models themselves are sound but it is not clear that the many issues are theoretically surmountable.	Other data set are clearly needed to tighten assumptions - especially the emissivity and atmospheric profiles.	Errors due to host of uncertainties need to be established.		Too many unsolved uncertainties to judge this.
(response)	all assumptions have been tested	more input data and TIR bands used	comprehensive error analysis done		revised significantly

Comments

(i) There is a fundamental issue here that needs to be constantly raised to remind other team members. This product and many others will only be available in clear sky conditions. (ii) Retrieval of land surface temperature is difficult using thermal emission techniques. The parameter is germane to many land surface interests, including energy budgets of land and canopies among others. Unfortunately the ATBD lacks clarity. (iii) There is a need to expand this team and include investigators who have worked with existing data such as AVHRR and ASTR. (iv) An algorithm has not been identified. A preliminary algorithm needs to be developed soon and preliminary tests need to be carried out on it.

Response to (i): Yes, the state of microwave technique for LST was reviewed (page 5).

Response to (ii):

Retrieval of LST is difficult using thermal emission techniques but it is more accurate than using microwave techniques. More LST applications were discussed in 2.1 (page 2).

Response to (iii):

The MODIS LST team is using AVHRR data. A collaboration has been established with investigators who have worked with existing data, especially with Dr. Zhaoliang Li who works with the France LST group ledi by Francois Becker and Imarc-Philisppe Stoll. Dr. Li and myself developed the MODIS day/night LST algorithm during his visit to UCSB in 1995.

Response to (iv):

Two LST algorithms have been identified and being validated by field measurement data and aircraft data.

Comments from John Salisbury: The parameters necessary to calculate accurate temperatures from infrared emittance of the surface are well understood. The problem is to quantify them with sufficient accuracy to reach LST and SST goals.

Response:

We are measuring surface emissivities of land materials in laboratory and fields for establishment of an emissivity knowledge base. We has also developed the day/night LST algorithm to recover surface emissivity from space.

Comment 2b from Samuel Goward: The major problem with the method as currently proposed, is the development of a land emissivity map.

Response:

It is truly not a good idea to develop a land emissivity map based on land cover types alone. So it is necessary to develop a LST method to retrieve surface emissivity from space.

Comment 2c from Samuel Goward: It may be that simultaneous execution of the three alternative "solutions" (p. 13) will provide insights concerning the emissivity factor. The investigator should explore this possibility. Currently the investigator proposed to use only 3 of the 16 available TIR measurements on MODIS. Creative exploration of land emissivity properties, looking for redundancies and correlations, may suggest clever ways to resolve this problem internal to the data stream rather than being depended on an unreliable "global" emissivity map.

Response:

This suggestion encouraged me to develop a LST algorithm to retrieval surface temperature and emissivity simultaneously for at-launch LST product rather than for post-launch product originally proposed in 1994. Because the day/night LST method uses the MODIS atmospheric temperature and water vapor profiles product as the initial atmospheric conditions, this LST method has used all information from all MODIS TIR bands although it uses seven TIR bands directly.

Comment 3 from Samuel Goward: Creation of the global emissivity map will be difficult, ... The proposed approach of a few ground measurements, combined with a NIS/NIR land cover classification is unlikely to be satisfactory.

Response:

In the revised ATBD, the above approach is used only for identification of pixels that are dense vegetation, water, snow, ice, not for the global emissivity map.

Comment 4 from Samuel Goward: More creative exploration of land surface TIR spectral properties, in relation to atmospheric TIR spectral attenuation properties is needed to achieve the goals of this data product. The answers to this problem are most likely to be found in cross-band correlations across the entire 16 channel TIR configuration of MODIS. An aggressive investigation of surface and atmospheric emissivity properties is call for to seek out the needed answers.

Response:

Thanks to this comment. It is exactly the theoretical basis for the statistical approach of the MODIS day/night LST algorithm which has been developed recently. Seven MODIS TIR are used in this algorithm because the surface signal in other bands are very weak.

Comment 5 from Samuel Goward: The validation approach is not adequate. It appears to only evaluate sensor calibration. Use of high altitude lakes does not test the capability of the procedure to adjust for either atmospheric attenuation or land surface emissivity. An alternative approach to validation should be determined.

Response:

Yes, high altitude lakes is only for evaluation of MODIS calibration. We use other test sites and approaches for validation of the LST algorithm and product (pp. 41-44 and 52-54).

Comment 6 from Samuel Goward: No schedule for generating data product is specified in this document.

Response:

The schedule for delivery of the LST code is given on page 50. The schedule for data product generation will be decided by DAAC ECS.

Comment 1 from Yann Kerr: This product is probably a key parameters and is thus very important. I regret that the text is not very clear and does not seem to me to address the key points. NB: emissivity is not a MODIS parameter but from a data base!

Response:

A new day/night LST algorithm has been developed to retrieve the surface emissivity from MODIS data. But for certain land cover types, such as dense vegetation, water, snow, ice, the accuracy of the retrieved emissivities may be not as high as those from our emissivity knowledge base.

Comment 2b from Yann Kerr: huge assumptions, sometimes not valid (i.e., emissivity). It is not consistent (complexity of the approach vs importance of the parameter).

Response:

It is true. We developed new algorithm to retrieve emissivity from MODIS data. Besides, we developed a method to detect night dew from MODIS data (pp. 34-39).

Comment 2c from Yann Kerr: consider the work done with the ATSR. work and test with AVHRR data.

Response:

MODIS is not designed to observe a same point at two viewing angles in the almost same time as ATSR does but it has more TIR bands than ATSR. We are using AVHRR data.

Comment 3 from Yann Kerr: emissivity has not be addressed. an approach like that was used to transfer 5S into "smac" should be considered. I do not see a description of the algorithm.

Response:

See response to comment 2c. The 5S code is not suitable for TIR. A clear description of the algorithms are given in the revised ATBD.

Comment 4 from Yann Kerr: Work in collaboration with the ASTER team. The emissivity problem is largely underestimated. What about temporal variability of emissivity?

Response:

Temporal variations in surface emissivity is fully considered in the new LST algorithm. We work with the ASTER team closely, especially in field work for validation.

Comment 5 from Yann Kerr: Do not believe the proposed approach is a validation.

Response:

Revised, see pp. 41-44 and 52-54. We have developed approaches to address the temporal, spatial, and angular variations in LST by the sue of multiple instruments.

Comment 2a from an anonymous reviewer: This approach (the split-window LST method) will require a significant amount of prelaunch work to develop the coefficients for the full range of emissivities and atmospheric climate zones.

Response:

After revising, the split-window LST algorithm is mainly used for land cover types with high emissivities. The MODIS atmospheric profile product will be used to give the range of the atmospheric condition. The concept of climate zone was no longer used.

Comment 2b from an anonymous reviewer: potential problems with the varying emissivity ...

Response:

Emissivity variations fully considered in the new LST method, even for night dew (pp. 34-39).

Comment 5 from an anonymous reviewer: Significant amount of prelaunch validation using aircraft and field measurements will be required.

Response:

Yes, we have conducted several field campaigns in the last two years. See sample results on pp. 41-44.

Comment 6 from an anonymous reviewer: The product can be ready at launch, but the author leaves open the option to switch to another technique if the first method proves unsatisfactory, or if the accuracy of the MODIS total column water is sufficient to provide improved LST using this atmospheric variable. This implies that parallel development on alternative algorithms should occur.

Response:

Yes, the parallel development on the day/night LST algorithm has been done.

Appendix B: Response to the review comments to the version 2 ATBD

Summary of the ATBD review for MOD-12 in May 1996.

technical/scientific soundness of algorithm	value of the data product to the science community	soundness of validation strategy	extent to which 1994 review issues	extent to which product is useful	assessment of plans of plans for comparison
3	6	5	3	6	3
details of separating Earth's surface into known & unknown emissivity for deciding which algorithm to use	p22 separate climate by latitude and longitude?	p23 it not clear where air surface T & water vapor come from	p46-47 only mentioned briefly	inaccuracy in this product not necessarily lead to severe limitations limitations	not well defined
response (1)	response (2)	response (3)	response (4)	response (5)	response (6)

response (1):

See step 5) on page 49 for the generalized split-window method. The day/night LST algorithm can be used for any pixels as long as the dew model (pp. 34-39) shows that there is no significant change in surface emissivity.

response (2):

The concept of climate zone was left from the original ATBD. It is not used any more because the air surface temperature and column water vapor in the MODIS atmospheric profiles product (MOD30) can be used to select the coefficients in their right ranges.

response (3):

See response (2) above.

response (4):

More details are given on pp. 49-50.

response (5):

It is true. But it is possible to improve the surface energy models only if we have accurate surface temperature. The analysis of global surface temperature changes also needs accurate surface temperature.

response (6):

The MODIS LST product will be compared with AM-1 ASTER LST product and the surface parameters from PM-1 AIRS data.

Recommendation 1 from John Price: The robustness of the approach is unclear in regions with unknown emissivity. Day-night temperature data set requirements pose many problems, including: image-to-image registration, changes of the atmosphere between data acquisitions, cloud cover which will make 12-hour temperature pairs much less likely than individual clear scenes, scattered sunlight in the day images for the shorter wavelengths (< 3 um), etc. Solution for 14 variables in terms of 14 measurements is straightforward theoretically, but subject to countless error sources. It appears that the procedure may fail in areas which are of interest to ASTER: when the surface emissivity is less than about 0.96 and is wavelength dependent on the thermal infrared (MODIS bands 31 and 32).

Response:

Simulations show that the day/night method works well as long as the uncertainty in the day/night registration is less than 15-20% (pp. 46-47). The specification for the error in MODIS pointing knowledge is smaller than 200m. So mis-registration is not a problem if we apply this algorithm to pairs of data at 5km by 5km resolution. The NSR could be

increased by a factor of 5 after this average.

Change of the atmospheric condition between data acquisitions is not a problem because we use independent atmospheric variables for daytime and nighttime (p19).

The day/night LST algorithm does not require the 12-hour day and night coverage as ATI (apparent thermal inertia) does for the HCMM data (see page 40 and related references).

Recommendation 2 from John Price: Furthermore, the day-night approach is not practical for latitudes north of 45 deg. N, i.e. it will not produce useful data sets even if it can be implemented The basic reason is mentioned above, the likelihood of clear-sky data at both times during 24 hours is very low. If there is to be such a product it has to have a backup method which does not depend on 2x/day data.

Response:

First of all, there is no 12 or 24 hour requirement for the day/night approach. Cloud cover is a problem for high latitude regions. But the split-window method should work well in these regions because the land surface is covered by snow, ice, and dense vegetation in most of these regions. The main purpose of the day/night approach is to retrieve surface emissivity and temperature in semi-arid and arid regions over which cloud cover is minima (p40). We have also developed night-only and day-only options of the day/night algorithms. But the accuracies of these options are lower, in general (pp. 34-39).

Recommendation 3 from John Price: The ASTER surface temperature algorithm relies on the temperature sounding from MODIS, which in turn probably relies on some knowledge of surface emissivity. This is not being handled properly. This ATBD (MODIS surface temperature) could simply rely on the MODIS temperature and moisture profiles to reduce the problem to that of ASTER, if the MODIS atmospheric profiles are derived properly and within-pixel surface variability is small. But the independent solution is better if it can be provided, because it guarantees self consistency.

Response:

Simulations show that the ASTER algorithm and our different approach that bases on the essentially same physics (using the MMD-MIN relationship in MODIS bands and the least-square fitting method) used in our dew detection model (pp. 34-39) work quite well if the MODIS atmospheric profiles are derived properly and their accuracies are high. But this is not guaranteed because the instrument noise in the MODIS sounding channels may be high and the inaccurate surface conditions also result in uncertainties in the retrieved atmospheric profiles. Because the MODIS day/night LST algorithm uses independent variables for air surface temperature and column water vapor, it has the ability to simulate the variation in the atmospheric conditions and reduce the effect caused by the uncertainties in the profile through the self consistency in the multitemporal multichannel TIR observations.

Appendix C: Response to the comments to the version 3.1 ATBD (August 1996)

An International Land-Surface Temperature Workshop was held on September 17-19, 1996, at the University of California at Santa Barbara. Twenty five participants from USA, France, Australia and Japan attended the workshop. Twenty presentations were followed by two discussion sessions. It was a successful and productive workshop. Here is the author's response to oral and written comments received during and after the workshop.

Comment 1 from Samuel Goward: One consistent conclusion can be drawn from the various empirical and theoretical assessments presented at the meeting: Most AVHRR split-window equations work well (1C) for dry atmospheres but perform much poorer (5C) under high humidity conditions. Our assessment, with MODTRAN, suggests that this is because of high nonlinearity in the relation between spectral band differences and water vapor at high water vapor contents. Prof. Becker concurs that this is a problem which he and Dr. Li are currently working to address. How this problem would change with sensor configurations other than AVHRR (e.g. MODIS, ASTER, etc.) is not known.

Response:

In order to deal with nonlinearity problem, the MODIS generalized split-window LST algorithm uses different coefficients for different humidity and temperature ranges because the MODIS atmospheric profiles product can provide the necessary information for us to determine the suitable ranges. The atmospheric optical depth depends on viewing angle, that is why we developed the view-angle dependent split-window LST algorithm for further improvement.

Comment 2 from Samuel Goward: Much discussion of the role of emissivity in LST estimation occurred. Several key points are worth noting; 1) For about 70% of land areas (the vegetated-soils part) emissivity variability does not appear to be an important issue, particularly in the 10-14 μm region. This suggests the possibility of geographically stratified approaches to LST were, for much of the land areas, emissivity can be ignored. 2) For the other 30% of the land areas (semi-arid to arid), the major emissivity contrasts are primarily in the 8-10 μm region. In the 10-12 μm region only a few surface types have important emissivity features. In the 12-14 μm region no currently measured land surface materials appear to have important (to LST) emissivity features. This suggests that a) 10-12 μm based LST algorithms may not be impacted much by emissivity variability and b) "universal" LST estimation, ignoring emissivity, may be possible using 12-14 μm observations (such as in MODIS). 3) The ASTER Gillespie-Hook TES approach to emissivity assessment, evaluating between-spectral-band correlations, shows significant promise as a means to further reduce the residual emissivity problems encountered in the 10-12 μm region.

Response:

This is the physics basis of our generalized split-window LST algorithm. Our measurements show that the emissivity of structured leaf samples is around 0.99, so we can ignore the emissivity effect for pixels covered by dense vegetation (using a fixed emissivity value at 0.99). The uncertainty of 0.01 in emissivity may result in an error of 0.3-0.6 °C in recovered surface temperature, depending on the atmospheric moisture condition. But there are considerable variations in emissivities of soil, sands, and rocks even in the 10-13 μm region. Beyond 13 μm the atmospheric absorption becomes a serious problem (see Fig. 1 in the ATBD). MODIS band 33 is located at 13.3 μm, we use this band in the day/night algorithm for retrieving the information of the atmospheric temperature. MODIS has only two bands (31 and 32) in the 10-13 μm region so they are not suitable for the method similar to the ASTER TES method.

Comment 3 from Samuel Goward: Wan and associated MODIS team members (Snyder, Zhang, Feng) presented the currently proposed day-night multi-spectral MODIS LST algorithm. Based on theoretical work by Wan and Li, the method solves the n+1 problem by assuming constant day-night emissivity. Considerable concern was expressed about this method. Efforts under the early NASA HCMM mission to employ this approach for thermal "inertia" analysis in general were not successful. Basic problems in image registration, cloud cover, changing surface conditions and sensor calibration stability mitigate the approach. Proposed solutions, including 5 by 5 pixel averaging do not appear to provide an effective resolution of this problem. Goward made a recommendation that a by-component (i.e., 1-band, 2-band, 3-band, etc.) assessment of the proposed multispectral, multi-temporal method be undertaken to determine what is gained over current two-band approaches with each step of the process. In particular, a single scene, per-pixel method should be developed for at-launch use.

Response:

See response to recommendation 1 from John Price in Appendix B for the comment day/night registration (pp. 46-47 in the ATBD). See response to recommendation 2 from John Price in Appendix B for the comment regarding HCMM (see discussion on pp. 34-39 in the ATBD). We come through the long way from 1-band, 2-band, 3-band, etc. In version 1 of

this ATBD, we focused on 2-band method. In version 2, we tried 3-band methods. Then we tried 4-band, 5-band, 6-band, and finally 7-band method. The critical question is how much do we know the atmospheric condition and surface emissivity, and their accuracies of these knowledge. If we know everything, single band is enough. If we know the surface emissivity in bands 31 and 32, we can use the split-window LST method. If we do not have any confident information of the atmosphere and surface emissivity, we need at least seven MODIS bands for simultaneous retrieval of surface emissivity and temperature (page 19). Considering this comment and the comment made in 1994 (comment 2b from Samuel Goward in Appendix A), it seems that the generalized split-window LST algorithm and the day/night LST algorithm are the good combination for the global LST. We recently developed a single scene, per-pixel method for investigation of the diurnal change of emissivity caused by night dew (pp. 34-39). It works quite well if we know enough information of the atmospheric condition, so we can use it for detection of a significant change in surface emissivity. But the accuracy of this night-only method is lower than the day/night LST algorithm.

Comment from Francois Becker: It is important to understand the requirements for accuracies of LST and surface emissivity from different applications, including GCM and survey, and their sensitivities in wide ranges of atmospheric and surface conditions.

Response:

Yes! A specific LST algorithm may work well in cold and dry conditions, but it may be poor in hot and wet conditions. So it is important to develop a LST algorithm working well in wide ranges of conditions. As an example from our field measurements at a silt playa in Railroad Valley, NV, on 4 June 1996, the measured LST at 12:25 PDT is 57.5 °K and the measured LST at 19:55 PDT is 24.5 °K. The day-evening LST difference is larger than 30 °K (p44 in the ATBD).

Comment from Xubin Zeng: The LST accuracy needed in climate models is 1 °K. The error in calculated sensible heat flux is not a constant but a function of the surface-to-air temperature difference, i.e.,

$$\frac{\delta H}{H} = \frac{\delta T_s}{T_s - T_a} \quad ,$$

where T_s is LST and T_a is the air surface temperature.

Response:

In general, the surface-to-air temperature difference decreases with the increase of atmospheric humidity. As we know the LST retrieval is more difficult in wet conditions, so this is a challenge. In order to meet the accuracy requirement from climate modeling, we need to try our best to develop LST algorithms as accurate as possible in the wide ranges of atmospheric and surface conditions.

Comment from Merv Lynch: The accuracy and role of geostationary sensors for providing higher temporal sampling of land temperature should be investigated. Such sensors offer a higher probability of achieving cloud free conditions for a given location and also would provide data sets at time more appropriate for model assimilation.

Response:

It is a very good suggestion.